ASSESSMENT OF THE EFFECT OF MITOTANE ON EXPRESSION PROFILE

OF THE GENES INVOLVED IN MITOCHONDRIAL METABOLISM IN HUMAN

ADRENOCORTICAL, LUNG, BREAST AND COLON CANCER CELL LINES

PhD thesis

Author: Urszula Waszut

Supervisor: dr hab. n. med. Dorota Dworakowska

Department of Nuclear Medicine

Chair of Nuclear Medicine and Radiology Informatics

Faculty of Health Sciences with Subfaculty of Nursing

And Institute of Maritime and Tropical Medicine

Head of the Department: Prof. dr hab. n. med. Piotr Lass

Medical University of Gdańsk

Gdańsk 2017

OCENA WPŁYWU MITOTANU NA EKSPRESJĘ GENÓW

ZAANGAŻOWANYCH W REGULACJĘ METABOLIZMU

MITOCHONDRIALNEGO W LUDZKICH LINIACH KOMÓRKOWYCH RAKA

KORY NADNERCZA, PŁUC, PIERSI I JELITA GRUBEGO

Praca Doktorska

Autor: Urszula Waszut

Promotor: dr hab. n. med. Dorota Dworakowska

Zakład Medycyny Nuklearnej

Katedra Medycyny Nuklearnej i Informatyki

Radiologicznej

Wydział Nauk o Zdrowiu z Oddziałem Pielęgniarstwa

i Instytutem Medycyny Morskiej i Tropikalnej

Kierownik: prof. dr hab. n. med. Piotr Lass

Gdański Uniwersytet Medyczny

Gdańsk 2017

Wyniki zawarte w niemniejszej pracy były prezentowane na międzynarodowych konferencjach naukowych wliczając: *Endocrine Society's 97th Annual Meeting w San Diego, USA* (5–8 marca 2015) oraz XXI Zjazd Polskiego Towarzystwa Endokrynologicznego w Katowicach (15– 17 września 2016).

Acknowledgements:

Podziękowania:

Mój dług wdzięczności głownie należy się Pani Promotor dr hab. med. Dorocie Dworakowskiej za możliwość uczestnictwa w grancie Fundacji na Rzecz Nauki Polskiej, poświęconym ciekawemu obszarowi badań i za okazane mi wsparcie. Składnam podziekowania dla Pani Promotor za pomoc merytoryczna w częśći badowczej i statystycznej oraz finansową (udzielenie stypendiium FNP oraz środków z funduszu Kings College Hospital Charity 'Endocrine Cancer Research Fund'.

Pragnę także wyrazić moją wdzięczność dla pracowników naukowych (Viapath) Departamentu Patologii Molekularnej i Biochemii, Szpitala Kings College w Londynie, którzy pomogli mi w sposób praktyczny, a także okazali przyjaźń i wsparcie. Chciałabym szczególnie podziękować Dr Mel Smith za udostępnienie laboratoriów i sprzętu badawczego oraz za udzielone doradztwo i sprawdzenie moich tekstów związanych z zagadnieniami biologii molekularnej, a także Dr Salvador Diaz-Cano z Departamentu Histopatologii w King College Hospital za udzieloną pomoc. Dr Normanowi Taylorowi z Zakładu Biochemii Klinicznej pragnę podziękować za korektę pisowni, wyszukanie i udostepnienie tekstów, do których nie miałam otwartego dostępu. Pragnę także podziękować, dr hab. Piotrowi Wężowi jako osobie, która wykonala statystyke w ramach grantu, oraz szczegunie dr Paulinie Szyszce za współpracę i wzajemną pomoc podczas projektu badawczego.

Z Wdziecznością podziękowania dla Magdaleny Dąbrowski za przyjaźń oraz wsparcie finansowe, kończąc dziękuje mojej rodzinie za ich miłość i wsparcie, wspominając szczególnie mojego ojca, któremu chcę podziękować za pomoc w układzie rysunków, tabel oraz sprawdzenie tekstu pod względem poprawności technicznej. Biorę pełną odpowiedzialność za wszelkie pozostałe błędy.

Table of contents

List of abbreviations:

AKT	protein kinase B	**JNK**	c-Jun N-terminal kinase
AMP	adenosins monophosphate	**KCH**	King's College Hospital
AMPK	5' AMP-activated protein kinase	**KCNJ5**	Transcriptional factor
12S rRNA	12S ribosomal rRNA	**Keap1**	cytoplasm protein constitutively degrades Nrf2
16S rRNA	16S ribosomal rRNA	**Ki-ras**	Kirsten rat sarcoma viral oncogene homolog
		L	mtDNA light strand promotor
22 tRNA	transfer RNA, 22 translation mitochondrial adaptor molecules	**MAM**	mitochondrial-associated membranes
ACC	adrenocortical carcinoma	**MALDI-TOF**	matrix assisted laser desorption-ionization time of flight mass spectrometry
ACTH	adrenocorticotropic hormone	**LSP**	light strand promotor
ADIUVO	efficiency of adjuvant mitotane treatment	**MAPK**	mitogen-activated protein kinase
Apaf1	apoptotic protease activating factor 1	**MCF-7**	human breast adenocarcinoma cell line
ATP	adenosine triphosphate	**mt-PTP**	mitochondrial permeability transition pore protein
AVG	average	**mtDNA**	mitochondrial DNA
B1	isoform	**mTERF (MTERF)**	mitochondrial transcription termination factor
BAX	pro-apoptotic molecule BCL2-associated X protein	**MTK1/MEKK4**	human MAPK kinase, MTK1 (also known as MEKK4)
Bcl-2	B-cell lymphoma — anti-apoptotic protein	**mTOR**	mechanistic target of rapamycin
BCL-XL	B-cell lymphoma-extra-large (BCL-XL, or BCL2-like 1) isoform 1 gene	**mt-tRNAs**	mitochondrial transfer RNAs
bp	base pair	**NADH**	nicotinamide adenine dinucleotide-coenzyme (Appendix A)
C	complex	**NADP+**	nicotinamide adenine dinucleotide phosphate
cDNA	complementary DNA	**NADPH**	the reduced form of NADP+
c-Myc	regulator gene that codes for a transcription factor	**NDUFB5**	NADH dehydrogenase (ubiquinone) 1 beta subcomplex (Appendix A)
Acetyl-CoA	Acetyl coenzyme A	**NFP (grant)**	Foundation for Polish Science
COX	cytochrome c oxidase (Appendix A)	**NFκB**	nuclear factor kappa-light-chain-enhancer
COX2	mitochondrial encoded cytochrome c oxidase subunit 2	**NRF-1**	nuclear respiratory factor 1
COX4	cytochrome c oxidase subunit 4 isoform 1 (Appendix A)	**Nrf**	nuclear erythroid-derived factor
COX 7AL2	cytochrome c oxidase subunit VIIa polypeptide 2 like	**NVP-BEZ235**	imidazoquinoline derivative and PI3K inhibitor
Ct	cycle threshold	**o,p'DDD**	inhibitor of adrenal steroid synthesis (mitotane)

List of abbreviations

Abbreviation	Definition
C-terminus	carboxyl-terminus
CYP P450	cytochrome P450 — terminal oxidase enzyme
CYP11A1	cholesterol side-chain cleavage enzyme
CYP11B1	steroid 11β-hydroxylase
CYP11B2	aldosterone synthase
CYP17	17-hydroxylase / steroid 17-alpha-monooxygenase
CYP17A1	cytochrome 17A1
CYP21	21-hydroxylases
CYP21A2	cytochrome 21A2
CYP3A4	hepatic cytochrome P450 3A4
cyt b	cytochrome b
cyt c	cytochrome complex
Cdc2	cyclin B
Cdk2	cyclin dependent kinase
CHOP	C/ebp HOmologous Protein
DHA	dehydroepiandrosterone
DNA	deoxyribonucleic acid
DNase	deoxyribonuclease
dNTP	nucleoside triphosphate
eIF2A	eukaryotic translation initiation factor 2a
EGF	epidermal growth factor
ENS@T	european network for the study of adrenal
ER	endoplasmic reticulum
erlotinib	erlotinib hydrochloride (trade name "Tarceva")
everolimus	inhibitor of mammalian target of rapamycin (mTOR)
FAM	carboxyfluorescein
FATE1	fetal and adult testis expressed 1
FIRM-ACT	first international randomized trial in locally advanced and metastatic ACC
FFPE	formalin-fixed, paraffin-embedded
FOXO	forkhead transcription protein
GADD45B	growth arrest and DNA-damage-inducible (Appendix A)
GAPDH	glyceraldehyde 3-phosphate dehydrogenase (Appendix A)
gDNA	genomic DNA
GTP	guanosine-5'-triphosphate
GTPase	hydrolase enzymes activated by GTP
o,p'DDE	1,1-(o,p'-dichlorodiphenyl)-2,2 dichloroethene (mitotane analogue)
p,p'DDOH	2,2-bis(4-chlorophenyl)ethanol
p38	mitogen-activated protein kinase
P450	cytochromes P450 — CYPs
p53	tumour protein 53
p-value	probability value
PBS	phosphate-buffered saline
PCR	polymerase chain reaction
PET	Positron Emission Tomography
PGC1α	peroxisome proliferator–activated receptor alpha
PHB	prohibitin inhibits DNA synthesis, regulator of proliferation
PHB1p	PHB isoform 1
PHB2p	PHB isoform 2
PI3K	phosphoinositide 3-kinase
PINK1	PTEN-induced putative kinase 1
PPA1	inorganic pyrophosphatase 1
PPC	Positive PCR Control
PTEN	phosphatase and tensin homolog
qPCR	quantitative polymerase chain reaction
qRT-PCR	quantitative real-time polymerase chain reaction
RIN	RNA Integrity Number
RN	normalized reporter
ROS	reactive oxygen species (superoxide or H_2O_2)
rRNA	ribosomal RNA
RT	reverse transcriptase
RTC	Reverse Transcription Control
SOAT 1	Sterol-O-Acyl Transferase 1
serpin	SERine Proteinase Inhibitor
siRNA	small interfering RNA
SLC25A25	mitochondrial carrier; phosphate carrier (Appendix A)
ST DEV	standard deviation
StAR	steroidogenic acute regulatory protein
SYBR Green I	asymmetrical cyanine dye used as a nucleic acid stain
Taq	Taq polymerase – thermostable DNA polymerase for PCR
TCA	tricarboxylic acid cycle

List of abbreviations

H1	full length polycistronic H1 strand transcript
H195R	adrenocortical carcinoma cell line
H2	full length polycistronic H2 strand transcript
HCT-116	human colorectal cancer cell line
HIF1α	subunit of a heterodimeric NRF-1
HIF1	hypoxia inducible factor 1
Hint	Histidine triad nucleotide binding protein
Hke-3	Ki-ras mutations of HCT-116 cell line
hnRNP	heterogeneous ribonucleoprotein particle
hnRNPA2/B1	heterogeneous nuclear ribonucleoproteins A2/B1
HSD	hydroxysteroid dehydrogenase
HSD3B1	3β-hydroxysteroid dehydrogenase
HSD3B2	hydroxy-δ-5-steroid dehydrogenase
HSP 1	mtDNA heavy strand promotor 1
HSP 2	mtDNA heavy strand promotor 2
hTERT	telomerase reverse transcriptase

TIGAR	TP53-inducible glycolysis and apoptosis regulator
TMX	thioredoxin
TR	containing a Tetracycline Response system
TRK	tyrosine kinase
VEGF	vascular endothelial growth factor
VDAC	voltage-gated anion channels
ΔΔCT	Delta Delta Ct method
ΔRn (Delta Rn)	intensity of fluorescence signal

NOTE 1: Numerous names of genes used in experiments can be also found in Appendix A at the end of the document.
NOTE 2: Despite carefulness some of genes names can differ from official notations, especially in product listings prepared by manufacturers.

Abstract

Abstract

Background: Adrenocortical carcinoma is a rare disease with poor prognosis. The most effective agent is mitotane, which selectively limits growth and bioactivity of adrenal tissue, but the basis for this action has yet to be established. It has direct effects on mitochondria, which have unique features in steroidogenic tissue and are known to be important in development of malignancy and in apoptosis. It might cause change in expression of genes related to mitochondrial energy metabolism, which is known to be disturbed during cytotoxic and apoptotic processes. There are many known changes in gene expression in adrenal tumours, based on use of fresh or snap-frozen material. If FFPE could be used, this would greatly expand the potential for study of these rare, very heterogeneous cancers, enabling exploitation of archival material and correlation with the histology of different regions of the tumour.

Aims: To compare expression levels of a panel of 84 genes involved in mitochondrial energy metabolism between human adrenocortical (H295R), breast (MCF-7), adolescent colorectal (HKe-3) and lung (H195R) cell lines under basal conditions and after exposure to the adrenolytic agent mitotane and to consider whether the greater sensitivity to this agent of adrenal cells involves different expression to that in other cancer cells. In addition, to develop extraction of mRNA from FFPE with the aim of achieving sufficient quality for gene expression studies.

Materials and methods: Gene expression was assessed in the four cultured cell lines after proliferation experiments using the *Mitochondrial Energy Metabolism Plus PCR Array* from Qiagen which includes genes of the respiratory complexes I - V and associated mitochondrial proteins. Extraction of mRNA from FFPE adrenocortical carcinoma samples was optimized, with testing of quality at each step and final testing on an mTOR array in comparison with normal adrenal tissue.

Results: At baseline, there was a range of activities of mitochondrial energy metabolism genes in the ascending order: MCF-7, H295R, H1975, Hke-3. Mitotane led to more than two fold overexpression in a number of subunits of complexes I -V in both H295R and Hke-3, which were the most sensitive cell lines. This 'mitotane-sensitive' group showed statistically significant overexpression of six genes of complexes I and III, which are potentially ROS-generating and four genes of complex V, which generate high energy phosphates, together with four genes of the COX complex. In the two less sensitive cell lines, only one gene, in complex II, was upregulated. FFPE-derived RNA was successfully prepared for gene expression analysis.The most important findings were several-fold over-expression of VEGFs (VEGF C 16 fold change) and strong downregulation of PIK3CD (37 fold change) which encodes a protein important for immunology interaction in tissue, as well as upregulation of some important downstream effectors of the TRK receptor.

Conclusions: For adrenal H295R cells, there were no clear differences in comparison with the other cell lines, with genes of all complexes represented and no single group dominating. However, upregulation in respiratory complex subunits after mitotane suggests this is a key event in the processes of cell stasis and death, perhaps via increased generation of ROS and high energy phosphates, leading to loss of mitochondrial continuity and cytochrome c leakage, Ca^{2+} influx, and increased expression of proapoptotic COX subunits and GADD45B. The preliminary findings on gene expression using material from FFPE blocks do indicate that this methodology can make an important contribution to future studies.

Keywords: mitotane, mitochondrial energy metabolism, cell culture,gene expression, apoptosis, adrenocortical carcinoma

Streszczenie

Streszczenie

Wprowadzenie Rak kory nadnerczy jest rzadką chorobą o złym rokowaniu. Najbardziej skutecznym stosowanym lekiem jest mitotan, który ogranicza aktywność biologiczną i wzrost komórek raka kory nadnerczy, jednak spójny mechanizm jego działania nie został jak dotąd ustalony. Bezpośrednie obserwacje wykazały istotną rolę mitochondriów, które posiadają specyficzną budowę w tkankach steroidowych, ze względu na ich rolę w rozwoju nowotworu i programowanej śmierci komórek (apoptozie). Mitotan może powodować zmiany w ekspresji genów związanych z mitochondrialnym metabolizmem energetycznym, który wiadomo, że jest zakłócony w trakcie zmian cytotoksycznych i apoptozie.Wiele zmian w ekspresji genów zostało wykazanych przy użyciu mrożonej próbki guza, jednakże jeśli można by zastosować materiał parafinowany, znacząco zwiększa to potencjał badania tych rzadkich, bardzo heterogenicznych raków, umożliwiając wykorzystanie materiału archiwalnego i korelację z histologią różnych regionów guza.

Cele: Celem projektu było zbadanie poziomu ekspresji genów uczestniczących w mitochondrialnym metabolizmie energetycznym pomiędzy liniami komórkowymi raka kory nadnercza (H295R), piersi (MCF-7), jelita grubego (HKe-3) i płuca (H195R) w warunkach podstawowych i po ekspozycji na adrenolityczny mitotan. Rozważenie, czy występuje większa wrażliwość na ten czynnik w komórkach nadnerczy wiąże się z inną ekspresją tych genów. Dodatkowo sprawdzenie wystarczającej przydatności dla badania ekspresji genów mRNA izolowanego ze starych bloków parafinowych.

Materiały i metody: Ekspresję genów została zbadana w czterech liniach komórkowych w hodowli, po eksperymentach dotyczących proliferacji z wykorzystaniem macierzy qPCR Qiagen z genami biorącymi udział w metabolizmie mitochondrialnym, która zawiera geny kompleksów oddechowych I-V i powiązanych białek mitochondrialnych. Izolację mRNA z guzów parafinowych zoptymalizowano, testując jakość etapowo, ostatecznie przeprowadzony został eksperymenty na macierzy mTOR w porównaniu z normalną tkanką nadnerczową.

Wyniki: Wyjściowa ekspresja genów metabolizmu mitochondrialnego wskazująca na jego aktywność jest rosnaca kolejno dla: MCF-7, H295R, H1975, HKe-3. Porównanie wpływu mitotanu na badane linie komórkowe, wykazała wiele zmian w ekspresji genów, w zróżnicowany sposób. Mitotan spowodował nadekspresję w podjednostkach kompleksów I -V zarówno w H295R jak i Hke-3, które były najbardziej wrażliwymi liniami komórkowymi. Ta grupa "wrażliwa na mitotan" wykazała statystycznie istotną nadekspresję sześciu genów kompleksów I i III , które mogą generować ROS i cztery geny kompleksu V, wytwarzające wysokoenergetyczne nukleotydy adeninowe i cztery geny kompleksu IV- COX. W dwóch mniej wrażliwych liniach komórkowych wystąpiła nadekspresja tylko jednego genu w kompleksie II. RNA z FFPE z powodzeniem został wykorzystany do analizy ekspresji genów. Najważniejsze wyniki to silna nagekspresja VEGFów i białka kodowanego przez PIK3CD, ważnego dla prawidowych interakcji immunologiczych w tkance, a także nadekspresja niektórych ważnych efektorów receptora TRK.

Wnioski Dla linii H295R nie było żadnych wyraźnych tendencji, czy genów jednej dominującej grupy danego kompleksu oddechowego, w porównaniu do innych linii komórkowych, dla wyjściowej ekspresji metabolizmu mitochadrialnego. Jednakże nadekspresja genów kompleksów oddechowych sugeruje procesy, które mogą być kluczowe w procesie śmierci komórki jak zwiększona produkcja wolnych rodników, czy wysokoenergetycznych fosfataz i przepływ jonów Ca2+, prowadzące do utraty ciągłości błony mitochondrialnej, oraz promujący apoptozę wzmożony wzrost ekspresji podjednostek oksydazy cytochromowej i czynnika GADD45B. Wstępne opracowanie dotyczące ekspresji genów za pomocą materiału z bloków parafinowych wskazują, że ta metodologia może w istotny sposób przyczynić się do przyszłych badań.

Słowa kluczowe:mitotan, mitochadrialny metabolism energetyczny, chodowle komórkowe, ekspresja genów, apoptoza, rak kory nadnercza.

I. Introduction

1.1 Mitotane: basis for understanding possible mechanisms of action.

1.1.1 Historical background

Mitotane (o,p'DDD) is an adrenolytic drug recommended for treatment of primary and recurrent adrenocortical carcinoma (ACC) (Breuner et al. 2000), (Fassnacht, Kroiss, and Allolio 2013), (Else et al. 2014),(Libe and Assie 2014), and also in Cushing syndrome (Fleseriu and Castinetti 2016). Though it has had limited success, no pharmacological options of better efficacy have yet become available. Mitotane synthesis from the insecticide DDT and its recognition as an agent that selectively damages adrenocortical tissue originates in the 1940s. Since 1959, mitotane has been used for treatment of inoperable ACC (Kasperlik-Zaluska 2000), but its role in prolonging survival has been in question. In 2002, the European Commission granted the drug orphan designation under the trade name Lysodren, based on the low prevalence of the disease. A large retrospective study by Terzolo *et al*., which investigated mitotane use as an adjuvant treatment (Terzolo et al. 2007), has led to its widespread adoption in this setting.'It remains a question whether continuing mitotane use assists disease-free and overall survival in low-grade and radically operated ACC patients. This is being addressed in an ongoing international study (ADIUVO), which randomises patients to treatment or no treatment (Terzolo and Berruti, n.d.), (Postlewait et al. 2016). This initiative builds on ongoing highly successful collaboration established through the European Network for the study of Adrenal Tumours (ENS@T). Addition of chemotherapeutic agents to mitotane has been assessed in the international FIRM-ACT study, where the treatment aim was to prevent metastasis development or further growth of a tumour that had not been fully resected. Additional treatment with a combination of etoposide, deoxyrubicin and cisplatin was compared with streptozocin, with switching to the alternative if disease progression occurred. The first was associated with a better response rate and progression - free survival but there was no difference in effect on overall survival, which was still regarded as dismal, with medians of 14.8 and 12.0 months, (Fassnacht et al. 2012), (Waszut, Szyszka, and Dworakowska 2017).

Introduction

Mitotane sensitivity differs widely between species but with correlation of morphological and functional toxic effects. The dog is an especially sensitive species and has been the most studied, with demonstration of gross destruction of the zona fasciculata and zona reticularis of theadrenal cortex. In contrast, observations in the human are fragmentary and harder to interpret, although high doses do cause adrenal atrophy, while in contrast, rats, mice, rabbits and monkeys are relatively insensitive (Fang 1979). Extensive investigations into the mechanisms of adrenocorticolytic activity, reviewed below, offer tantalising clues. However, no entirely coherent understanding has yet emerged of the characteristics of this tissue that cause it to be especially targeted by mitotane.

1.1.2 Clinical effectiveness and clinical monitoring

A therapeutic range in blood of 14 to 20mg/L (43.75–62.5 µM) is universally accepted; monitoring of blood levels is necessary (van Ditzhuijsen, van de Weijer, and Haak 2007). The drug is highly lipophilic and accumulates in body fat. In consequence, attainment of these levels requires many weeks and there is a slow fall over months if treatment is stopped. This, together with its limited effectiveness and associated toxicities means that therapeutic management has been a recurring challenge.

The survey of mitotane use as an adjuvant referred to above (Terzolo et al. 2007) included 177 patients after radical surgery at 8 centres in Italy and 27 in Germany. Outcomes for 47 Italian patients who received treatment were compared with two control groups, 55 from Italy and 75 from Germany, which had not received adjuvant mitotane after resection. The authors concluded that mitotane treatment prolongs recurrence-free survival, but this has been challenged (H. Huang and Fojo 2008) on grounds including possible ascertainment bias and limitations of analysis of data from a rare disease such as this. These authors emphasise that the findings infer that mitotane only delays time to recurrence without impact on survival but concede that mitotane may help prolong disease-free survival in some patients. They also note that the descriptions of several studies reporting biochemical and tumour regression rates as high as 85% have never been substantiated in subsequent trials. Only one third of patients are considered to be responders, with the only predictive marker of response being the drug level in plasma.

16

Introduction

Others (Hescot et al. 2013), (Takeshita et al. 2013) maintain that if the therapeutic range is maintained, which is reached after 3 months of treatment on average, then indefinite therapy may produce growth arrest of tumour deposits and prevent recurrence and improve overall survival rates. A relatively high proportion of treated patients show side effects, particularly gastrointestinal and neurological, with 80% having at least one undesirable effect. Although high doses reduce the time taken to reach therapeutic levels, there is a greater risk of unacceptable side effects, so lower doses may be preferable to achieve better overall outcomes (H. Huang and Fojo 2008). Radical surgery together with maintenance of drug levels in the therapeutic range currently offer the best hope of long term remission (Else et al. 2014).

Mitotane decreases cortisol secretion and this has been utilized to assist control of Cushing's syndrome (Schteingart et al. 1980) (Howlett, Rees, and Besser 1985). When used in an adjuvant setting, a glucocorticoid, most commonly hydrocortisone (cortisol), must also be given to compensate for this. The dose requirement for hydrocortisone replacement is increased by mitotane, as a result of enhancement of metabolic clearance via induction of hepatic CYP3A4 and other hydroxylases (Ghataore et al. 2012), (Takeshita et al. 2013) and decrease of bioavailability of cortisol via increase of corticosteroid-binding globulin. Total blood cortisol is thus a poor means of monitoring the biologically-available cortisol level. Free cortisol is not a widely available assay, so it has been recommended to monitor ACTH instead (Schteingart et al. 1993). In assessing effects of mitotane on normal adrenal tissue, concomitant use of hydrocortisone with mitotane renders it impossible to distinguish direct effects on the non-affected adrenal following ACC surgery from the effects of suppression of the hypothalamo-pituitary-adrenal axis.

The influence of mitotane on aldosterone secretion is less clear. (Fukushima, Bradlow, and Hellman 1971) found that four Cushingoid patients whose cortisol was corrected by mitotane did not have lower aldosterone, while Schteingert *et al.* 1980 found mostly normal aldosterone and renin values in 8 patients while on a 120 meq sodium diet. Renin quantification in patients under treatment has nevertheless been recommended as part of routine monitoring and in practice, many patients are judged to require mineralocorticoid supplementation (Fassnacht and Allolio 2009), (Schteingart et al. 1980).

17

Introduction

1.1.3 Effects on adrenal tissue and cells

It has proved difficult to demonstrate clearly the effects of mitotane treatment on the human adrenal glands. There are few reported studies of the effects of mitotane treatment on human adrenal tissue. The most direct approach is that of Touitou *et al.*, (1978) who compared adrenal glands removed from 5 Cushingoid patients receiving mitotane with those from 2 untreated patients with Cushing's and 2 removed from adults within an hour of death in traffic accidents. Adrenal weights were not lower in the mitotane-treated patients, but initial weights may well have been increased by presence of tumour or ACTH-dependent adrenocortical hyperplasia. Histological changes were listed. These appear to be normal after mitotane but are unfortunately insufficiently detailed to differentiate mitotane effects. Incubation of adrenal homogenates was carried out for 2h with radiolabelled steroid precursors. Rates of conversion of 11-deoxycortisol to cortisol and cortisone (in parentheses) were much lower in treated patients (mean 1.8 (0.6) %) than controls (11 & 11 (1.5 & 2.1) %) or untreated patients (34 & 64 (7.3 & 2.5) %). Conversion rates of corticosterone to aldosterone were lower for patients (mean 0.14 %) than for one control (0.32 %). Also studied were two adrenal glands derived from a single patient with Cushing's syndrome with adrenocortical hyperplasia. The first was removed after treatment for one month with mitotane and the second after a further 4 months with no treatment. Yield (treated, untreated) of cortisol was 22, 64 %, cortisone, 2.3, 2.8 % and of aldosterone 0.56, 0.94 %. In contrast, direct addition of mitotane as a powder to the adrenal homogenates was without effect over the same time course. This was suggested by the authors to show that activation of mitotane *in vivo* was necessary, but stands in contrast to findings in cultured adrenal cells (see below). This might be explained by lack of dissolution of this lipophilic compound, or a requirement for a longer time course of activation or activation may only take place in intact adrenal cells. The effects on steroidogenesis may reflect a generalised damage to adrenocortical cells or a specific inhibition of CYP 11 B1 (11-hydroxylase) and CYP 11 B2 (aldosterone synthase), but both of these enzymes are located in the mitochondria and so are most likely to refect mitochondrial disruption (see below).

Microscopic and ultramicroscopic effects of mitotane, with evident change in mitochondria, have been shown in cultured adrenal-derived human adrenocortical cancer cell lines SW13 and H295R (Poli et al. 2013). Mitotane rapidly accumulated intracellularly, increasing in a dose and time-dependent way after incubation with the

agent, as did effects on viability and proliferation. By 2 hours after a single exposure, swelling and depolarisation of the mitochondrial membrane and progressive dissolution of the inner matrix were visible by electron microscopy. There was no significant effect on fibroblasts. These findings support the proposal that the main role of mitotane is induction of oxidative stress within adrenal tissue (Stigliano et al. 2008).

Mitotane exposure of Feng-8 cells (feminizing adrenal neoplastic cells believed to be derived from the zona reticularis) in culture resulted in microscopically visible evidence of a toxic reaction, including air bubbles at the cell surface and shrinkage of the cells, followed by detachment of some from the dish. Blockage of cell division, growth and function occurred in a dose-related manner with progressive loss of cell protein at concentrations above 8.4×10^{-5} M. Interestingly, when cells that had survived and remained attached were returned to mitotane-free medium, they recovered normal function with no sign of any residual toxic effect (Fang 1979).

These effects are not seen in the zona glomerulosa. In the same time frame, there is a reduction of steroidogenesis and significant reduction of mitochondrial P450 and haem content (Martz and Straw 1977), (Schteingart et al. 1993).

Active intracellular conversion of mitotane *in vivo* and by human hepatocytes *in vitro* has been demonstrated, but there are no comparable studies of mitotane conversion by H295R cells. Direct *in vitro* effects of the major known products of mitotane *in vivo* have not, however, been confirmed (Takeshita et al. 2013). In early studies, (Touitou, Bogdan, and Luton 1978) using fresh homogenates of 'normal' adrenals, incubated for 2h, showed no effects on steroidogenesis of the unsaturated metabolite o,p'DDE or p,p'DDMU at a concentration of 10^{-2} M, or of p,p'DDOH at 2.1×10^{-3} M. However, it must be noted that mitotane at similar concentrations was inactive in this system.

1.1.4 Mechanisms of adrenocortical cell death and stasis in response to mitotane.

Numerous observations suggest that there are several different processes by which mitotane induces arrest of adrenocortical cell proliferation or cell death. These may include direct toxic effects, arrest of the cell cycle and apoptosis. There is much higher sensitivity to mitotane of adrenocortical tissue and derived cell lines in comparison with other tissues, including carcinoma tissue. This may be due to generation of unique toxic

products within the adrenals (Section 1.1.3) or to other particular features of adrenal biochemistry that render them susceptible to mitotane or its products, but the mechanism(s) have so far proved elusive.

1.1.5 Activation of mitotane

The specificity of mitotane for adrenocortical tissue may derive from metabolic transformation of the drug to an active product via an enzyme system that is unique to this tissue. It was established early that extensive transformation of radiolabelled mitotane occurs *in vivo*, and these products undergo covalent binding, with good correlation between rates of transformation and binding and bioactivity across species (Martz and Straw 1977). Evidence that supports unchanged mitotane not being the effective agent is the lack of a direct effect on fresh adrenal homogenates described above (Touitou, Bogdan, and Luton 1978). Addition of mitotane to a cytochrome P450 fraction from bovine adrenals gave rise to a light absorption difference spectrum similar to that caused by steroid binding (Young et al. 1973). Formation of adducts with electrophoretic mobility corresponding to P450scc, but not adrenodoxin, in canine, bovine and human adrenocortical homogenates has been demonstrated (Cai et al., 1997). Mitotane metabolism and covalent binding are closely correlated across species (Martz and Straw 1980).

Comparison of activity of mitotane analogues on Fang-8 cells (derived from a feminising ACC) has shown a common requirement for a dichloro- or trichlorethylene structure (Fang 1979). The essential dichloromethyl moiety undergoes P450-catalysed hydroxylation followed by rapid dechlorination to generate an acyl chloride (Figure 1).

The generation of the acyl chloride almost certainly is mediated by a mitochondrial cytochrome P450 (Poli et al. 2013), which does not seem to be CYP11B1, since mitotane shows equal toxicity towards the ACC cell lines expressing (H295R) and not expressing (SW13) this enzyme (Hescot et al. 2013). However, transfection of the gene for CYP11B1, but not for CYP11A1 or CYP11B2, into monkey kidney COS cells caused them to take up a mitotane analogue and generate metabolites (Lund and Lund 1995). Other evidence against CYP11B1 is that it not subject to competition by the specific inhibitors etomidate and metyrapone. The less specific agent ketoconazole, which inhibits among others CYP11A1, CYP17 and CYP11B2, is a competitor, pointing to an

Introduction

alternative mitochondrial P450, possibly active in xenobiotic metabolism in the adrenal cortex (Schteingart 2000) (Veytsman, Nieman, and Fojo 2009).
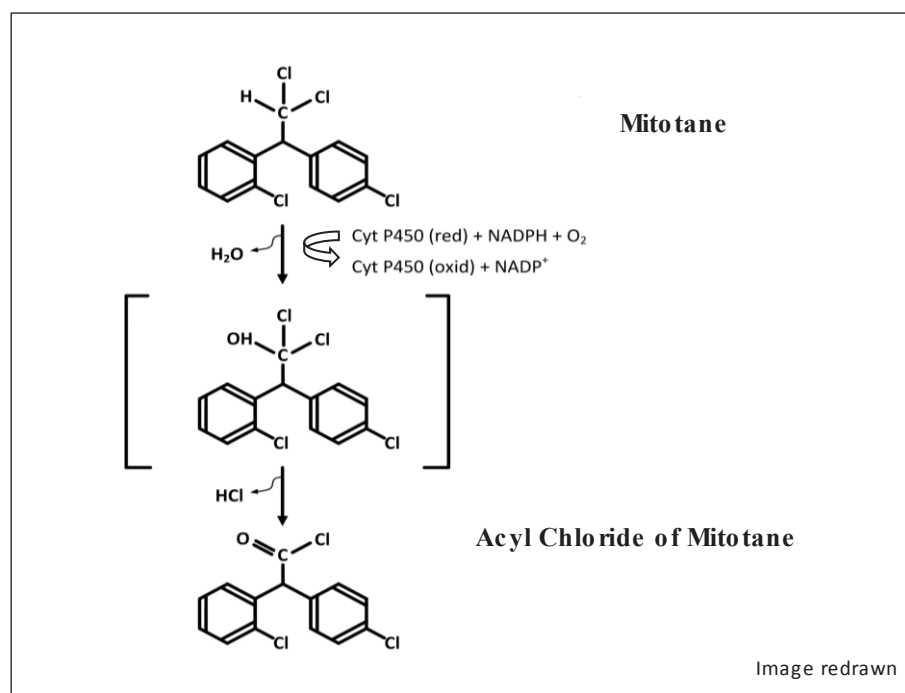
Figure 1. Mitotane transformation to an active form (adapted from Nelson & Woodard (1949), also presented in Waszut et al.(2017)).

Binding between mitotane and a cytochrome P450 has been directly observed using an antibody to CYP11A1. This offered a plausible candidate, given that it mediates a metabolic transformation inhibited by mitotane (below), but this was not competed for by its substrate, cholesterol, nor the CYP11A1 inhibitor, aminoglutethimide (Cai, Benitez, et al. 1995). Another candidate is CYP2W1. This is highly expressed in fetal life and in some cancers, most notably colon cancer, and whilst a clear physiological role has not been established, it shows catalytic activity towards a range of substrates including some procarcinogens. Ronchi et al (2014) reported CYP2W1 immunoreactivity in normal and malignant adrenocortical tissue, with increased expression in steroid-secreting compared with non steroid-secreting tumours and a modest positive effect of immunoreactivity on disease progression and survival time during mitotane treatment. However, Nole et al (2016), using an antibody claimed to be more specific for CYP2W1, did not find expression in either normal adrenocortical tissue or in adrenocortical tumours (Ronchi et al. 2014) (Nolé et al. 2016).

The acyl chloride is a highly reactive molecule, which can bind to particular binucleophiles in target cells to bring about an adrenolytic effect, or via induced oxygen

activation. Although not conclusively proven, metabolic transformation and oxidative damage through production of free radicals are generally accepted as the mechanisms that mediate this drug cytotoxicity, with some transformation occurring in the tumour (Veytsman, Nieman, and Fojo 2009). Most of the binding is to proteins, with one sixth to phospholipids. (Cai, Counsell, et al., 1995), (Hong, for Cancer Research, and Hait 2010). Addition of water otherwise gives rise to the acetic acid derivative o,p'DDA, which is extensively excreted in urine and has recently been shown to be inactive, with no useful antitumour properties in adrenal cells, being unable to activate oxidative stress and apoptosis in H295R cells, nor cause down-regulation of the genes involved in steroidogenesis that had been previously described by these authors (Hescot et al. 2014), (Waszut, Szyszka, and Dworakowska 2017).

1.1.6 Proteins involved in response to mitotane

Mitotane and its active metabolites produce irreversibly bound protein adducts on incubation with H295R cells (Asp et al. 2010). Modulation of the proteome in the H295R cell line seems to most closely relate to processes of stress response and energy metabolism (Schteingart et al. 1993). Important further insights have been provided by studies using these cells by Stigliano *et al.* (Stigliano et al. 2008) who used two-dimensional electrophoresis and MALDI-TOF to identify proteins that undergo change. These included proteins involved in energy metabolism, stress response, cytoskeletal structure and tumourigenesis. Sampling at 15 min, 1, 5, 24 and 48 h after mitotane exposure showed both increased and decreased expression, with opposite changes at different time points for some proteins.

Proteins modulated by mitotane included those involved in energy metabolism such as: D-3 phosphoglycerate dehydrogenase isoforms, and nucleotide diphosphate kinase (which play a role in cholesterol trafficking to the inner mitochondrial membrane) and the glycolytic enzymes triose phosphate isomerase and enolase. Proteins involved in stress response include peroxiredoxins 2 and 6 (with antioxidant functions), heat shock proteins B1 (HSP 27) and the 70 kDa protein 1A, together with heat shock cognate 71 kDa protein. These stress response proteins play roles in protection of cells against oxidative stress and cytotoxic effects and possibly conferring drug resistance. The next group of proteins affected by mitotane is related to the cytoskeleton and comprises

profilin, which is involved in actin filament polymerization, and tubulin, which is an intrinsic component of mitochondrial membranes. This mitotane effect would interfere with mitochondrial membrane permeability and thus cholesterol trafficking (Stigliano et al. 2008).

Proteins modulated by mitotane that are involved in tumourigenesis play roles in growth, ageing, transcription and RNA splicing. This may be effective in reversing the changes to cell function that permit the growth of an ACC. Histidine triad nucleotide binding protein (Hint) is a hydrolytic enzyme that may function as a tumour suppressor, being involved in apoptosis by inhibition of TCF-β-catenin-mediated transcription, an activity that is constitutive in H295R cells. The prohibitin (PHB) protein level was initially diminished and then increased. Consistent overexpression of its isoforms PHB1p and PHB2p has been observed in neoplastic tissue from a wide range of anatomical sites. Although PHB proteins were originally considered to be putative negative regulators of the cell cycle, recent studies indicate that they act as chaperones in the assembly of subunits of mitochondrial respiratory chain complexes, binding directly to newly synthesised mitochondrial translation products and stabilising them against degradation. They may also play roles as structural scaffolds. Their overexpression in tumours may lead to reduction of oxidative stress and tumour insensitivity to this condition (Nijtmans et al. 2002). Diminution of PHB expression by mitotane again suggests that mitochondrial injury and oxidative damage are the main sites of mitotane action. There was a decrease of heterogeneous nuclear ribonucleoprotein (hnRNP) isoforms A2/B1, proteins acting as multifunctional transcription and translation factors in human adrenal tissue. Importantly, B1 expression is boosted in various adrenal hormone- secreting tumours, with a negative correlation between B1 expression and steroidogenesis. Increase of cathepsin D is also a significant factor, which is activated by hnRNP (Stigliano et al. 2008).

1.1.7 Mitochondrial effects

Mitochondria are the structures within the adrenal cells that are primarily responsible for mitotane susceptibility, The primary effect may be induction of mitochondrial degeneration, resulting in adrenal atrophy, although a direct effect on mitochondrial stability has not been clearly shown. Possible alternative modes of its action remain

Introduction

unclear (Feng et al. 2014), (Martz and Straw 1977), although covalent binding of macromolecules, including proteins, is regarded as being the main factor in mitochondrial degeneration (Cai, Benitez, et al., 1995). This has been suggested to be via a dose-related cellular toxic effect, causing rupture of mitochondrial membranes (Stigliano et al. 2008).

In a study by Hescot *et al.*, (2013) drastic morphological alterations in ACC cell line mitochondria were brought about by treatment with 50 μM mitotane. The interconnected filamentous tubular network displayed a punctiform pattern when the morphology was analysed by immunocytochemistry, indicating mitochondrial fragmentation. Changes also include marked swelling and refraction of cristae and appearance of electron-dense myelin-like remnants of the inner mitochondrial membranes, followed by vacuolation of cytoplasm after a longer duration of exposure (Poli et al. 2013). These changes are not seen in the zona glomerulosa.

Mitochondrial P450 systems employ adrenal ferredoxin (first found in steroidogenic tissues), also called ferredoxin-1, to transfer electrons from NADPH to CYP P450. This initially suggested a source of mitotane specificity, but this same ferredoxin has also been detected in mitochondria of a number of other tissues including the testes, ovaries, placenta, kidney, liver and brain, with all taking part in P450-dependent hydroxylation reactions (Redick et al. 1977). Specificity may instead lie with a particular P450, perhaps an as yet unknown nonsteroidogenic enzyme that is unique to adrenocortical mitochondria, since since there is no firm proof for any of the known forms (Section 1.1.15). Mitochondrial hydroxylations are known to be associated with generation of reactive oxygen species (ROS) so that the process of activation of mitotane might itself be contributory to mitochondrial damage (Germano 2010), (Kufe et al. 2010).

To offer an additional viewpoint to that described above, there may be characteristics contributing to mitotane sensitivity that are common to steroidogenic tissues rather than being unique to adrenal tissue. There are features of mitochondrial ultrastructure, such as presence of lamellae and a tubular association of the cristae (figure 2), that are common to adrenal and gonadal tissue (Vafai and Mootha 2012), (Prince 2002).

In sum, specificity of mitotane for adrenocortical tissue and a targeting of the mitochondria most plausibly depends upon a unique activation taking place within zona fasciculata and reticularis tissues. Mitotane does also diminish gonadal androgen synthesis and so might contribute to activation in this tissue, while activation elsewhere, such as in the liver, is unlikely be significant. A toxic intra-adrenal product could be retained or further transformed in lipid-rich cellular components, since these compounds

are lipophilic, and so may not be detectable in blood. The absence of activity among known mitotane metabolites should thus not be regarded as evidence against this proposed mechanism. Since the effects of mitotane on the respiratory chain complexes appear to be confined to inhibition of complexes I and IV, this may not be a point at which mitotane acts (Hescot et al. 2013).

Image redrawn and modified
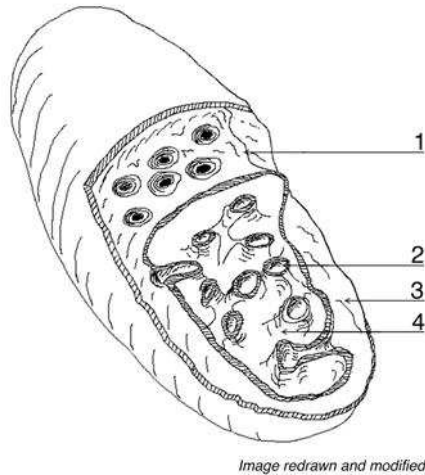
Figure 2 *Mitochondria with tubular cristae characteristic of steroidogenic tissue. Matrix and the outer membrane surround the organelle. Internal features are: inner membrane (1), tubular cristae (2), intracristal space (3), matrix (4) (adapted from* Freya and Mannellab (2000)*, (Ovalle and Nahirney 2013)* also presented in *Waszut, Szyszka, and Dworakowska (2017)).*

1.1.8 Mitotane effects on mitochondria that may lead to apoptosis

Apoptosis, or programmed cell death, is an orderly process of cell removal that results in generation of cell fragments that can undergo phagocytosis. This contrasts with necrosis, which is an unplanned cell death caused by acute cell damage due to factors such as exposure to poison or traumatic injury. It may result from anoxia via disruption of the blood supply or another cause. Necrotic cells can cause further damage, such as by triggering immune responses. Overabundant apoptosis also causes tissue atrophy.

There are several routes of apoptosis, with different elements of a cascade being involved (Figure 3). Two major pathways may be distinguished: the *extrinsic* pathway, which starts through activation of pro-apoptotic receptors on the cell surface by molecules known as *proapoptotic ligands* (Alberts et al. 2002) and the *intrinsic* pathway, also called the *mitochondrial* pathway, which is initiated from within the cell. This is activated in reply to signals resulting from DNA damage, loss of cell-survival factors, or other cell

stress, such as toxins, so mitotane may have an action via this entire pathway, but there is also ample evidence for direct actions of mitotane on the mitochondria.
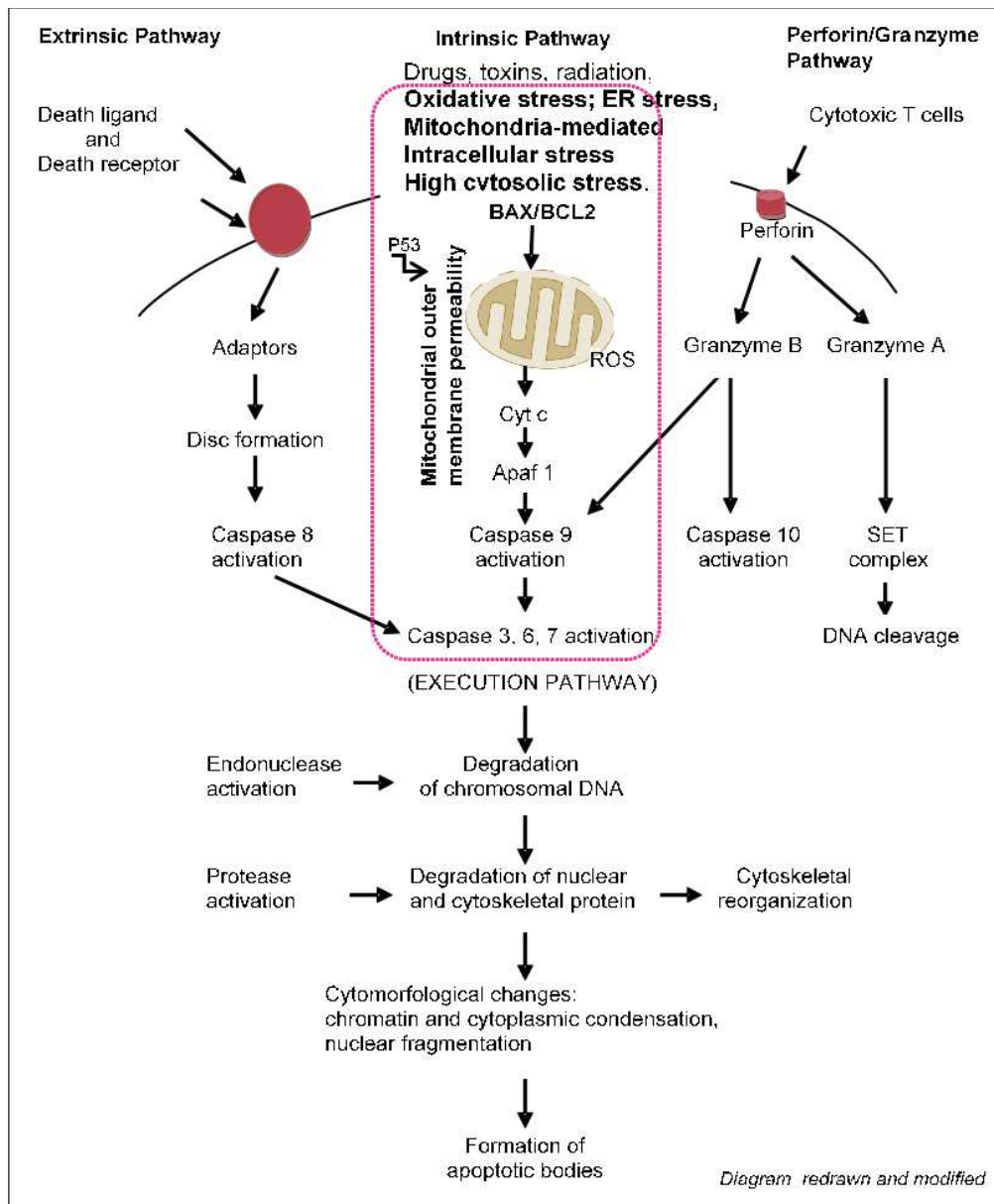
Figure 3 *Major apoptotic pathways (redrawn from Bali et al. (2013), with additions from Ashkenazi, 2008 and Beesoo et al. (2008),.* ***The mitochondrial pathway that is initially induced by mitotane is outlined.***

The core of this pathway involves activation of BAX and BAK within the mitochondrial membrane, causing opening of megachannels (permeability transition pores) via association of the pore protein mt-PTP with the proapoptotic protein BAX. This results in dissipation of the transmembrane potential, increase of ROS (Ricci, Gottlieb, & Green, 2003) efflux of cyt c and collapse of ATP generation.

Introduction

The cyt c associates with the adaptor Apaf-1 to recruit procaspase 9 to form the apoptosome. In the presence of ATP, caspase-9 is activated. This in turn activates effector (executioner) caspase 3, 6 and 7, which leads to the degradation of cell components (Ashkenazi, 2008).

High-energy ATP or other phosphates can contribute to apoptosis induction. Interestingly, when all mitochondria in cells are ruptured after cyt c release and caspase activation, this results in necrosis, but when some mitochondria are functional and produce enough ATP, apoptotic cell death occurs (Whelan and Zuckerbraun 2013).

The Figure 4 summarises the major factors described that enhance mitochondrial membrane permeability.
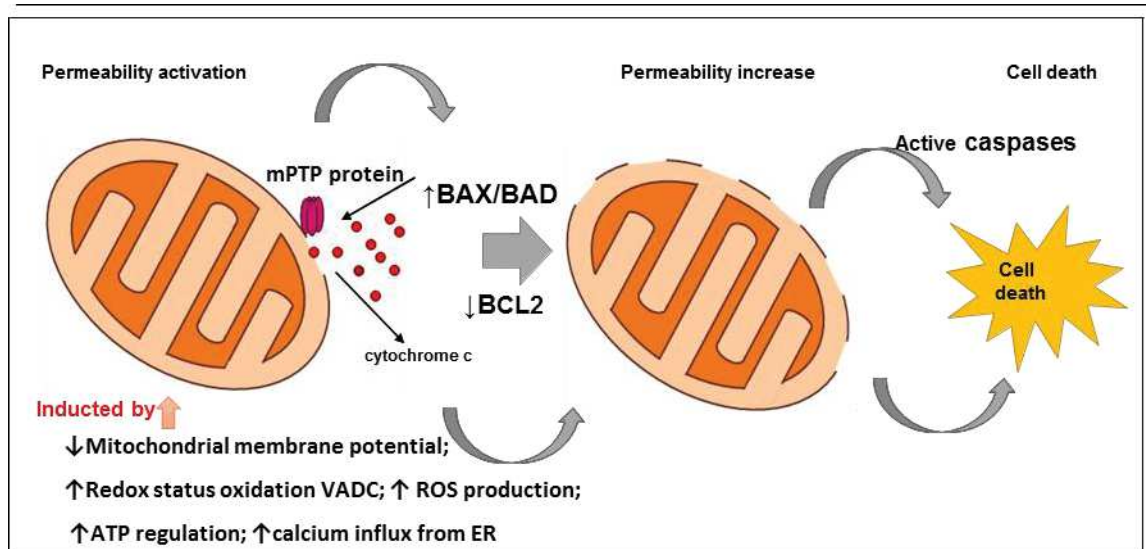
Figure 4 *Mitochondrial membrane permability pore induction.*

Promotion of apoptosis and cell death by mitotane has been shown in H295R and SW13 cells by Poli *et al*., (2013), using cytofluorimentric separation, with increase of both apoptotic live and apoptotic dead cells, detected by tagging for caspase 3/7 activity, within the range 30–50 µM mitotane, accompanied by loss of membrane potential and a sharp reduction in oxygen consumption. These events coincided with damage to the mitochondrial cristae. Lehman, Wrzesiński & Jagodziński (2012) directly demonstrated increase of caspase 3/7 activity in the medium of H295R cells exposed to 62.5 & 100 µM mitotane.

Considering possible mechanisms by which mitotane promotes apoptosis in adrenocortical cells, one component of the intrinsic pathway, the tumour suppressor p53, which is stabilised by c-Myc, appears not to be involved, since mRNA expression levels

27

for c-Myc are unchanged by mitotane in H295R cells (Lehmann, Wrzesinski, and Jagodzinski 2013). Additionally, c-Myc is a characteristic coordinator for the S phase of the cell cycle, whereas mitotane treatment has been shown to delay the G2 phase (Cerquetti et al. 2008), alhough, at the G2/M checkpoint, p53 blocks cyclin-dependent kinase and the cyclin B complex, by inducing GADD45, p21, and 14-3-3 sigma protein. Cells arrested at this point are in the G2 phase (Jackson et al. 2005). Comparison of the effects of ionizing radiation, mitotane and their combination on the cell cycle in H295R and SW13 cell lines showed an inhibition of cell growth in both cell types by radiation with and without mitotane. Cells recovered spontaneously after radiation alone but remained arrested in the G2 phase after combination treatment. In the latter, cyclin B1 in the form of a complex with Cdc2 proteins was increased, as was Cdk2 kinase activity. Sequence analysis of p53 showed a large deletion of exons 8 and 9. The same arrest by combination therapy occurred in H295R cells with restored wild-type p53, suggesting that this mechanism is not mediated by the p53, c-Myc pathway (Cerquetti et al. 2008). (Waszut, Szyszka, and Dworakowska 2017)

1.1.9 Calcium signalling at the MAM, a crucial apoptosis trigger

Antiapoptotic members of the Bcl-2 family of proteins downregulate calcium flux through the plasma membrane and limit calcium transfer to mitochondria. Transmission is likely to take place at close points of contact between the ER and mitochondria, which can be fractionated as mitochondrial-associated membranes (MAM). This is one of the most important factors triggering apoptosis (Alberts et al. 2002). The MAM has specific characteristics in adrenocortical tissue, since steroid synthesis requires coordination of activity between mitochondrial and ER enzymes (reviewed by Doghman-Bouguerra & Lalli, 2017) and these might make it vulnerable to mitotane effects, as detailed below. Calcium flux at the MAM appears to be a critical control point for signalling between ER and mitochondria. This interaction can provide opportunities for cancers to limit apoptosis by diminishing passage and one at which mitotane can act to promote calcium influx and thus apoptosis. The cancer-testis antigen FATE1 is localised to the MAM and decreases calcium flux by widening the ER-mitochondrial distance and is overexpressed in some cancers. Doghman-Boughuerra (2016) developed H295/TR SF-1 cells, in which overexpression of SF-1 was deoxycycline dependent and was found to induce high

FATE1 expression. Using this model, they demonstrated a decreased apoptoptotic response to mitotane, but when FATE1 was knocked down, it was increased. Patients with adrenocortical tumours and receiving mitotane who had relatively high tumour expression of FATE1 had worse outcomes than those in whom it was low (Doghman-Bouguerra et al. 2016). Another factor regulating calcium flux at the MAM is the thioredoxin TMX1, offering another potential drug target (Krols, Bultynck, and Janssens 2016); (Waszut, Szyszka, and Dworakowska 2017).

Lipid signalling is also critical to MAM function. Drugs designed to inhibit esterification of cholesterol by sterol-O-acyl transferase 1 (SOAT1) were found to be toxic towards adrenocortical tissue. The SOAT inhibitor ATR-101 has been shown to activate a caspase response in H295 cells concomitant with increase of free cholesterol and ER stress responses (LaPensee et al. 2016). Mitotane has recently been shown to also inhibit this enzyme and mimic many of the drug actions on signalling systems that enhance apoptosis. In a very comprehensive series of studies in H295 cells, Sbiera et al (2016) (Sbiera et al. 2015) have directly shown mitotane inhibition of this enzyme and an association with increase of free cholesterol and numerous other lipids, while genes involved in lipid metabolism and steroidogenesis were downregulated. Many genes associated with ER stress were upregulated, including CHOP activated by eIF2A, important elements of the signalling cascade that results in calcium loading of the mitochondria and triggers proapoptotic mitochondrial Bax and suppresses antiapoptotic Bcl-2. These effects were not seen in other cell types, which the authors ascribed to lower baseline expression of SOAT1 (Sbiera et al. 2015), (Waszut, Szyszka, and Dworakowska 2017).

1.1.10 Effects of mitotane on cellular biochemistry and steroidogenesis.

Appendix C shows the pathways of steroidogenesis in the human. Inhibition of cholesterol side chain cleavage and 11-hydroxylation are the most consistent findings. Mitotane results in loss of activity of the steps in the steroidogenic pathways that are mitochondrial, i.e.: StAR synthesis, CYP11A1, CYP11B1 and CYP11B2. In contrast, the steps catalysed by microsomal enzymes have not been conclusively shown to be affected.

Some gene expression analyses using qPCR have supported previous microarray findings that mitotane does not induce under-expression of the genes coding for the

enzymes above, but does suppress other genes, including those coding for the steroidogenic enzymes HSD3B1, HSD3B2 and CYP21A2 (Asp et al. 2010), (A Zsippai et al. 2012). However, Lehmann *et al.* (2012) observed decrease of mRNA for CYP11A1 and CYP17A. These findings have offered the possibility that the observed steroid inhibitory effects are not only mediated by inhibition of CYP11s or by adrenolytic activity but by a direct effect on levels of other steroidogenic enzymes (A Zsippai et al. 2012).

An alternative basis of 'inhibition' of 11β-hydroxylase CYP11B1 and of cholesterol to pregnenolone conversion involving StAR protein might be via deleterious effects on the mitochondria rather than on gene expression or by direct competitive inhibition. Mitotane action is not attenuated by the specific 11-hydroxylase blocking agents metyrapone and, etomidate, providing evidence against direct inhibition.

An alternative mode of mitotane action may be by mimicking steroids via binding to steroid receptors or duplicating their non-genomic effects (see section 5.2). As small organic diphenolic compounds, they share features with other well-known endocrine disruptors, including natural compounds such as lignans and equol and synthetic mimics, such as diethylstilbestrol.

1.2. Mitochondria as semiautonomic structures with major roles in energy metabolism and apoptosis.

The mitochondria are responsible for efficient energy accumulation and management within the organism and thus have intimate connections with most biosynthetic pathways. The process of oxidative phosphorylation produces cellular energy, regulates mitochondrial and cellular redox status, generates most of the ROS and regulates Ca^{2+} concentration (Hebe, Blackburn, and Miller 2011). The oxidative phosphorylation chain is further described in the Section 1.3.

Mitochondria on the one hand influence nuclear gene expression via messaging systems termed *retrograde mitochondrial signalling* and on the other, require a nuclear contribution to produce most of their structural and functional protein, since most of the required genes are located in nuclear DNA, comprising those responsible for mitochondrial structural elements, those for glycolysis and most of the genes for oxidative metabolism. They also include genes for the transcriptional machinery needed for expression of the mitochondrial genome as well as those required for nuclear genes

Introduction

(Whelan and Zuckerbraun 2013). Proteins that are coded for by nuclear genes that are destined for the mitochondria are tagged with a presequence that is a 20- 35-mer peptide. They are maintained in an unfolded state by chaperone proteins to enable passage across the mitochondrial membranes (Coope and Hausman 2006). The normal circular human mitochondrial genome, or mitochondrial DNA (mtDNA) encodes the structural genes for 12S and 16S ribosomal rRNAs, some subunits of NADH-coenzyme Q oxidoreductase, cyt c oxidase, cyt b, ATP synthase, and 22 tRNAs. Transcription takes place from both of the complementary strands, termed *heavy* (H, guanine-rich) and *light,* (L, cytosine-rich). Synthesis of mRNA starts from three promotors: two H promotors, *heavy strand promotors 1 & 2* (HSP 1 & HSP 2) and one L — *light strand promotor*, LSP (Figure 5).
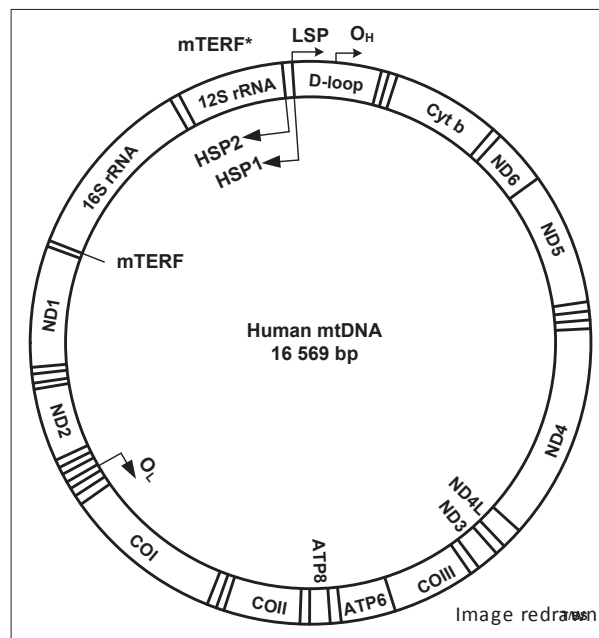
Figure 5. Gene sequences within mitochondrial circular DNA (taken from Asin-Cayuela & Gustafsson (2007)).

The mitochondrion needs to synthesise enough rRNA to fulfil the simultaneous translation requirements of the 13 mRNAs within the polycistronic transcripts. This is the reason that transcription takes place in two versions — besides synthesis of the full length polycistronic H2 strand transcript, promoted by HSP 2, which covers almost all the length of the heavy strand, a shorter transcript, H1, promoted by HSP 1, ends at the 16S rRNA, and is transcribed at 20 times the level of H2. This ensures that a sufficient amount of 12S and 16S rRNA is available for protein translation. The shorter H1, with well-defined start and stop sites, requires association with mTERF to enable early termination.

Introduction

These promotors are found in the mtDNA non-coding region and recruit mitochondrial RNA polymerase to drive this transcription, leading to the production of three polycistronic transcription units. Transcription from the H-strand results in an RNA unit that is processed into two mt-rRNAs, fourteen mt-tRNAs and mt-mRNAs that encode twelve proteins. Transcription of the L-strand produces RNA that is cleaved to produce eight mt-tRNAs and only one mt-mRNA that encodes a single protein. Full polycistronic transcription from the L strand has never been observed under experimental conditions (Temperley et al. 2010). These initial polycistronic precursors are next cleaved by endogenous nucleases at the 5' and 3'ends. The process of 'tRNA editing' is possible thanks to the tRNA sequence between rRNA and mRNA having a cloverleaf structure that is recognised by the enzyme processing the primary transcript. The mRNA and rRNA became polyadenylated by mitochondrial polymerase, which stabilises their structure and is needed to create a stop codon (Schapira and Dimauro 1994), (Asin-Cayuela and Gustafsson 2007), (Temperley et al. 2010). Figure 6 presents the mitochondrial genome translation mechanism.

Nuclear DNA gene expression is also controlled epigenetically, meaning that it is sensitive to the environment. The processes of gene expression are compound-dependent, controlled by a set of nuclear-encoded transcription factors. For example, nuclear respiratory factor 1, NRF-1, has specific binding sites in the promotors of the genes for the electron transport chain and cyt c. Further, these nuclear factors are coordinated by coactivators, some of the family members of which provide a link between the products of mitochondrial function or malfunction and subsequent adjustments of nuclear gene expression. Mitochondrial dysfunction is often found to correlate with alterations in nuclear gene expression. Further, there are other crucial factors that control nuclear gene expression, such as the ATP/ADP concentration: each mitochondrial promotor has been shown to have a unique sensitivity to the mitochondrial ATP level (Whelan and Zuckerbraun 2013).

Mitochondria have been called 'fundamental arbiters of life and death of the cell'. It has been shown that pathways of intermediary metabolism involved in energy capture are important components and regulators of mitochondria-linked events of cell death and survival. These may involve interaction of signalling molecules with the mitochondrial membrane. Several chemotherapeutic agents have been shown to act on targets in the respiratory chain (Cerquetti et al. 2008).

> This diagram reflects a linear view of the genetic map of the heavy (H) and light (L) strands of human mtDNA. The long horizontal arrows indicate precursor polycistronic transcripts, while short vertical lines indicate the locations of tRNA genes and the vertical arrows indicate the processing sites where precursors are punctuated by antisense tRNAs or are not punctuated by tRNAs. Black and white blocks represent mature transcripts for H- and L-strands, respectively. Asterisks denote the protein coding transcripts that require the addition of the poly (A) tail to generate a stop codon.

Figure 6. *Gene expression in human mitochondria. (Taken from Zeviani et al. (2015)).*

The mitochondrial permeability transition pore can be activated by factors which include a decreased membrane potential, with predominant role of ROS. The important mechanism of apoptosis involving mitochondrial membrane permeabilization and cyt c release has been described in the Section 1.1.8 and 1.1.9 when increased Ca^{2+} transmition plays a crucial role.

ROS are products of oxidative phosphorylation. Mitochondrial stress has been shown to result in excess production of ROS, and thay may contribute to cyt c release. ROS have also been found to be important second messengers for mitochondrial communication in both physiological and pathological circumstances. For example, expansion of ROS production can be an important second messenger in inducing factors such as nuclear erythroid-derived factors (Nrfs) that transfer to the nucleus and stimulate antioxidant response elements. ROS production induces conformation change of Keap1 protein, activating Nrf2 which transfers to the nucleus to stimulate antioxidant response elements, leading to enhanced mitochondrial biogenesis for inducing factors such as NRF-1. The NRF-1 with Nrf2, mediates the genomic coordination between nuclear and mitochondrial

genomes, and indirectly regulating the three mitochondrial-encoded COX subunit (Whelan and Zuckerbraun 2013). If oxygen species overwhelm the protective capacity of antioxidants, enhanced lipid peroxidation leads to increased permeability and progression to programmed cell death.

1.3 Cell lines used in the experiments

This section presents characterisation and data describing morphology and energy metabolism of the cell lines used in studies.

H295R — The human adrenocortical carcinoma-derived H295R cell line, which expresses most of the important steroidogenic enzymes, was developed and validated to measure the expression of 10 genes involved in steroidogenesis. It has been used as a sensitive and integrative screen for the many effects of chemical agents on steroidogenesis (Hilscherova et al. 2004), (Gazdar et al. 1990). It was developed from an adrenocortical carcinoma in a 48-year-old black female who presented with weight loss, acne, facial hirsutism, oedema and diarrhoea. The tumour was first visualised using computer tomography in 1980. The excised tumour was $14 \times 13 \times 11$ cm. More than 30 secreted steroids have been identified by gas chromatography, mass spectroscopy and radioimmunoassay. These cells appear to contain all of the adrenocortical enzyme systems that presumably were present in the original tumour, including CYP11A, HSD3B2, CYP11B1, CYP21, CYP17, CYP11B2, 3-hydroxysteroid sulfotransferase, and a low level of aromatase (CYP19). The original strain, first designated NCL-H295, has been grown under various conditions to promote fast growth and retention of steroidogenic characteristics. Growth over 3 months in specially supplemented medium caused the cells to transform from forming floating aggregates or loosely attached cells to a tightly adherent monolayer. The population doubling time was reduced from five to two days. The adapted strain of this line was named H295R (Rainey, Saner, and Schimmer 2004).

Hke-3 Cell line — Ras genes encode small GTP-binding proteins with ability to strongly influence gene expression, acting as major switches in the signal transduction processes. Mutated Ki-ras is one of the most frequent genetic events in human cancer. Point mutations that activate the Ki-ras proto-oncogene are present in about 50% of human colorectal tumours, which then play a key role in colorectal tumourigenesis

through altered cell differentiation and cell growth (Escandell et al. 2008). A colorectal cancer cell line which differed only by the presence of an activated Ki-ras allele was called HCT-116, whereas Hke-3 was derived from HCT-116 by deletion of the activated mutant Ki-ras allele. Compared with parental cells, Hke-3 was described as morphologically altered. It had lost the capacity for anchorage-independent growth, grew more slowly both *in vitro* and in nude mice, and showed reduced expression of c-Myc (Shirasawa *et al.*, 1993).

It was observed that oncogenic Ki-ras mutations correlated in particular with alterations in an energy metabolism, including increase of glucose and glutamine consumption, lactic acid accumulation, changed expression of mitochondrial genes, and reduction of mitochondrial activity (Gaglio et al. 2011).

Mitotane appears to require transformation into active metabolites for therapeutic action, which is connected with mitochondrial P450-mediated hydroxylation (described in Section 1.1.5). The observed susceptibility of this cell line in response to mitotane might thus be connected with Ki-ras disruption. Since a well-known side effect of mitotane is gastroenterological disturbance, what might reflect its greater sensitivity of the Hke-3 cell line to mitotane.

H1975 is a cell line derived from a lung carcinoma, popularly called non-small-cell lung cancer. It is an adherent cell line with a mutation in the epidermal growth factor receptor (EGFR) (Zhao et al. 2015).The process of tumourigenesis often involves a shift in key regulatory steps of energy metabolism, in which cancer cells become highly dependent on glycolysis rather than oxidative phosphorylation. As described above (in section 1.1.2). This may result from different oncogenic signaling pathways. Aberrant signaling from the EGFR though the PI3K/AKT pathway, in particular, was found to change gene expression connected with glycolytic transporters and enzymes. In non-small cell lung cancer, a mutated EGFR is a crucial oncogenesis driver. Mutation in the kinase domain of EGFR enhances EGFR tyrosine kinase activity, with downstream signaling causing tumour progression. H1975 cells bear an activation point mutation in exon 21(L858R) of EGFR and a T790M mutation in tyrosine kinase of EGFR. The T790M mutation makes this cell line resistant to erlotnib – an inhibitor of the EGFR receptor via binding to the intracellular portion, in contrast to responsive HCC827 cells, another non-small lung cell line.(De Rosa et al. 2015). Their findings indicate that normal inhibition of cell proliferation via EGFR pathway involve mitochondrial reactive oxidative phosphorylation.

35

The "Reverse Warburg Effect"

(a)

Stromal fibroblasts   Cancer cells

ROS

HIF1α ⟷ NFκB

Autofagy/ Mitofagy

Aerobic gycolysis & Recycled nutrients (lactate, ketones, glutimine & others)

Protection against apoptosis (cell death)

Oxidative mitochondrial metabolism

(b)

Fibroblasts   MCF7

Co-Culture

(a) Via oxidative stress, cancer cells activate two major transcription factors in adjacent stromal fibroblasts (HIF1α and NFκB). This leads to the onset of both autophagy and mitophagy, as well as aerobic glycolysis, which then produces recycled nutrients (such as lactate, ketones, and glutamine). These high-energy chemical building blocks can then be transferred and used as fuel in the tricarboxylic acid cycle (TCA) in adjacent cancer cells. The outcome is high ATP production in cancer cells, and protection against cell death.

(b) Homotypic cultures (upper panels) of MCF-7 cells (right) and hTERT-fibroblasts (left) were immunostained with a mitochondrial membrane antibody (red). Note that mitochondrial mass is lower in monocultures of MCF-7 cells compared to fibroblasts. However, co-culture of MCF-7 cells with fibroblasts (lower panel) induces a dramatic increase in mitochondrial mass in the 'central MCF-7 cell colony.

Image redrawn

Figure 7. *Demonstration of the reverse Warburg effect using MCF-7 cells (taken from Sotgia et al. (2011)).*

MCF-7 — is a cell line that was first isolated in 1970 from the breast adenocarcinoma of a 69-year old Caucasian woman. It has ideal characteristics particular to the mammary epithelium, possessing oestrogen receptors (ER) and the ability to covert oestrone to oestradiol (Horwitz, Costlow, and McGuire 1975). These cells has been used to demonstrate that oestrogenic organochlorine pesticides, including o,p'-DDT, mimic the endogenous oestrogen, estradiol-17β and suppress apoptosis (Burow et al. 1999).

MCF-7 has been used to study the reverse Warburg effect (Figure 7). Co-culture with fibroblasts, which more closely mirrors the microenvironment of a naturally occurring tumour, promotes a very significant increase in mitochondrial mass. In contrast, when

cultured under homotypic conditions, the cells have a very low mitochondrial mass, which characterises the conventional Warburg effect (Sotgia et al. 2011).

Since homotopic culture was used in the current study, it could be that the strongest relative unresponsiveness after mitotane treatment, on energy metabolisms level, is partly caused by the described lack of mitochondria

1.4 Heterogeneity in context of ACC study and gene expression study from formalin-fixed, paraffin-embedded adrenocortical carcinoma tissue

ACC is rare, accounting for 2–11% of adrenal masses. It is highly aggressive, causing approximately 0.2% of all cancer deaths in the US, with a mean survival time of only months. The molecular pathology of malignancy is currently poorly understood. ACC has been thought not to evolve from adenomas. For these rarely observed cancers, long-term follow up data suggest that mutations can arise in signalling pathways (Allolio and Fassnacht 2006), (Kassi et al. 2010).

Comparison of gene expression in benign versus malignant adrenal tumours and in malignant tumours that are aggressive versus those that are more quiescent shows that differentiation is readily achieved, with genes for IGFs and WINT QT and B-catenin signalling pathways to the fore (reviewed by (Fonseca et al. 2012), and (Assié, Jouinot, and Bertherat 2014). Changes in cell-cycle checkpoints are also important (Szabo et al. 2010). These differences may have prognostic value and thus guide personalised management. For example, the best predictor of malignancy and overall survival in one study was the combined expression of BUB1B and PINK1, which significantly correlated with MacFarlane staging (de Fraipont et al. 2005). None of these studies on large numbers of specimens, which were flash frozen in most cases, have attempted to differentiate different portions of the tumour, even though a cardinal feature is a high degree of heterogeneity at both gross and microscopic levels.

The H295R cell line, as a cultured model of ACC tumours, cannot reflect all features of malignant tumours, especially their heterogeneity, which is found between patients as well as within regions of the single tumour mass. It is therefore important to study material derived directly from patients, to enable development of understanding of the

altered signalling pathways or mechanisms of proliferation *in vivo* and also changes that take place in response to treatment by drugs such as mitotane.

Mechanisms that determine the processes of cellular differentiation and positioning are beginning to be understood (Pignatti et al. 2017). The normal adult adrenal cortex is organized into concentric zones of *zona glomulosa* and *zona fasiculata and zona reticularis*, each specialized to produce distinct steroid hormones. In adrenocortical carcinomas, arrangement of the tissue appears chaotic, so these processes of control are probably disrupted. A single report of gene expression in different portions of tumour that were considered histologically malignant and non-malignant (Bernard et al. 2003) led to the conclusion that malignant tissue might evolve from non-malignant tissue. Gene expression analysis has been used to identify the patterns associated with normal histological differentiation. Similarly, (Azizan et al. 2012) found different gene expression patterns in zoma glomerulosa-like and zona fasiculata like portions of aldosterone-producing adenomas.

Material from patients is usually stored as FFPE blocks. It would therefore enable the largest number of patients to be studied if RNA and DNA of adequate quality could be isolated. Since the material is solid, direct comparison of histology and gene expression is theoretically possible. The only retrieved published study of FFPE from ACC patients (Lombardi et al. 2006) did not differentiate portions of the tumours and showed a poor success rate, with only 4 of 14 blocks producing useable material. If extraction and amplification methods could be sufficiently improved, then a much more comprehensive picture of the disruption of control pathways that lead to tumour development might emerge and also enable better management of individual tumours.

II. Aims of the study

1. To examine expression levels of a panel of 84 genes involved in mitochondrial energy metabolism between human adrenocortical (H295R), breast (MCF-7), colon (HKe-3) and lung (H195R) cell lines under basal conditions and after exposure to the adrenolytic agent mitotane.

2 To calculate changes in gene expression using the d/dCT method and thus compare the impact of mitotane exposure on adrenal-derived cells in comparison with the other cell lines.

3.To consider whether changes that are specific to the adrenals or take place in adrenals at lower drug concentrations can explain the adrenolytic action of mitotane via actions on energy metabolism that might lead to initiation of apoptosis.

4.To develop extraction of mRNA from different portions of sections cut from formalin fixed, paraffin-embedded preparations of adrenocortical tumours obtained at surgical removal in order to explore the feasibility of obtaining material of sufficient quality to compare gene expression within and between these tumours.

III. Materials and methods

3.1 Biological material, reagents, equipment and software

This section summarizes biochemical materials and reagents, equipment, software and information from handbooks that were used during the studies. Tables also include short forms of complicated/long names used further in the document in order to improve text readability. Items are listed in order of appearance.

3.1.1 What was essentially used in the experiments

This section summarizes biochemical materials and reagents, equipment, software and information from handbooks that were used during the studies. Tables also include short forms of complicated/long names used further in the document in order to improve text readability. Items are listed in order of appearance.

Studies were conducted on biological material. These are summed up in Table 1.

Table 1. Essential biological material used for experiments.

Source/ Vendor	Biological material	Description	Short form used in text

Guy's Hospital	**Cell lines: H295R, H1975, HKe-3, MCF-7**	Cell lines derived from various types of carcinoma, as described in Section 2.2.1.	H295R, H1975, HKe-3 & MCF-7
QIAGEN	**Human Mitochondrial Energy Metabolism Plus RT² Profiler PCR Array ***	For pathway-focused gene expression analysis using laboratory-verified assays	*HMEM PCR Array*
		Profile 84 related genes simultaneously.	
		(Detailed description in Section 3.1.2. and Appendix B).	
Department of Histopathology KCH	**Formalin-fixed tissue embedded ACC paraffin blocks.**	Paraffin-embedded tissue blocks made from surgically removed adrenocortical carcinoma tumours from patients over many years.	**FFPE**
QIAGEN	**Human mTOR Signalling RT² Profiler™ PCR Array ***	PCR Array profiling the expression of 84 key genes involved in the mammalian target of rapamycin (mTOR) signaling pathway. Description in Appendix C.	*mTOR PCR Array*

* NOTE**:** In some places in the document the term *RT² Profiler PCR Array* is used. In such cases it refers to the technical QIAGEN RT² Profiler™ PCR Array type, not to particular genomic material positioned inside the array.

Table 2. *Reagents and buffers.*

Source/ Vendor	Reagent/Buffer	Description	Short form used in text
QIAGEN	RNeasy Plus Mini Kit	For purification of up to 100 µg total RNA from cells/tissues using gDNA Eliminator columns.	*RNeasy Plus Mini Kit*
QIAGEN	RNAprotect® Cell Reagent	RNAprotect Cell Reagent provides immediate stabilization of RNA in sorted or cultured cells.	*RNAprotect Cell Reagent*

Materials and methods

Source/ Vendor	Reagent/Buffer	Description	Short form used in text
QIAGEN	Buffer RW1	Buffer RW1 is for washing membrane-bound RNA when following RNeasy and AllPrep procedures.	*Buffer RW1*
QIAGEN	Buffer RPE	Buffer RPE is for washing membrane-bound RNA in RNeasy, miRNeasy, and AllPrep procedures.	*Buffer RPE*
QIAGEN	RNase-Free Water	RNase-Free Water is pure, quality-tested water suitable for use in all experiments that require RNase-free water.	*RNase-Free Water*
QIAGEN	QIAamp® DNA Blood Mini Kit	For purification of genomic, mitochondrial, or viral DNA from blood and related body fluids.	*QIAamp DNA Blood Mini Kit*
QIAGEN	Buffer AL	For DNA purification using QIAamp and DNeasy Kits.	*Buffer AL*
QIAGEN	Buffer AW1	Wash Buffer AW1 is for a stringent wash with low concentration of quinidine.	*Buffer AW1*
QIAGEN	Buffer AW2	Wash Buffer AW2 is a Tris-based ethanol solution to remove salts.	*Buffer AW2*
QIAGEN	Buffer AE	Elution Buffer.	*Buffer AE*
QIAGEN	RNeasy FFPE Kit	For purification of total RNA from formalin-fixed, paraffin-embedded tissue sections.	*RNeasy FFPE Kit*
QIAGEN	Buffer PKD	Buffer PKD functions as a Proteinase K Digestion Buffer. (In RNeasy FFPE Kit)	*Buffer PKD*
QIAGEN	Buffer RBC	For binding adjustment conditions. (In RNeasy FFPE Kit)	*Buffer RBC*
QIAGEN	QIAamp DNA FFPE Tissue Kit	For purification of genomic DNA from formalin-fixed paraffin-embedded tissues.	*QIAamp DNA FFPE Tissue Kit*

Source/ Vendor	Reagent/Buffer	Description	Short form used in text
QIAGEN	RT² PreAMP cDNA Synthesis Kit	For preamplification of cDNA from small or FFPE samples of RNA for analysis on RT² Profiler PCR Arrays.	*RT² PreAMP cDNA Synthesis Kit*
QIAGEN	REPLI-g FFPE Kit	For whole genome amplification from purified genomic DNA, blood, and cells.	*REPLI-g FFPE Kit*
QIAGEN	Buffer GE	gDNA Elimination Buffer.	*Buffer GE*
QIAGEN	RT mix	5x Buffer BC3, Control P2,	*RT mix*
		cDNA Enzyme Synthesis Mix, RNase Inhibitor, RNase-free water (acc. to RT² PreAMP cDNA Synthesis Handbook).	
QIAGEN	BC3: 5X Reverse Transcription Buffer 3	RT reaction buffer.	*5X BC3 Buffer*
QIAGEN	cDNA Synthesis Enzyme Mix	Includes dNTPs and random primers.	*cDNA Synthesis Enzyme Mix*
QIAGEN	RNase Inhibitor	To inhibit RNase activity.	*RNase Inhibitor*
QIAGEN	Proteinase K	For release the RNA. (In RNeasy FFPE Kit)	*Proteinase K*
QIAGEN	RNase-Free DNase I	Endonuclease for digesting single- and double-stranded DNA.	*RNase-Free DNase I*
QIAGEN	DNase Booster Buffer	For optimized removal of genomic DNA contamination.	*DNase Booster Buffer*
QIAGEN	Control P2	Control factor for RT reaction effectiveness.	*Control P2*
QIAGEN	RT² PreAMP PCR Mastermix	Buffer for preamplification (multiplex cDNA).	*RT² PreAMP PCR*
	7.5 PreAMP Pathway Primer Mix	Primers for preamplification pathway specified transcript.	*Mastermix*
QIAGEN			

Materials and methods

Source/ Vendor	Reagent/Buffer	Description	Short form used in text
			7.5 PreAMP Pathway Primer Mix
QIAGEN	HotStart DNA Taq Polymerase	Enzyme for amplification.	*HotStart DNA Taq Polymerase*
QIAGEN	Side Reaction Reducer	For reducing potential nonspecific reactions in the downstream PCR Array applications.	*Side Reaction Reducer*
QIAGEN	QuantiTect Probe RT-PCR Kit	For one-step qRT-PCR using sequence-specific probes for gene expression analysis.	*QuantiTect Probe RT-PCR Kit*
QIAGEN	2x QuantiTect Probe PCR Master Mix	HotStarTaq® DNA Polymerase, QuantiTect Probe PCR Buffer, dNTP mix, including dUTP, ROX™ passive reference dye, 8 mM MgCl2.	*2x QuantiTect Probe PCR Master Mix*
QIAGEN	QuantiTect RT Mix	Mix of Omniscript® Reverse Transcriptase, Sensiscript® Reverse Transcriptase.	*QuantiTect RT Mix*
Applied Biosystems®	TaqMan® Probe	Hydrolysis probes designed to increase the specificity of quantitative PCR.	*TaqMan Probe*
Applied Biosystems®	FAM™	EcoRI-ACT FAM™ Selective Amplification Primer	*FAM*
QIAGEN	RT² SYBR® Green Mastermix	Contains all of the optimized reagents and buffers needed for SYBR® Green based real-time polymerase chain reactions in all real-time PCR instrumentation.	*RT² SYBR Green Mastermix*
Affymetrix	ROX™ Passive Reference Dye	Inert dye, the fluorescence of which does not change during the reaction in real-time PCR instruments.	*ROX Passive Reference Dye*
QIAGEN	RT² qPCR Primer Assay	For accurate and reliable gene expression analysis using laboratory-verified assay.	*RT² qPCR Primer Assay*

Table 3. *Equipment used in experiments.*

Vendor	Equipment name	Description	Short form used in text
QIAGEN	gDNA Eliminator spin column	Cell or tissue lysates are spun through gDNA Eliminator spin columns to remove genomic DNA. (In the *RNeasy Kit*).	*gDNA Eliminator spin column*
QIAGEN	QIAamp® Mini spin column	Mini spin column for DNA purification.	*QIAamp Mini spin column*
QIAGEN	RNeasy MinElute Spin Column	Mini spin column for RNA purification.	*RNeasy MinElute Spin Column*
Thermo Fisher Scientific	Thermo Scientific NanoDrop™ 1000 Spectrophotometer	The full spectrum (220nm-750nm) spectrophotometer.	*Thermo Scientific NanoDrop 1000 Spectrophotometer*
Starlab	0.2ml PCR Tubes		*0.2ml PCR Tubes*
Eppendorf	Eppendorf® Safe-Lock microcentrifuge tube	1.0 to 2.0 mL microcentrifuge tubes.	*Eppendorf tube*
Applied Biosystems®	Veriti® Thermal Cycler	Thermal Cycler.	*Veriti Thermal Cycler*
Corbett Life Science	Rotor-Gene 6000	Real-time PCR cycler.	*Rotor-Gene 6000*
Applied Biosystems®	ViiA™ 7 Real-Time PCR System	Real-Time PCR System.	*ViiA 7 Real-Time PCR System*

Table 4. *Software and most important handbooks used for data analysis.*

Vendor	Handbook (edition) or Software	Description	Short form used in text
QIAGEN	RNAProtect® Cell Reagent Handbook (QIAGEN 2010)	Principles and procedure of immediate stabilization of RNA in sorted or cultured cells.	*RNAProtect Cell Reagent Handbook*

Vendor	Handbook (edition) or Software	Description	Short form used in text
QIAGEN	RNeasy® FFPE Handbook (QIAGEN 2013a)	Principles and procedure of purification of total RNA from formalin-fixed, paraffin-embedded tissue sections.	*RNeasy FFPE Handbook*
QIAGEN	QIAamp® DNA FFPE Tissue Handbook (QIAGEN)	Principles and procedure of purification of genomic DNA from formalin-fixed, paraffin-embedded tissues.	*QIAamp DNA FFPE Tissue Handbook*
QIAGEN	REPLI-g® Mini/Midi Handbook (QIAGEN, 2011a)	Principles and procedure of whole genome amplification from purified genomic DNA, blood, and cells.	*REPLI-g Mini/Midi Handbook*
QIAGEN	RT² PreAMP cDNA Synthesis Handbook (QIAGEN, 2011b)	Principles and procedure of synthesis and preamplification of cDNA from small RNA samples and RNA from formalin-fixed, paraffin-embedded samples.	*RT² PreAMP cDNA Synthesis Handbook*
QIAGEN	QuantiTect® Probe PCR Handbook	Principles and procedure of one-step qRT-PCR using sequence-specific probes for gene expression analysis.	*QuantiTect Probe PCR Handbook*
QIAGEN	Life Technologies® ViiA-7® (ViiA 7 Software v1.2) instrument setup instructions for RT² Profiler PCR Arrays (QIAGEN, 2013)	RT² PCR Array specific protocol sheet.	*Life Technologies ViiA-7 instrument setup instructions for RT² Profiler PCR Arrays*
QIAGEN	RT² qPCR Primer Assay Handbook (QIAGEN, 2013c)	Principle and procedure of gene expression analysis by real-time RT-PCR.	*RT² qPCR Primer Assay Handbook*
Corbett Life Science	Rotor-Gene 6000 Series Software 1.7	Software for PCR cycles generating and control for Rotor-Gene 6000 PCR cycler and reporting.	*Rotor-Gene 6000 Series Software 1.7*
Applied Biosystems®	ViiA™ 7 Software, v. 1.3	For editing the PCR thermal cycling conditions, full remote control, status monitoring of instruments, default protocols for standard applications, analyses or results.	*ViiA 7 Software, v. 1.3*
QIAGEN	RT² PCR Array Data Analysis version 3.5 software	Array data analysis software, using ΔΔCT method, dedicated for RT² PCR Arrays.	*RT² PCR Array Data Analysis version 3.5 software*

Vendor	Handbook (edition) or Software	Description	Short form used in text
		http://pcrdataanalysis.sabiosciences.com/pcr/arrayanalysis.php	

1.3 Description of genes included in the QIAGEN Human Mitochondrial Energy Metabolism Plus RT² Profiler PCR Array.

This preliminary study set out to establish whether the particular susceptibility of human adenocarcinoma cell lines to mitotane might be related to different expression of mitochondrial genes. Those genes code components of the coenzyme respiratory chain, since it is known that the mitochondria play an important role in apoptosis via generation of chain components such as cyt c.
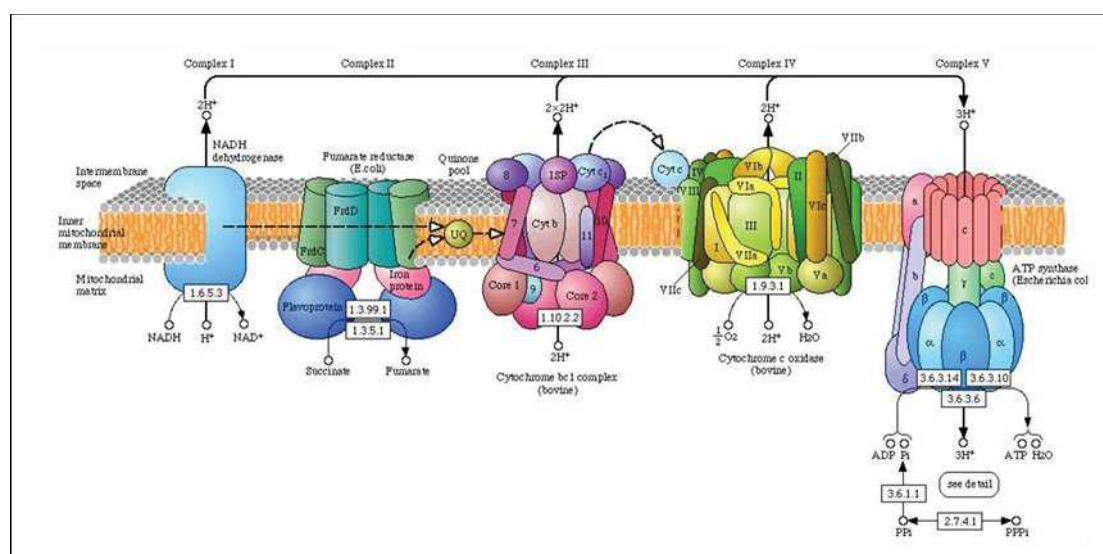
Figure 8. *Components of the coenzyme respiratory chain (Taken from Grossman & Kamholz (2015).*

The diagram above shows the oxidative phosphorylation complex and its constituent subunits.The electron transport chain comprises multiple subunit complexes. NADH is oxidised by complex I, (NADH dehydrogenase) and electrons from complex I and II are transferred to coenzyme Q and passed on to complex III, also known as cyt c reductase and thence to complex IV, also known as cyt c oxidase (COX) and finally to O_2 to generate H_2O. As the electrons traverse complexes I, III and IV, protons are pumped out across the inner mitochondrial membrane, generating an electrochemical gradient, which is used by complex V to condense ADP and inorganic phosphate to form ATP. Succinate dehydrogenase, also termed succinate-coenzyme Q reductase, or respiratory complex II, participates in both the TCA and the electron transport chain. In step 6 of the citric acid cycle, it catalyses the oxidation of succinate to fumarate with the reduction of ubiquinone

to ubiquinol. This process occurs in the inner mitochondrial membrane by coupling the two reactions together.

The QIAGEN *Human Mitochondrial Energy Metabolism Plus RT² Profiler PCR Array (HMEM PCR Array)* profiles 84 genes. Most of them are nuclear and code for the mitochondrial coenzyme respiratory chain, together with mitochondrial gene precursors and polycistronic transcripts H1 and H2 units.

The nuclear genes encoding components of the electron transport chain and oxidative phosphorylation complexes comprise:

Complex I (NADH-Coenzyme Q Reductase: NDUFA1, NDUFA10, NDUFA11, NDUFA2, NDUFA3, NDUFA4, NDUFA5, NDUFA6, NDUFA8, NDUFAB1, NDUFB10, NDUFB2, NDUFB3, NDUFB4, NDUFB5, NDUFB6, NDUFB7, NDUFB8, NDUFB9, NDUFC1, NDUFC2, NDUFS1, NDUFS2, NDUFS3, NDUFS4, NDUFS5, NDUFS6, NDUFS7, NDUFS8, NDUFV1, NDUFV2, NDUFV3);

Complex II (Succinate-Coenzyme Q Reductase: SDHA, SDHB, SDHC, SDHD);

Complex III (Coenzyme Q-Cytochrome c Reductase: CYC1, UQCR11, UQCRC1, UQCRC2, UQCRFS1, UQCRH, UQCRQ);

Complex IV (Cytochrome c Oxidase: COX4I1, COX5A, COX5B, COX6A1, COX6A2, COX6B1, COX6C, COX7A2, COX7A2L, COX7B; COX8A)

Complex V (ATP Synthase: ATP5A1, ATP5B, ATP5C1, ATP5F1, ATP5G1, ATP5G2, ATP5G3, ATP5H, ATP5I, ATP5J, ATP5J2, ATP5L, ATP5O, PPA1).

The array consists also of primers for the genes of associated proteins involved with mitochondrial processes and mitochondrial genes polycistronic precursors H1 and H2. Other proteins and mitochondria polycistronic units also used by the company as biomarkers of pathway activity as whole (Pathway Activity Score): ARRDC3, ASB1, CYB561D1, DNAJB1, EDN1, GADD45B, HSPA1A, HSPA1B, LRP5L, MitoH1, MitoH2_12106, MitoH2_14573, MitoH2_4162, MitoH2_5726, RNU11, SLC25A25.
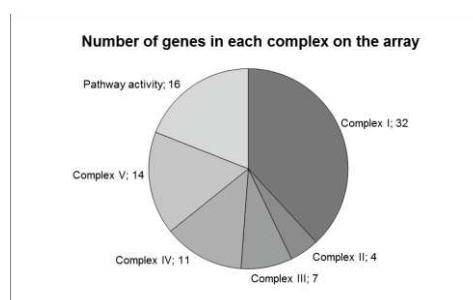

Figure 9. Number of genes in each complex on the HMEM PCR Array.

Materials and Methods

The complete list of genes, as supplied by the manufacturer, forms Appendix A, at the end of the document.

3.2 Protocol of experiments

3.2.1 Cell culture: treatment with mitotane and control normal serum. Preparation of samples for gene expression analysis.

Four human adenocarcinoma cell lines were used in the studies: H295R derived from an adrenocortical carcinoma, H1975 derived from a lung carcinoma, HKe-3 derived from a colon carcinoma, and MCF-7 from breast cancer, described in the introduction (Section 1.4). These cell lines were cultured by Paulina Szyszka at Guy's Hospital within the framework of the same grant. She studied cytotoxicity of mitotane by monitoring cell number and used caspase-3-like activity as an index of apoptosis. Mitotane showed anti-proliferative activity in all four cell lines but H295R was much the most sensitive. Using these measures, she established mitotane concentrations of 10 μM for H295R cells and 40 μM for the other cell lines. Incubation times were 24 and 48 hours respectively, when optimum cytotoxic effects of mitotane were observed. The H295R cells were seeded in 10 cm dishes at a density of 790 × 103. Remaining cell lines were seeded in 6 cm dishes at a density of 230 × 103 (HKe-3, H1975) and 570 × 103 (MCF-7) (Dworakowska et al. 2015). Dr Szyszka also examined the toxic effects of mitotane in combination with the cytotoxic agent Erlotinib (Dworakowska et al., 2014) and other agents (Table 8).
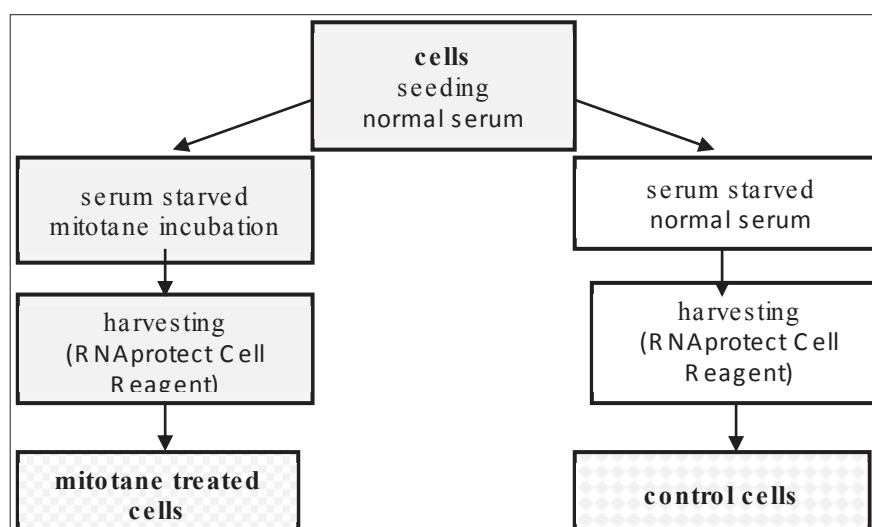
Figure 10. *Mitotane experiment workflow.*

Cells were allowed to grow for 24h and then were serum-starved for 4h. After that time, the medium was replaced with complete medium (control) or medium containing mitotane at 10 µM (H295R) or 40 µM (HKe-3, H1975, MCF-7) concentration. Cells were harvested 24h (H295R) or 48h (HKe-3, H1975, MCF-7) later. Cell pellets were stored in *RNAprotect Cell Reagent* at –20°C until the next step of the experiment. Each experimental group was run in triplicate in three independent incubations. Next, each set of cells was pooled. Three quarters of the volume of each pool were used for further transcriptomic studies (section 3.2.2).

3.2.2 Isolation of total RNA from cultured cells

For each of cultured cells line (H295R, HKe-3, H1975, MCF-7) the following process of RNA isolation was carried out, using the *RNeasy Plus Mini Kit* in accordance with the protocol in the *RNAProtect Cell Reagent Handbook*. Cells were first centrifuged and resuspended in *RNAprotect Cell Reagent*, then centrifuged again. The cell pellet was then suspended in *Buffer RLT*, to provide complete homogenization. This buffer includes guanidine isothiocyanate, which has strong denaturing properties, immediately destroying RNases, ensuring that no degradation of RNA occurs in samples.

In order to remove genomic DNA (gDNA), homogenate was passed through a *gDNA Eliminator spin column* at 73% ethanol suspension, centrifuging for 1 min at 9000 g.

Figure 11. *Workflow of Total RNA extraction from cultured cells with RNeasy Plus Mini Kit.*

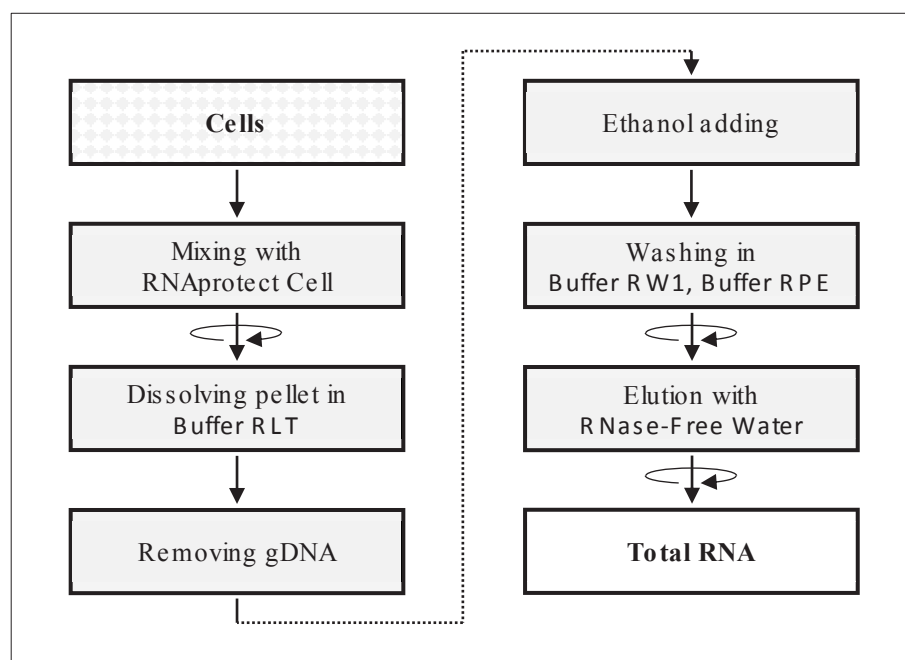RNA purification was carried out on *RNeasy MinElute Spin Columns.* The technology enables selective binding of the RNA to a silica membrane within the column. In combination with special high salt buffers with RNA stabilizing reagent, it is designed to sufficiently purify all RNA molecules longer than 200 nucleotides (including ribosomal 5.8S rRNA & 5S rRNA and tRNAs, which comprise 15–20% of total RNA, in addition to mRNAs) with high quality suitable for qPCR analysis. The system allows the attachment of up to 100 µg of material. The flow-through homogenate from the last step was mixed well with 350 µl 90% aqueous ethanol and 700 µl of the solution was applied to the *RNeasy MinElute Spin Column*, which was then centrifuged (9000 g for 30 s). The flow-through containing the contaminants was discarded. The spin column membrane was washed with 700 µl *Buffer RW1* and *Buffer RPE* in sequence for 30 s and 2 min respectively at 9000 g. To remove any traces of ethanol and buffers, and to ensure that the RNA was pure, a 1 min centrifugation at maximum speed with the lid closed and in a new collecting tube was carried out. *RNase-Free Water* (30 µl) was added directly to the spin column membrane and then total RNA was eluted into previously labelled collection tubes after the 1 min centrifugation at maximum speed. The eluates, representing total RNA were then frozen at $-70\ ^{0}$C.

One quarter of the volume of the pooled material was used for extraction of DNA using the *QIAamp DNA Blood Mini Kit* according to the manufacturer's instructions. Protocol as directed for cultured cells, blood and body fluids was applied. The cells were

centrifuged at 300 g for 5 minutes. The supernatant was gently removed in order not to disturb the cell pellet. The cell pellet was resuspended in PBS to a final volume of 200 µl. *Proteinase K* (20µl) was added, followed by 200 µl *Buffer AL*. Incubation at 56°C for 10 min resulted in efficient lysis. To remove drops from the inside of the lid after brief centrifugation, 200 µl of 96% ethanol was added to the sample. After mixing by pulse vortexing for 15 s the tubes were briefly centrifuged. All the sample liquid was gently applied to the *QIAamp Mini spin column*, avoiding wetting the rim. The columns were closed and centrifuged at 6000 g for 1 min and the collection tubes containing the filtrate were discarded. *Buffer AW1* (500µl) was carefully added. After centrifugation at 6000 g for 1 min, the 2 ml collection tubes were exchanged. The columns were carefully opened and 500 µl *Buffer AW2* was poured in, without wetting the rim, and centrifuged at full speed for 3 min. The collection tubes were exchanged, followed by centrifugation at full speed for 1 min. A new collection tube was fitted, 200 µl *Buffer AE* was added onto the column membrane, followed by a 5 minute incubation in order to increase the DNA yield, followed by centrifugation at 8000 g for 1 min. The samples containing the purified DNA were stored at –20°C

3.2.3 Extraction of total RNA and DNA from FFPE.

A series of microsections were received from Dr Salvador Diaz-Cano (Department of Histopathology KCH). These sections had been cut from paraffin-embedded tissue blocks prepared from tumour tissue that had been surgically removed from patients with ACC or ACA. They were of thickness 0.7 mm and each of them was attached to a slide in the standard way. The first each of them had been stained and subjected to the histological evaluation by Dr Diaz-Cano, who designated areas of the tumour as central or peripheral. Staining is known to affect the quality of extracted RNA and suitability for its application in further downstream steps. Following the labelling of the first section, further sections of waxed tissue were dissected using a scalpel blade into central and peripheral material and next transferred to two separate Eppendorf tubes. These pooled portions of material, derived from one patient, were then used for RNA extraction. Remaining sections were used for extraction of DNA, after dissection of the two zones as before. The number of sections needed to get sufficient RNA was first established (Section 3.3.5).
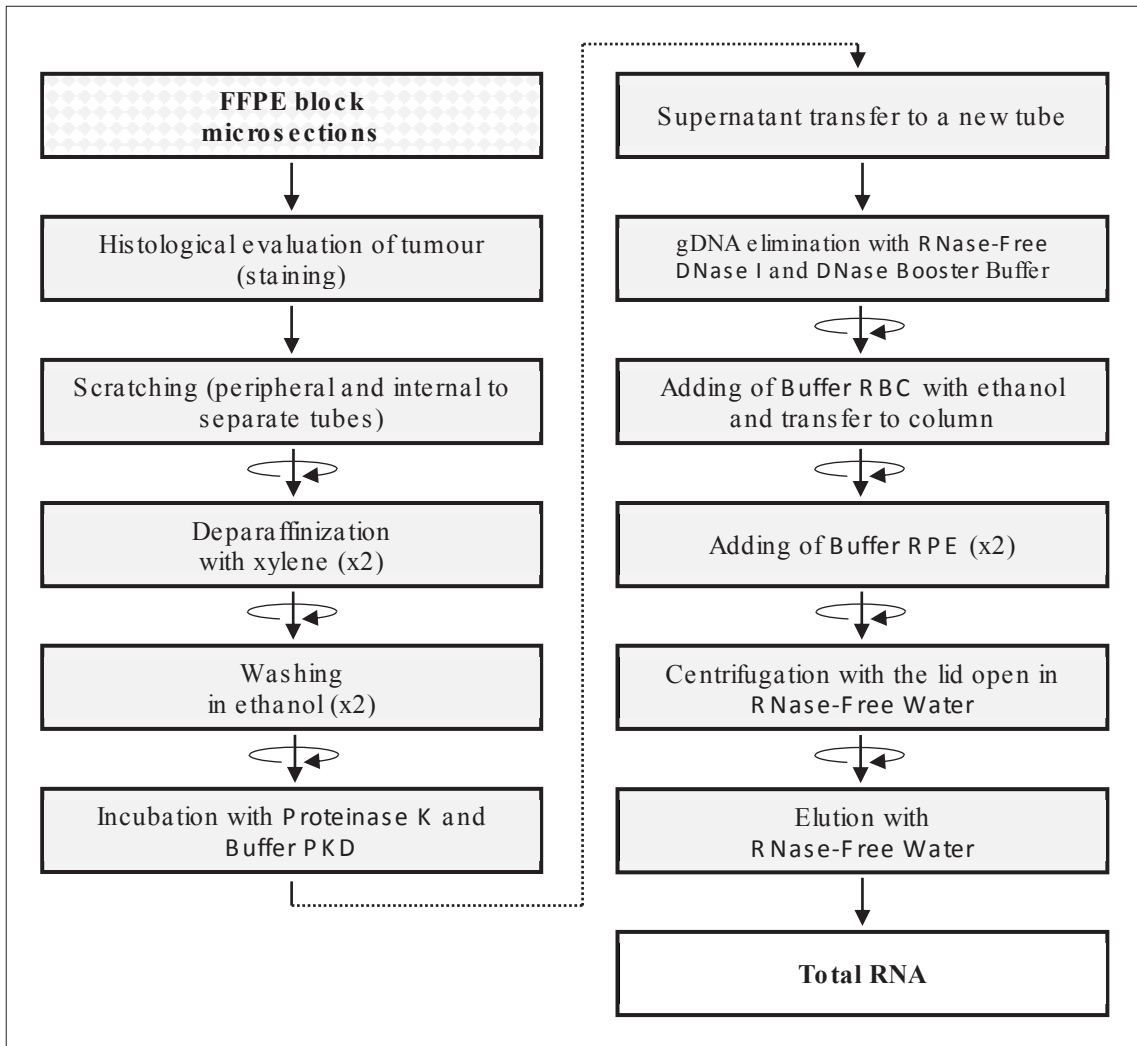
Figure 12. *Workflow of Total RNA extraction from FFPE, using RNeasy FFPE Kit.*

Extraction of total RNA from FFPE was carried out following the *RNeasy FFPE Handbook* using the *RNeasy FFPE Kit*. This kit is specifically designed to reverse as much as possible the chemical modifications of RNA caused by formaldehyde, such as crosslinking, which cannot be detected by standard 'lab on-a-chip' quality control. RNA originating from FFPE often has lower molecular weight in comparison to others. By isolating RNA molecules longer than 70 nucleotides, the kit provides recovery of RNA fragments, making them suitable for gene expression analysis.

Each sample was first dewaxed in the fume cupboard using 1 ml xylene. After thorough vortex mixing and centrifugation at maximum speed for 5 minutes, the xylene containing the paraffin was carefully poured off, taking care not to disturb the pellet remaining at the bottom, and then the dewaxing step was repeated. In the same way, each sample was then

washed with 96% aqueous ethanol. The pellet was left in the fume cupboard until completely dry.

Incubation with optimized lysis buffer containing *Proteinase K* was next carried out in order to release the RNA. A temperature gradient was applied, which allows the removal of chemical modifications of RNA, with a higher temperature incubation removing partial cross-linking. Modification of time and temperature improved the concentration and quality of the RNA (further described at "Optimization" – Section 3.3.5). Each sample was poured into 240 µl *Buffer PKD*. After vortexing, 10 µl *Proteinase K* solution was added. The sample was then mixed gently by pipetting and incubated overnight at 56ºC, followed by 10 min incubation at 80ºC the following day. After cooling on ice, the samples were centrifuged for 15 min at 13,500 rpm. The supernatants were transferred to new tubes.

DNA was removed by incubation with 10 µg *Free DNase I* in 25 µl *DNase Booster Buffer* for 15 min. *Buffer RBC* with ethanol was added to adjust binding conditions of RNA to the *RNeasy MinElute Spin Column*, while impurities were effectively washed from the column. *Buffer RBC* (500 µl) and ethanol (100 µl) were added to each sample. After thorough mixing, 700 µl was transferred to a column, followed by 30 s centrifugation at 9000 g. *Buffer RPE* (500 µl) was then layered onto the column membrane, followed by centrifugation for next 30 s. Centrifugation was repeated for 2 min. Changing a new collection tube under the column and placing the columns in the centrifuge and especially running with the lid open for 1 min were procedures aimed at ensuring that there would be no remaining contamination of total RNA.

For the last step, 17 µl *RNase-Free Water* was carefully poured onto the column membrane, followed by centrifugation at full speed for 3 minutes to elute the RNA. Obtained RNA (2 µl) was immediately taken from the original tube and combined with 2 µl of *RNase-Free Water* in mini tubes and kept on ice ready for measurement of the concentration of total RNA.

Extraction of DNA from FFPE was carried out for the first samples using the *QIAamp DNA FFPE Tissue Kit*, according to the *QIAamp DNA FFPE Tissue Handbook*. Thereafter, for the majority of samples, the *REPLI-g FFPE Kit* was used, following protocol taken from the *REPLI-g Mini/Midi Handbook*.

Purity and concentration of nucleic acids was measured using a *Thermo Scientific NanoDrop 1000 Spectrophotometer*.

Materials and Methods

3.2.4 Research workflow

During the research, several cross-dependent experiments were conducted. The sequence of experimental blocks was initially planned and then modified according to the needs occurring during the progress of the research.
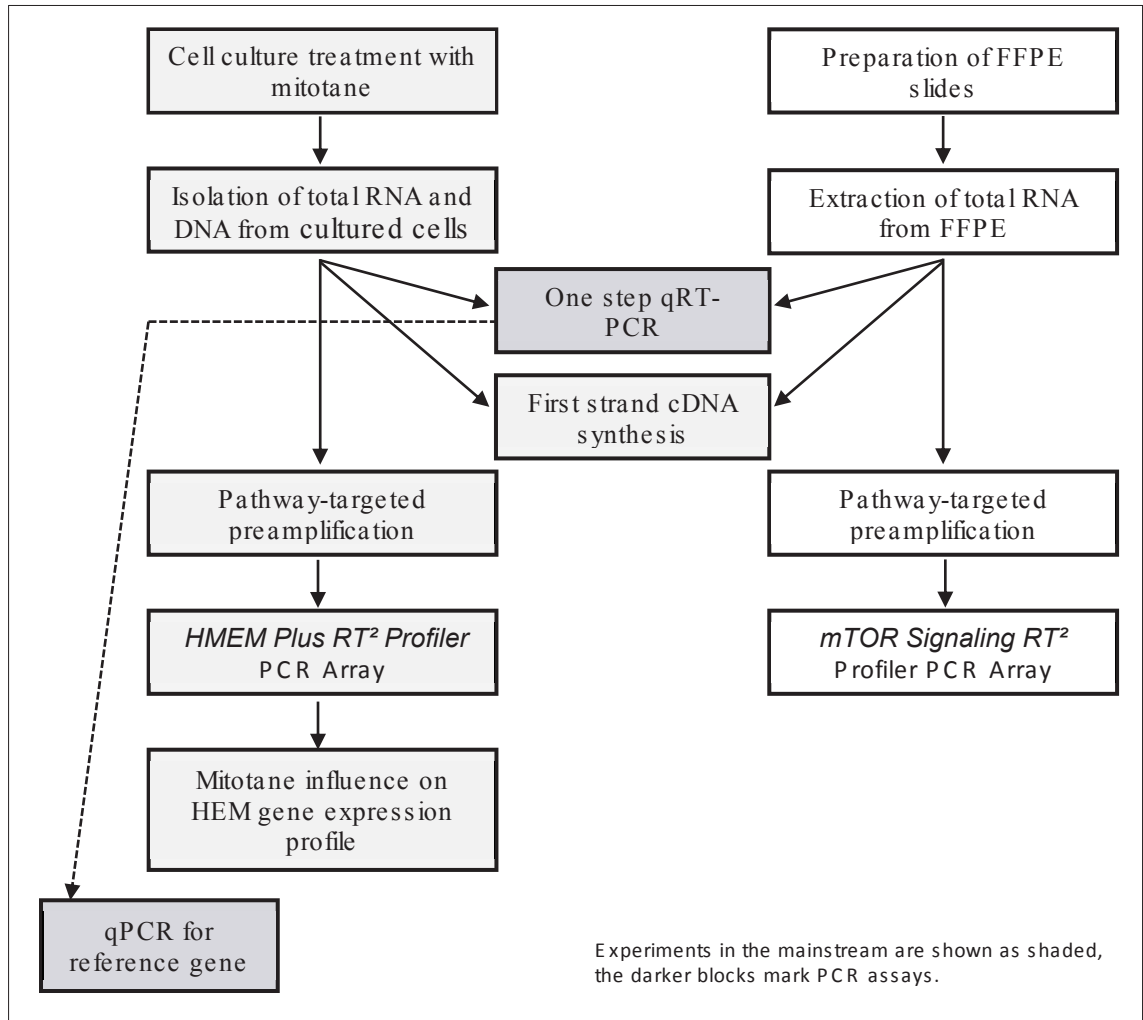
Figure 13 *Research workflow*

The following protocols were used for both cell lines and FFPE

3.2.5 One step (quantitative) qRT-PCR

This procedure was carried out using the *QuantiTect Probe RT-PCR Kit,* according to the *QuantiTect Probe PCR Handbook*. The reaction mix for each sample contained 15 ml *2x QuantiTect Probe PCR Master Mix*, 0.5 ml *QuantiTect RT Mix* 2 µl total RNA and 2 µl *RNase-free Water*. A volume of 20 µl was carefully pipetted into 200 µl tubes. Tubes then were placed in the sample rotor of the *Rotor-Gene 6000* real-time PCR cycler. The

reaction parameters and cycling condition were set up using the *Rotor-Gene 6000*. One sample contained 1 µl of primers and probes for beta-Actin. These primers and probes are unlabelled PCR primers and *TaqMan Probes* with a *FAM* (carboxyfluorescein) dye label on the 5' end, together with *minor groove binder* and *nonfluorescent quencher* on the 3' end.

Table 5. *Parameters of the cycles set for one-step qRT-PCR with TaqMan Probes.*

Cycle	Cycle Point
Hold 1 @ 50°C, 30 min 0 s	—
Hold 2 @ 95°C, 15 min 0 s	—
Cycling (50 repeats)	Step 1 @ 95°C, hold 10 s
—	Step 2 @ 57°C, hold 20 s, acquiring to Cycling A

3.2.6 First strand cDNA synthesis and pathway-targeted preamplification

Total RNA (90 ng for cell lines and 200ng for FFPE) was used for the reverse transcription reaction, using the *RT² PreAMP cDNA Synthesis Kit*.

At first, the total RNA (1 µg/µl) samples were diluted as follows:

Control: Hke-3 — 1:8,   H1975 — 1:14,   MCF-7 — 1:14,   H295R — 1:2;

Mitotane: Hke-3 — 1:2,   H1975 — 1:8,   MCF-7 — 1:14,   H295R — 1:2.

No method of RNA extraction provides a sample free of gDNA. As a first step, gDNA needs to be removed because it can act as an effective template during PCR, resulting in a false positive signal unrelated to mRNA. Removal was achieved by incubation with *Buffer GE* at 42°C for 5 min. This buffer presumably contains DNase. Lack of presence of gDNA is monitored by quality control on the array (see further explanation in results).

For each sample, 10 µl *RT mix* was added. The solution was prepared by combining *5X BC3 Buffer* (3 µl), *cDNA Synthesis Enzyme Mix* (2 µl), which includes dNTPs and random primers', *RNase Inhibitor* (1 µl) and *RNase-Free Water* (3 µl). 'Random primers' are a pool of hexanucleotides and pentanucleotides of all possible sequences, which are crucial elements during complementary strand synthesis, representing the total RNA of the cell.
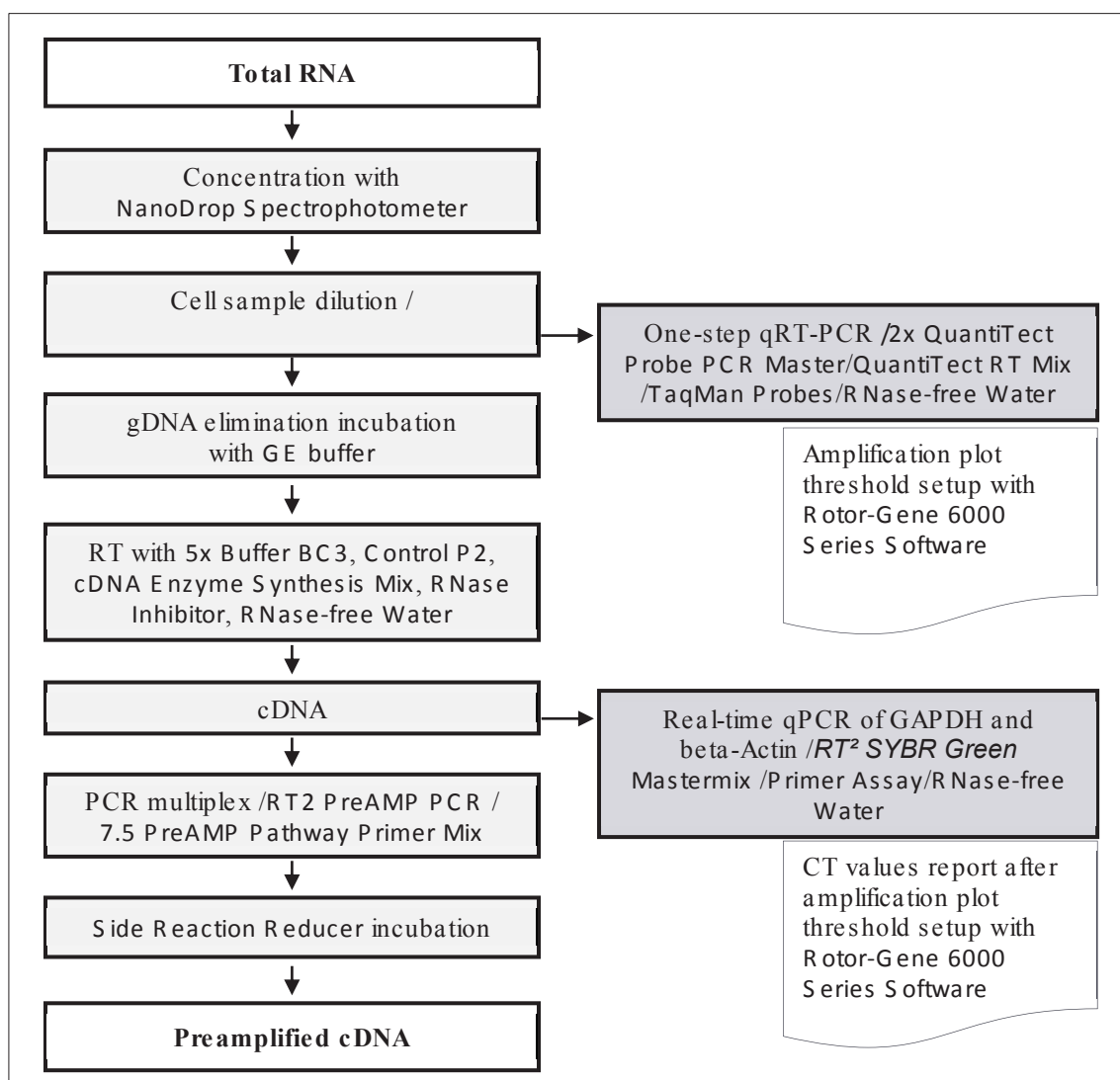
Figure 14. *Workflow of cDNA synthesis with preamplification using RT² PreAMP cDNA Synthesis Kit, also qRT -PCR with the QuantiTect Probe RT-PCR Kit , and Real Time qPCR with RT2 qPCR Primer Assay.*

'Additionally, *Control P2* was added. First strand cDNA was synthesised (42°C for 30 min, then 95°C for 5 min) with built-in external RNA quality control, yielding 20 µl product. Preamplification of cDNA was carried out in duplicate for each of the 8 cell groups, using 5 µl of product, with 12.5µl the *RT² PreAMP PCR Mastermix* and *7.5 PreAMP Pathway Primer Mix* specified for each type of array. Cycle conditions were: 10 min 95°C *HotStart DNA Taq Polymerase*, activation followed by 12 cycles of 95°C for 15 s and 60°C for 2 min. Next, *Side Reaction Reducer* was added and incubated at 37°C for 15 min, followed by inactivation at 95°C for 5 min.

Materials and Methods

The cDNA synthesis and preamplification reaction procedures were carried out according to the *RT² PreAMP cDNA Synthesis Handbook*. Incubations and cycling were processed with use of an *Veriti Thermal Cycler*.

3.2.7 QPCR amplification prior to use on the *RT² Profiler* PCR Array

Real-time qPCR for gene expression profiling is a very sensitive and reliable method that allows detection and quantification of cDNA. During the accumulation of product of the PCR reaction in each cycle of amplification, fluorescence emitted from a reporter molecule SYBR Green I (asymmetrical cyanine dye used as a nucleic acid stain) is detected in real time. This allows the monitoring of the PCR reaction during the early and further exponential phases, where the first significant increase in the amount of amplification product correlates with the initial amount of target template, reflected further as the cycle threshold (Ct) value.

RT² SYBR Green Mastermix contains a fluorescent dye, SYBR Green I, that binds only to two-stranded DNA. Minimal fluorescence is emitted from the dye in solution. The intensity of the fluorescence signal (Delta RN or ΔRN) correlates with DNA amplicon amount, which is related to the initial sample input amounts (Rulli 2014). The amplification plot is therefore an image of ΔRN in the cycle.

The main amplification reactions were carried using a *ViiA 7 Real-Time PCR System* instrument equipped with *ViiA™ 7 Software, v. 1.3. RT² Profiler PCR Array*. In this study, 384-well (4 × 96) plates were used. Each of the 96 wells in one line of the array contains primers for one of the selected genes. Four samples can be uploaded into one array. Following the method in the *RT² Profiler PCR Handbook*, qPCR reaction ingredients were mixed: Preamplified cDNA, *RT² SYBR Green Mastermix* (contains *HotStart DNA Taq Polymerase*), dNTPs and *RNase-free Water*. Samples (10 μl) were loaded by an 8-channel pipette. A four colour numbered cap system enabled samples 1 to 4 in sequence to be loaded correctly onto the array plate. Finally, the array plate was sealed against evaporation and centrifuged.
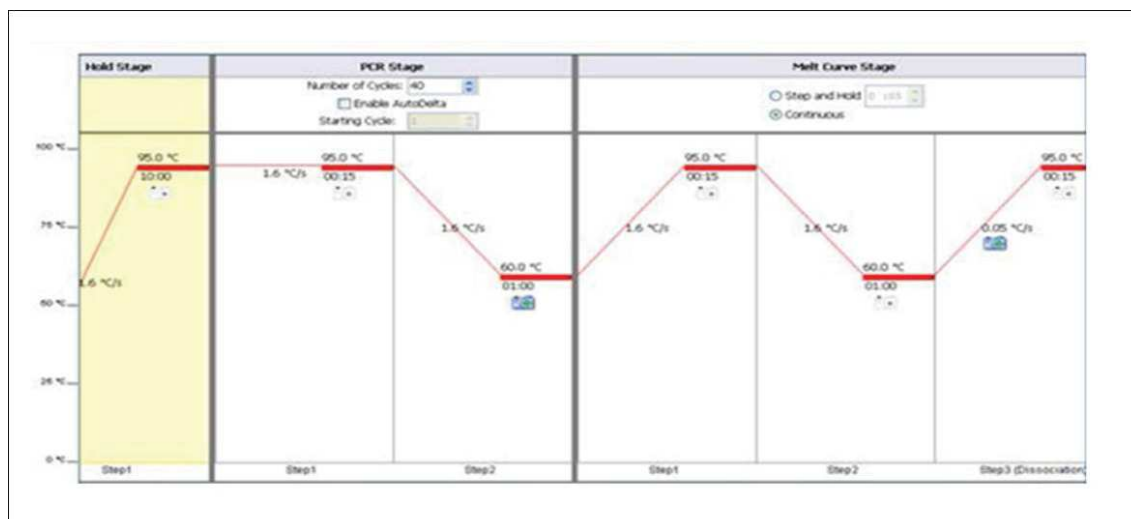
Figure 15. *Scheme showing the amplification cycling ViiA 7 Real-Time PCR System setup instructions for RT² Profiler PCR Arrays (Taken from ViiA™ 7 Software, v. 1.2).*

The centrifuged plate was placed in the thermocycler, which had been precalibrated for use with SYBR Green I. Before that, reaction parameters according to the protocol in *Life Technologies ViiA-7* instrument setup instructions for *RT² Profiler PCR Arrays* were set up. Parameters included plate type and size, the use of SYBR Green I reagents, the use of *ROX Passive Reference Dye*, specification of times, plate layout with targets and samples; together with run method parameters as follows: 10 µl volume per well, cycling conditions: Hold Stage, 50°C, 2.00 min; PCR Stage, 40 cycles 95°C, 0.15 min, 60°C, 1.00 min, Melt Curve Stage with default settings. During the PCR run, the data is shown on the screen as amplification plots (Figure 14 and further). On completion, data are analysed using the supplied software. Analysis involves defining 'baseline' and 'threshold' using the log view of the amplification plots. By specifying the background signal as within the lower ⅓ of the phase diagram of linear amplification, the values for Ct become visible and results can then be exported to an Excel file.

3.2.8 Real-time PCR of GAPDH and Beta Actin

In order to check on the quality and quantity of the RNA prepared for use on the Qiagen PCR Array, it was considered useful to carry out qPCR on a sample of genes. The primers for GAPDH and beta-Actin were already available, so these genes were chosen. For results, see Section 3.3.6. As noted by D'haene, there is no need for the reference genes

to be measured in the same run as the gene of interest during relative quantification, so long as all samples are treated equally (D'haene 2013).

First strand cDNA synthesised after the RT reaction (not preamplified) was used as the template for the qRT-PCR reaction. A 1:10 dilution at *RNase-free Water* was made first. The PCR component mixes were prepared following directions in the *RT² qPCR Primer Assay Handbook.* In these PCR experiments two mixes from QIAGEN's Primer Assays were used – the first containing Beta Actin primers and the second, GAPDH primers.

Components for one reaction were: 12.5 µl of *RT² SYBR Green Mastermix* (containing *HotStart DNA Taq Polymerase* activated by heating at 95°C), 1 µl *Primer Assay* (10 µM), 10.5 µl *RNase-Free Water*. A volume of 24 µl was carefully added to special tubes in duplicate into which 1 µl cDNA template had been added earlier. Tubes were placed in the sample rotor of the *Rotor-Gene 6000*. The reaction parameters and cycling condition were set up on the associated computer. The report was generated by *Rotor-Gene Software*.

The cycling conditions are shown in Table 6.

Table 6. *Parameters of the cycles set for two-step qPCR with SYBR Green I.*

Cycle	Cycle Point
Hold 1 @ 50°C, 30 min 0 s	—
Hold 2 @ 95°C, 10 min 0 s	—
Cycling (45 repeats)	Step 1 @ 95°C, hold 15 s
—	Step 2 @ 60°C, hold 1 min 0 s, acquiring to Cycling A

3.3 Technical results with quality evaluation

Use of quantification and quality checking at each stage are very important. Gene expression methodology is exacting and difficult, because the final results are only achieved after a long protocol with multiple steps, each requiring measurement, verification, and calculation. The complexity of the method justifies presentation of intermediate experimental results in this thesis.

Materials and Methods

3.3.1 Total RNA yields and cDNA assessment in the mitotane-treated cell experiments

RNA yields after extraction from H295R cell lines treated or not with mitotane are shown in Table 7.

Table 7. *Yield of RNA from untreated and treated cultured cells.*

Cell line name	Control TOTAL RNA [µg/µl]	Mitotane TOTAL RNA [µg/µl]
Hke-3	750	148
HI973	1264	360
MCR7	1327	707
H295R	216	201

Examples of the RNA concentration results from earlier experiments on H295R cell lines treated with various inhibitors are presented in Table 8. The lower concentrations in the 3 last samples reflect stoppage of cell growth and cell death after using 3 inhibitors in combination.

Table 8. *RNA concentration in H295R cells, untreated and treated with various combinations of inhibitors.*

Inhibitor	TOTAL RNA [µg/µl]
C	1955
EGF (100 ng/ml)	135
Erlotinib (20 µM)	256
EGF + Erlotinib	113
Everolimus (60 nM)	159
NVP-BEZ235 (10 nM)	75
Everolimus + NVP-BEZ235	83
EGF + everolimus + NVP-BEZ235	53
Erlotinib + everolimus + NVP-BEZ235	29

The table below shows the cDNA yield obtained after RT reaction of diluted RNA template, checked on the *Thermo Scientific NanoDrop 1000 Spectrophotometer*. The cDNA yield obtained after RT reaction was diluted to be in the range 1:2–1:14 RNA template. Determination of cDNA concentration is needed before carrying out the preamplification reaction, especially when total RNA has been derived from cultured cells, because the cDNA yield can be high and it is important to protect the costly array plates from overloading. Also, it is useful to know the concentration of cDNA prior to

further processing. The ratios 260/230 are artefactorily diminished at high concentrations of sample (Held 2001). The table below shows the presence of cDNA at high concentration from a strongly diluted initial sample of RNA, obtaining at least 10 times multiplication from 90 ng/µl initial RNA.

Table 9. cDNA concentration assessment prior to the preamp and array runs for samples used in the experiment, after RT.

Cell line name	Control			Mitotane		
	Conc[ng/µl]	260/280	260/230	Conc.[ng/µ]	260/280	260/230
HKe-3	1606	1.64	2.06	1116	1.65	2.02
HI973	1067	1.62	1.98	928	1.62	2.00
MCR7	1067	1.62	2.0	928	1.62	1.98
H295R	1104	1.64	1.91	955	1.64	1.96

3.3.2 Results for total RNA and DNA extraction from FFPE, with method adjustments to improve yield

In order to gain the best possible results of extraction, each step was separately verified. The first important step was to determine the number of sections needed to get a sufficient amount of nucleic acid. It was necessary to find out if the 5–6 sections for total RNA extraction and 1–2 for DNA purification of each series, that had been prepared already at the Department of Histopathology, would be sufficient. Taking into consideration the process of dissection of the 0.7 mm waxed tissue from the slide by using a thin scalpel blade, and the fact that the volumes of the selected peripheral and internal zones can differ by up to 60%, it was important to ensure that the yield would be sufficient. It needs to be emphasised that adenocarcinoma or nodule tumours can be small, so that the 5–7 sections might be the maximum number that could be obtained. Once the minimum required number was established to enable duplicate experiments to be carried out, it would be possible to estimate if there was sufficient amount of material to continue.

The second improvement was carried out according to the advice provided in 'Genomic Technology, FFPE and RNA extraction a troubleshooting guide', GenomeWeb site (Johnson 2014). The experimental protocol was improved by enhancing the *Proteinase K* step. The time of incubation at 50°C with *Proteinase K* was extended from the 3 h suggested in the QIAGEN protocol to up to 12 hours, as it was observed that this had a very significant impact on the total RNA concentration and quality.

Materials and Methods

In the protocol, two options were recommended for the volumes of ethanol and *Buffer RBC* that are passed through the column, namely 320 µl or 500 µl *Buffer RBC* with 720 µl or 1200 µl ethanol. The higher volumes were found to give higher concentrations of total RNA.

The total yields in each case for central and peripheral areas of tumour sections are shown in ng/µl. The concentrations were obtained by analysis using a *NanoDrop Spectrophotometer*. Total RNA was obtained from the FFPE-derived peripheral and internal zones of ACC and ACA tumours in the range 30–380 ng/µl. Additionally, for comparison, RNA from one normal cortex was extracted at a concentration of 280 ng/µl.

Table 10. *Concentration of Total RNA extracted from FFPE, showing yield of RNA originating from the internal part of the tumour or the peripheral part for each case.*

No.	Patient case No.	INTERNAL **Total RNA [ng/µl]**	PERIPHERAL **Total RNA [ng/µl]**
1	10-8431 ACA	30	170
2	11-6580 ACC	63	108
3	10-4143 ACA	114	40
4	10-9614 ACC	131	184.1
5	115-10219ACC	54	88.32
6	10-6232ACA	256	115
7	09-4816ACC	251	261
8	10-2161 ACC	105	42
9	10/16266 ACC	236	115
10	11/1324ACC	102	242
11	09-18501 ACA	40	96.42
12	09/15605 ACC	380	89.56
13	12-7230 ACA	300	197
14	10/3326 ACA	81	183.7
15	12 -2635ACC	162	281
16	101/11541 ACC	14	99.65
17	09-16010ACA	54.87	72.96

When DNA was extracted from separate sections from the same blocks, high concentrations were found (3200–4900 ng/µl in 35 µl).

3.3.3 Nucleic acid purity parameters

It is important to note that absorbance ratios are only an indication of purity rather than a precise measure (Held 2001). Total RNA in the experimental material, measured

64

Materials and Methods

by a *Thermo Scientific NanoDrop 1000 Spectrophotometer* showed the expected curve shape and the parameters A260/A230 A260/A280 in the range of 1.89–2.05. Avoidance of the use of phenol and use of specialised kits give the least risk of co-extracting any impurities. There is a risk that the guanidine isothiocyanate used in the method would result in the presence of impurity, as shown by both ratios being < 1.4, but this was not observed in the experiment.

### 3.3.4 QRT-PCR reaction carried out with TaqMan Probes

This section considers the total RNA quality prior to amplification.

A quantitative real-time polymerase chain reaction (qRT-PCR) was carried out using *TaqMan Probes* for the reference genes beta-Actin, to provide an initial assessment of whether the total RNA quality was adequate for amplification.

Quantitative results achieved by this method are presented below as amplification plots. These show the expected shape of the curve, with exponential and plateau regions, indicating that the qRT-PCRs were carried out properly. Threshold settings were adjusted to allow Ct values to be shown.

The beta-Actin primer report, showing representative results for four samples in duplicate for FFPE and ten in duplicate for cultured cells, is shown below. All FFPE-derived RNA samples that had been prepared were found to give positive results on RT-PCr for beta-Actin.

No.	Colour	Name	Type	Ct	No.	Colour	Name	Type	CT
1		1	FFPE RNA	18.95	13		7	FFPE RNA	23.84
2		1	FFPE RNA	20.27	14		7	FFPE RNA	21.89
3		2	FFPE RNA	21.61	15		8	FFPE RNA	17.67
4		2	FFPE RNA	22.39	16		8	FFPE RNA	17.58
5		3	FFPE RNA	21.02	17		9	FFPE RNA	18.97
6		3	FFPE RNA	21.28	18		9	FFPE RNA	20.22
7		4	FFPE RNA	19.30	19		10	FFPE RNA	14.20
8		4	FFPE RNA	19.54	20		10	FFPE RNA	12.29
9		5	FFPE RNA	21.66	21		cL9	Cultured Cell RNA	19.20
10		5	FFPE RNA	22.32	22		cL9	Cultured Cell RNA	18.86
11		6	FFPE RNA	17.49	23		cL10	Cultured Cell RNA	18.49
12		6	FFPE RNA	17.32	24		cL10	Cultured Cell RNA	17.92

Materials and Methods
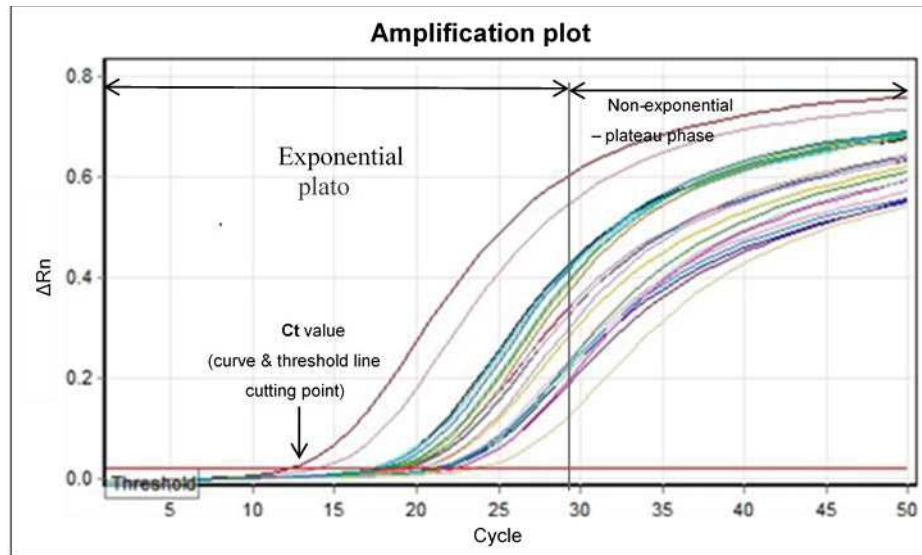
The duplicates for sample 10 at Figure 14 were unsatisfactory, with a difference of Ct values of more than 2. The same run was repeated and gave a better result (Figure 15).

No.	Colour	Name	Type	Ct
1		1	FFPE RNA	20.95
2		1	FFPE RNA	21.11
3		1	FFPE RNA	21.08
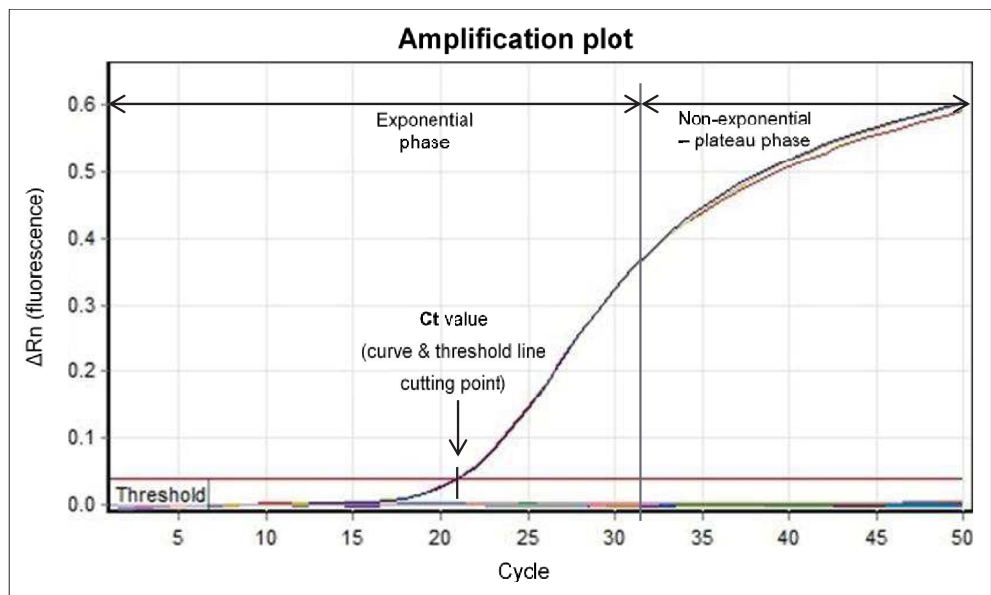
FFPE RNA was finally shown to also provide a usable template with qRT-PCR reaction carried out with *TaqMan Probes*. The standard curve has an exponential phase. The reaction overall is efficient according to PCR gold standards.

66

Materials and Methods

The threshold must be set up at the beginning of the exponential phase, cutting off the nonspecific background signal.

3.3.5 Optimization of the gene expression study method Real-Time PCR for RT2 Profiler PCR Arrays.

A first trial array experiment was set up to verify that all the specified reaction conditions were suitable. The trial was carried out using nucleic acids from cell lines and FFPE (400ng). The first two reaction results on the *mTOR PCR Array* revealed that the protocols (claimed to work for the *ViiA 7 Real-Time PCR System)* in the main *RT² PreAMP cDNA Synthesis Handbook*, were unsatisfactory, as shown by a delay in the amplification plot (Figure 16).

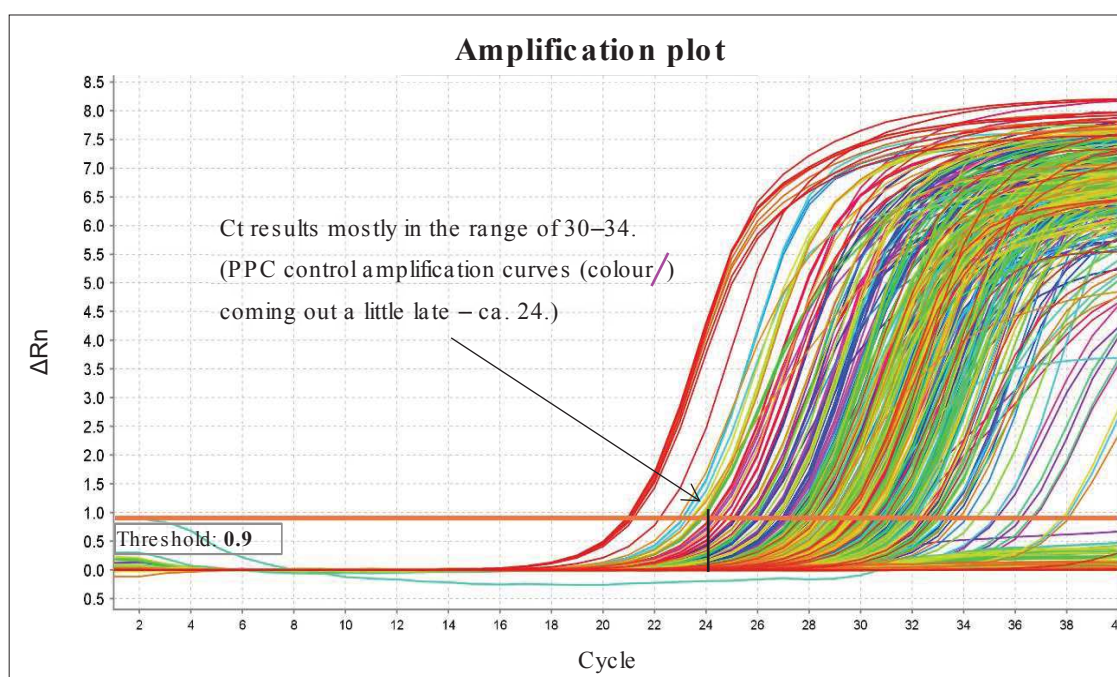*Figure 16. Positive results of PCR for cell lines in mTOR PCR Array.*

The next run *mTOR PCR Array* used the modified protocol with human RNA obtained from QIAGEN and RNA extracted from H295R cells in duplicate enabled confirmation that appropriate cycling conditions had been specified. Protocol accuracy was confirmed for the PCR control, which showed Ct values within the qPCR gold standard (Figure 17).

Using these conditions, the amplification plots for most genes fell within the desired range.
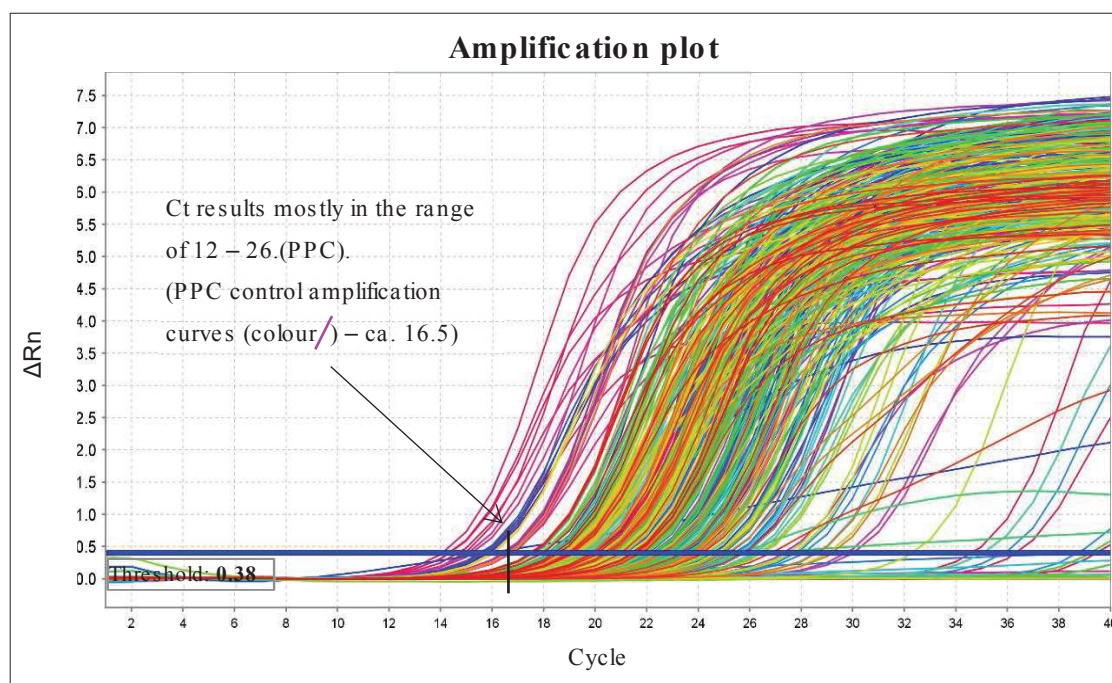

Figure 17. Positive results of PCR for cell lines in the mTOR PCR Array (after run with reaction parameters modified).

A further amplification plot was run for FFPE peripheral and internal zones of one ACC tumour, using the optimised condition for real time qPCR. On the amplification plot below, Ct curves are shown to be delayed, in spite of reaction conditions being correct (normal positive PCR control). In addition, the RT control data for these samples showed a pass, indicating that there were no problems with qPCR, with no indication of a positive influence or lack of inhibitors during the RT reaction. It can be concluded that not having sufficient yield and so not enough input template caused the observed delay in the curves for RNA from the FFPE samples.Templates of FFPE origin can always be expected to suffer some degree of degradation, but a proportion of the fragments will still be of sufficient length (Section 5.3).
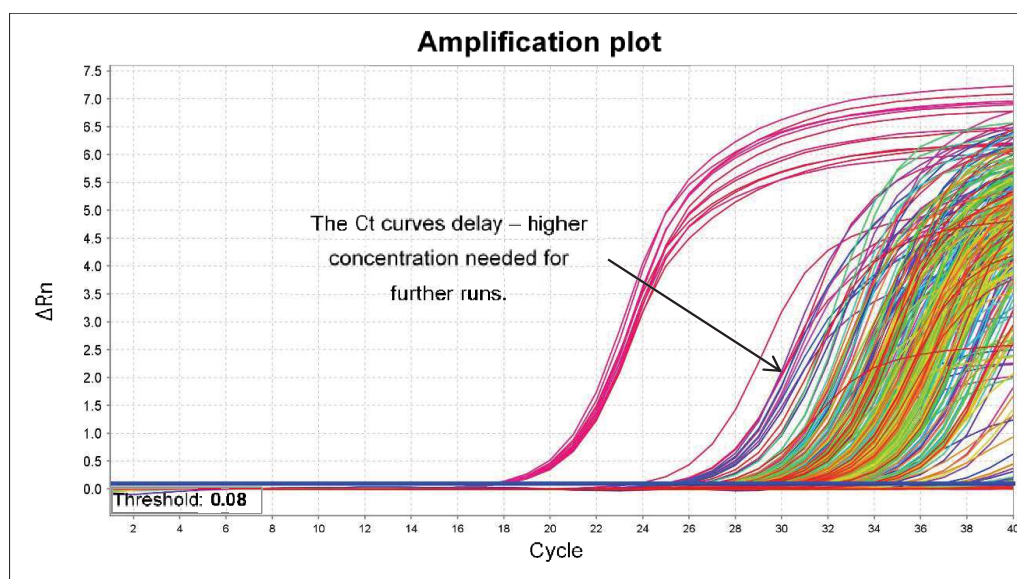
Materials and Methods

Figure 18 Amplification plot for FFPE originating from normal adrenal cortex and the peripherial zone of tumour.

However, this makes it difficult to estimate how much of a template is required. Because RNA from FFPE of adrenal cortex tumours may be very precious, using 200 ng input RNA was first attempted. Finally, it was established that the amount must be more than 500 ng. This was then confirmed on checking the QIAGEN company advice, which was that for use of FFPE RNA the requirement is between 500 ng to 1 µg input RNA.

3.3.6 Two-step qPCR results, reference gene for cell lines from mitotane induction and control

Table 11. Report showing representative results for beta-Actin for mitotane treated sample MCF-7 in duplicate.

No.	Colour	Name	Type	Ct
1		HKE3	Control	14.88
2		HKE3	Control	14.91
3		MCF7	Control	13.56
4		MCF7	Control	13.57
5		HI975	Control	13.26
6		HI975	Control	13.27
7		H295R	Control	13.92
8		H295R	Control	13.92
9		HKE3	Mitotane	16.56

69

Materials and Methods

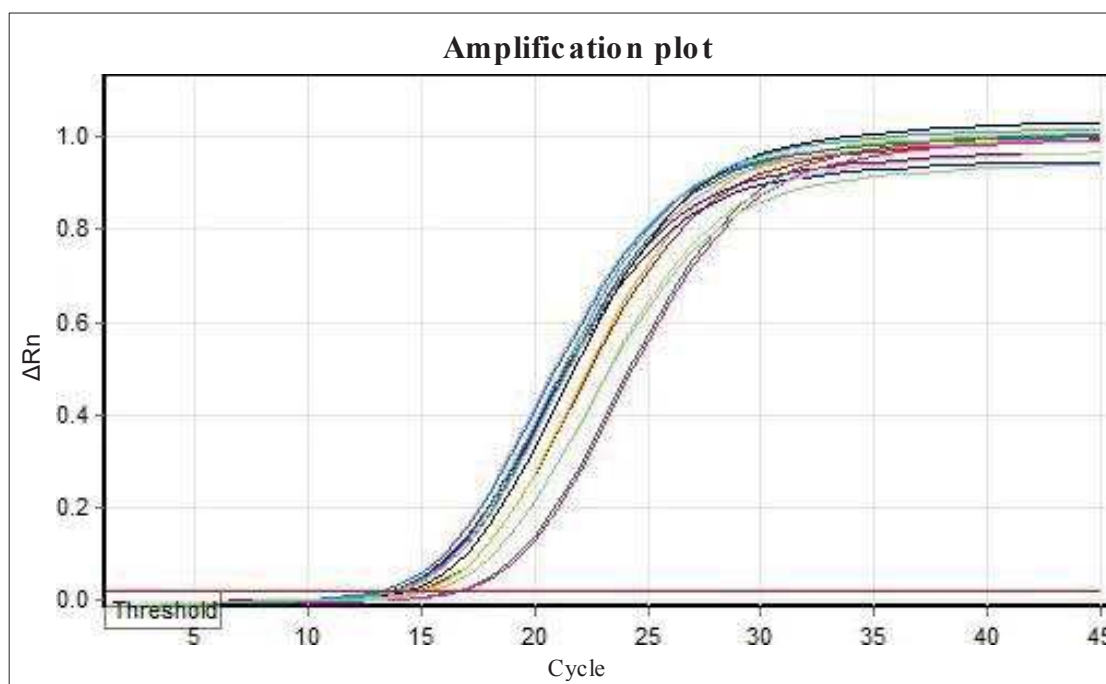| No.	Colour	Name	Type	Ct
10		HKE3	Mitotane	16.70
11		HI975	Mitotane	14.33
12		HI975	Mitotane	13.84
13		H2975	Mitotane	15.42
14		H2975	Mitotane	15.30

Figure 19. *Report showing representative results for beta-Actin for mitotane treated sample MCF-7 in duplicate.*

Beta-Actin and GAPDH expression analysis by real-time PCR, based on the cDNA template before preamplification, was carried out as an available array result validation. The results of the SYBR Green I-based method are presented as report tables with reaction parameters, Ct (cycle threshold) values and amplification plot, generated by *Rotor-Gene 6000 Series Software 1.7*. One example report for beta-Actin (MCF-7 mitotane treatment) is shown (Table 11, Figure 19), and other reports looked very similar. A table showing all Ct results in duplicates is given below, for sample dilutions1:10:

Table 12. *Ct values for reference genes used in mitotane experiments.*

Cell line name	Control		Mitotane treatment	
	beta-Actin Ct	GAPDH Ct	beta-Actin Ct	GAPDH Ct
H295R	13.92	14.89	15.42	15.69
	13.92	15.01	15.30	15.31
H1975	13.26	13.58	14.33	14.76
	13.27	13.64	13.84	14.48

Hke-3	14.91	14.73	16.56	15.59
	14.80	16.76	16.70	18.12
MCF-7	13.56	15.06	14.29	15.44
	13.57	14.88	14.23	15.78

3.3.7 Quality control provided for the array analysis results

Each *RT² Profiler PCR Array* is equipped with controls that allow checking of the quality parameters relating to the subsequent stages of the experiment, beginning with the RNA quality check. Examination of ΔΔCT values resulting from the experiment allows a retrospective check on these quality parameters. The software used for array result data calculation — *RT² PCR Array Data Analysis version 3.5*, gives a clear check on the value of controls, showing a pass when the results are in the appropriate range.

Control 1. *PCR Array Reproducibility:* Every thermocycler has a different level of sensitivity and the cycling condition must be optimised. A value of 20±2 assures reproducibility of the results. The assay must be reproducible in order for the data to be admissible when comparing runs between separate plates.

Control 2. *RT Efficiency:* Verification of the quality of the RNA. The main factor determining the effectiveness of RT is the state of the RNA, which can be impure, degraded or have chemical modifications that are inhibitors of proper transcription of the RNA into cDNA. This special control was possible thanks to the *Control P2* added during the RT reaction. When the control is passed, it means that the nucleic acid was good enough.

Control 3. *Genomic DNA Contamination***:** Elimination of genomic DNA is essential for production of truthful PCR results. It is important that gene expression analysis is not affected by gDNA amplification. This control can detect how effectively gDNA contamination was removed from the samples. It should have a Ct value less than 30 — a higher value indicates the presence of gDNA. All 16 samples in the experiment fulfilled the criteria for a pass.

Table 13. *Test results produced by the software for quality control with calculations supporting test results.*

1. PCR Array Reproducibility:			All Samples Passed	
Array	Sample 3	Sample 4	AVG	ST DEV
Average Ct (PPC)	18.29	18.19	18.24	0.07
ST DEV Ct (PPC)	0.75	0.06	0.41	--

Average Ct (RTC)	23.04	23.21	23.13	0.12
ST DEV Ct (RTC)	0.08	0.04	0.06	--

Criteria for the PCR Array Reproducibility: If the Average PPC Ct is 20±2 and no two arrays have an average PPC Ct of > 2 different from each other, then the sample and group pass.

2. Reverse Transcription Control (RTC):		All Samples Passed
Array	Sample 3	Sample 4
Delta Ct (AVG RTC - AVG PPC)	4.75	5.02
RT Efficiency	Pass	Pass

Criteria: If Delta Ct (AVG RTC - AVG PPC) ≤ 7, RT efficiency reports 'Pass'; otherwise, RT efficiency reports 'Inquiry'.

3. Genomic DNA Contamination (GDC):		All Samples Passed
Array	Sample 3	Sample 4
Ct (GDC)	35	35
Genomic DNA	Pass	Pass

Criteria: If Ct(GDC) ≥ 30, then the GDC QC reports 'Pass'; if 30 > Ct(GDC) ≥ 28, then the GDC QC reports 'Validate'; If Ct(GDC) < 28, then the GDC QC reports 'Inquiry'.

The passed control showed that high standards were maintained for all samples used in the experiment. The gold standard for a qRT-PCR reaction was fulfilled, which proves that the ΔΔCT method can be applied.

3.3.8 Usefulness of quality assessment of FFPE-derived total RNA in further gene expression analysis with qPCR arrays.

This section considers implications from the current study for usefulness of FFPE-derived total RNA in further studies with qPCR arrays.

Total RNA quality depends on a combination of purity and integrity of the RNA. Purity of the sample is the most common assessment for controlling RNA quality and also the most often quoted in terms of transcript quantity. The 'integrity' of the sample describes whether the mRNA molecules are intact or fragmented (Nolan, Hands, & Bustin, 2006). RNA purity is commonly verified using optical density measurements. The Thermo Scientific NanoDrop 1000 Spectrophotometer is based on measurement of the

Materials and Methods

260/280 ratio, which detects the presence of protein or residual guanidine. This technique is the best for concentration measurement (Desjardins & Conklin, 2010), but it cannot detect co-purified components which can inhibit qPCR amplification in an assay specific manner. Such an approach can be particularly relevant to FFPE sample extraction. Given the fact that patient samples in human clinical studies are especially valuable, even using partially degraded RNA from FFPE becomes a goal to provide enough material to carry out gene expression studies by microarray analysis and qRT-PCR (Die & Román, 2012). RNA integrity is based on the ratio of ribosomal bands 18s and 28s. The most commonly used method, formaldehyde gel electrophoresis with ethidium bromide staining, requires visual assessment of the ribosomal bands. However, this method is currently regarded as less reliable due to appearance of the rRNA bands being affected by the electrophoretic conditions, ethidium bromide fluorescence and an influence of the amount of RNA being loaded. Further disadvantages include use of toxic chemicals that require special waste disposal procedures and a lack of sensitivity and specificity in comparison with modern genomic techniques (Fleige & Pfaffl, 2006). A new method for RNA analysis is based on the Agilent Bioanalyser 7500. The method assesses ribosomal bands and the entire electrophoretic track of the sample. This enables actual presence or absence of degraded products to be automatically determined and expressed as the RNA Integrity Number (RIN), which ranges between 1.0 to 2.5 for tested material. The RIN value is much lower than, for example, freshly isolated human PBMC, which has a RIN of 9.0, which means integrity is excellent. An assessment of FFPE-derived RNA based on the bioanalyser, in contrast, has been found to be impractical (Chung et al., 2008), (Oberli et al., 2008), (Johnson, 2014). Although FFPE RNA appears to be highly degraded, based upon the bioanalyser quality assessment, it is most likely that there are uniformly fragmented sequences across the full length, with the majority of the transcript being 75–100 bp (Niesen et al., 2013). Meaningful results might be obtained by careful microarray analysis, if working with moderate template degradation. In the context of qPCR, the likelihood of fragmentation within the priming region is significantly reduced, since qPCR generates amplicons as small as 60 bp (Bustin, Benes, Nolan, & Pfaffl, 2005).

Die & Roman (2012) scrupulously reviewed the influence of RNA quality on gene expression profiling. The best alternative for assessing RNA integrity is the use of 3':5' assay (Nolan et al., 2006), adopted from microarray users. The ratio represents the integrity of all mRNA in a given RNA sample by amplifying different amplicons. This observation is based on evidence that cDNA yield from sequences near the 5'end of

73

partially degraded mRNA is significantly less than from sequences near the poly (A) 3' tail. From an experimental point of view, the 3' base amplification is the most practical. A Process of cDNA synthesis, when reverse transcriptase extends the transcript from the 3' to 5' end of mRNA or the cleavage in the case of mRNA degradation, enhances reliable detection of gene expression (Die, Obrero, Gonzalez-Verdejo, & Roman, 2011). The tolerance of some gene expression profiling studies to sample degradation has been shown by Lee et al. (2013) and Li & Reilly (2008). No effect was observed of RNA quality on gene expression. Another study observed a significant influence only on a small number of the genes (Opitz et al., 2010).

The HMEM PCR Array contains an RT control and a positive PCR control, which allows cDNA synthesis efficiency assessment, (controls were described in Results). The qPCR array includes 5 housekeeping genes. It seems reasonable to use all of these for final quality assessment as it can help address the potential problem of not knowing what inhibitors might be present in FFPE-derived material.

Final RNA quantification is improved by using a normalisation method. Reference genes normalise mRNA quantification by removing the within-sample differences. It has been demonstrated that normalising significantly improves the determination up to 4-fold, meaning 75% mRNA is degraded (Fleige & Pfaffl, 2006). However, gene-specific variation is higher in degraded versus intact samples. Although the process of normalization does not completely resolve the effect of compromised RNA quality, it is the most crucial, so long as data analysis has been performed using samples on comparable RNA. It should be remembered that small expression differences from lower quality RNA should be considered carefully as they can give a false positive result, showing as much as a 5 fold change within a particular assay. In these circumstances, the result should be revalidated to assess limits of detection of the assay (Die & Román, 2012), (Perez-Novo et al., 2005). It is therefore important to carry out FFPE on this precious patient material. Purification of nucleic acids from FFPE is still a relatively new field, especially important as regards rare cancers such as ACC. The experiments presented in the thesis represent a step in gaining experience of this still developing method.

3.4 Statistical method used for data analysis

The crucial normalisation of qPCR results uses the Delta Delta Ct ($\Delta\Delta$CT) method, which is the most reliable, commonly used approach (Livak and Schmittgen 2001). The described method makes one important assumption about the PCR, namely that the amplification efficiencies of the reference control gene and the target gene of interest are approximately equal. Specifically, $\Delta\Delta$CT assumes that each PCR cycle will exactly double the amount of material in the sample, (i.e.: amplification efficiency = 100%), and also assumes that the reference genes are uniformly and constantly expressed in all samples, as well as in one or more reference samples. The expression of the other samples is then compared to that in the reference sample. The $\Delta\Delta$CT method requires one or more approximations but returns results similar to non-approximation methods, such as the standard curve method (Zhang *et al.*, 2015). The formula for the method is shown below:

$\Delta\Delta$CT=(Ct(target, untreated)−Ct(ref, untreated))−(Ct(target, treated)−Ct(ref, treated))

The delta calculation and significance of results are expressed as probabilities (*p*-values) and were calculated using *RT² PCR Array Data Analysis version 3.5 software*, created for *RT² Profiler PCR Array* data analysis. The software is made available to use at a QIAGEN website: http://pcrdataanalysis.sabiosciences.com/pcr/arrayanalysis.php.

The statistical analyses were kindly cross checked by Dr Piotr Waż, using both Qiagen software and with the computing model for $\Delta\Delta$CT in the R software environment.

3.4.1 Choice of reference value

In accordance with currently accepted procedure, which specifies that at least the 3 most stable reference genes be used (Pfaffl 2004), (Perez-Novo et al. 2005) gene expression data was normalized using as the most stable gene across the array UQCRC1 and the three most stable housekeeping genes GAPDH, ACTB and HPRT1. These were selected because they showed the smallest variations for Ct value across the samples. The arithmetic means for these were used during calculations. This method reduces the possibility of error in circumstances when conditions are not perfectly stable.

IV. Results

This chapter present results of comparison of respiratory chain gene expression of the genes involved in mitochondrial metabolism between H295R and the other cell lines, under basal conditions and following mitotane exposure.

Cells for the gene expression studies were collected after incubation in medium (basal conditions) and also after exposure to mitotane for durations and at concentrations that had been established to obtain optimum cytotoxic effects, ie: a threshold at which a proportion of the cells died. (Dworakowska et al. 2015).

Results were calculated using the ΔΔCT method as described in Section 3.4.1. This measure, after first normalising to the reference genes value, describes how much expression of a gene is different between one preparation and another, which may be different cell lines, as first presented below or for one cell line under basal conditions compared with the same cell line exposed to mitotane, as presented after. These results are presented as *fold change.* This approach provides a normalised measure of the difference or change: it is not a technique that can provide absolute calculation of the amount of mRNA generated.

This preliminary analysis highlights those genes for which calculated changes greater than 2 or 3 are observed, as arbitrary measures of importance. The use of 2-fold change accords with published criteria (A Zsippai et al. 2012). However, this index is subject to biological variation, so to enable calculation of statistical validity, it was necessary to group findings to have enough biological replicates, and these outcomes are presented later in the chapter.

The figures below present various parameters of gene expression for the human adenocarcinomas of the adrenal cortex, colorectal tissue, breast and lung cell lines. Scatter plots and heat-maps are used, explained in Appendix B, as well as standard bar charts. The vertical axis scale in each bar chart is the same for all cell lines, allowing visual comparison of intensity of reactions.

The genes of interest are shown in scatter plots, giving overall visual presentation of overexpression (upper corner, shown red) or underexpression (lower corner, shown green). Boundaries are marked for genes showing this change.

The clustergram below, derived from hierarchical cluster analysis, showing all samples under study, is explained in Appendix B.

Figure 20. *Clustergram of gene expression in the HMEM PCR Array. Adjacent numbers are experimental duplicates (eg: Sample 1, Sample 2). It can be seen that these have similar levels of gene expression. The dendrogram to the left indicates genes which are coexpressed.*

4.1. Comparison of energy metabolism gene expression under basal conditions for all cell lines

The calculation of fold difference between cell types was used to address the question as to how energy gene expression differs between the cell lines under study and especially to consider whether adrenal cells are different from the others. This general overview of the energy metabolism gene profile provides a context for examining the effects of mitotane. These comparisons began with breast cancer cells in relation to the others, since in this tissue, the Warburg effect is known to be operative, with the cells containing few mitochondria and undergoing relatively inactive oxidative phosphorylation, so that expression of the genes of complexes 1 to 5 might be expected be lower than for adrenal cells.

Comparison of these results (as detailed below 3 panels in Figure 21a and 21b) shows, as expected, that MCF-7 cells are less active than the other cell lines, with the most genes less expressed than in the others. The left to right sequence shows a descending order of activity of the panel of genes under study, enabling the cell lines to be placed in the order (least to most active) MCF-7, H295R, H1975, HKe-3. Comparison of the results shown in the lower 3 panels supports this interpretation. Taking into account the identity of the genes differently expressed, the higher expression in HKe-3 is dominated by genes in complex 1 when compared with H1975 and H295R but not in comparison with H1975. Considering the adrenal H295R cells, there are no clear tends in comparison with the other cells lines, with genes of all complexes represented and no single group dominating.

a)

MCF-7 vs. Hke-3
MCF-7 vs. H1975
MCF-7 vs. H295R

H295R vs. Hke-3
H295R vs. H1975
H1975 vs. Hke-3
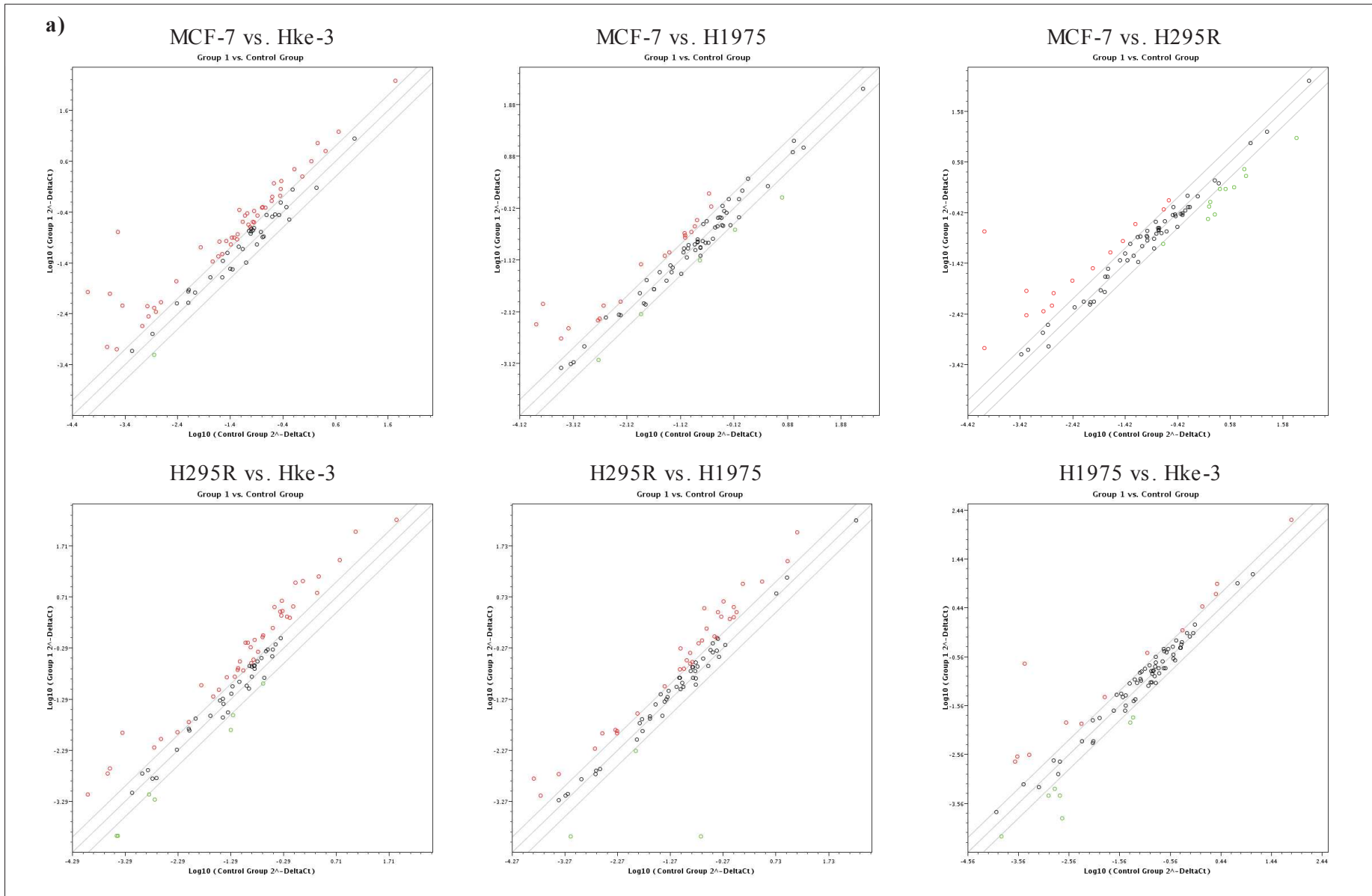
b)

MCF-7 vs. Hke3

complex	up	down	complex	up	down	complex	up	down
C I	NDUFA1	NDUFB8	C II	SDHA		CV	ATP5C1	
	NDUFA2			SDHC			ATP5G2	
	NDUFA3		C III	UQCRFS1			ATP5I	
	NDUFA4			UQCRQ			ATP5J2	
	NDUFA5		CIV	COX4I1			ATP5L	
	NDUFA8			COX5B		other	CYB561D1	ASB1
	NDUFAB1			COX6A1			EDN1	
	NDUFB10			COX6A2			GADD45B	
	NDUFB2			COX6B1			HSPA1A	
	NDUFB3			COX6C			MitoH2_5726	
	NDUFB4			COX7A2			RNU11	
	NDUFB5			COX7A2L				
	NDUFB7			COX7B				
	NDUFB9			COX8A				
	NDUFC1							
	NDUFC2							
	NDUFS2							
	NDUFS3							
	NDUFS4							
	NDUFV2							
	NDUFV3							

MCF-7 vs. H1975

complex	up	down	complex	up	down	complex	up	down
C I	NDUFA1		C III	UQCRFS1		C V	ATP5C1	
	NDUFA5			UQCRQ			ATP5F1	
	NDUFAB1		CIV	COX6A1			ATP5G2	
	NDUFB10			COX6B1			ATP5I	
	NDUFB7			COX6C			ATP5L	
	NDUFB9			COX7A2		other	CYB561D1	MitoH1
	NDUFC1			COX7A2L			EDN1	
	NDUFC2			CYC1			MitoH2_14573	
	NDUFS3						MitoH2_5726	
	NDUFS4						RNU11	
	NDUFV2						SLC25A25	
	NDUFV3							

MCF-7 vs. H295R

complex	up	down
C V	ATP5F1	ATP5I
		ATP5J
C IV	COX4I1	
	COX6A2	
	COX6C	
	CYC1	
C I	NDUFA1	NDUFA11
	NDUFA5	NDUFC1
	NDUFB10	NDUFS4
	NDUFV3	NDUFV1
other	CYB561D1	MitoH1
	EDN1	MitoH2_12106
	GADD45B	
	HSPA1A	
	RPLP0	

H295R vs. Hke-3

complex	up	down	complex	up	down	complex	up	down
C I	NDUFA11		C II	SDHA		CV	ATP5C	
	NDUFA2			SDHC			ATP5G2	
	NDUFA3		C III	UQCR11			ATP5I	
	NDUFA4			UQCRC2			ATP5J	
	NDUFA8			UQCRFS1			ATP5J2	
	NDUFAB1			UQCRH			ATP5L	
	NDUFB2			UQCRQ		other	EDN1	ASB1
	NDUFB3			ARRDC3			MitoH1	CYB561D1
	NDUFB4		CIV	COX5A	COX6A2		MitoH2_12106	DNAJB1
	NDUFB5			COX5B	CYC1		MitoH2_5726	HSPA1A
	NDUFB6			COX6A1			RNU11	
	NDUFB7			COX6B1				
	NDUFC1			COX6C				
	NDUFS4			COX7A2L				
	NDUFS6			COX7B				
	NDUFV1							
	NDUFV2							

H295R vs. H1975

complex	up	down	complex	up	down
C I	NDUFA1		C IV	COX6A1	COX6A2
	NDUFA11			COX6B1	
	NDUFB7			COX6C	
	NDUFC1		C V	ATP5C1	
	NDUFC2			ATP5G2	
	NDUFS4			ATP5I	
C II	SDHA	SDHC		ATP5J	
C III	UQCRH		other	MitoH2_1	DNAJB1
	UQCRQ				GADD45B
					HSPA1A
					HSPA1B

H1975 v Hke-3

complex	up	down
C I	NDUFA3	NDUFA1
	NDUFB2	NDUFC2
C II	SDHA	
	SDHC	
C IV	COX7B	
C V	ATP5G2	ATP5F1
	ATP5J2	
other	EDN1	ASB1
	GADD45B	CYB561D1
	HSPA1A	
	MitoH1	
	MitoH2_5726	
	RNU11	

Figure 21. *a)* *The expression of energy metabolism genes under basal conditions. These are shown as differences between cell lines presented as Scatter plots. Results in red show genes over two fold more expressed, green, over two fold less.* *b)* *Tables of results listing genes greater than two-fold different, grouped according to respiratory complexes. The ratio calculations are based on the 2nd over the first cell line of the named pairs.*

Results

4.2. Mitotane response: preliminary analysis based on over 2-fold changes

Changes in gene expression specified as Ct values were used to derive relative quantification of treated cells versus the untreated control group in the form of fold change. These show how much expression of a certain gene, or gene profile, was up or down regulated as a result of treatment.

The following profiles show normalised results for the genes with over 2-fold change in expression after 24 hours of mitotane treatment for H295R, and 72 hours for the other three cell lines. Under- or over-expression is marked in green and red respectively.

Scatter Plots present the gene expression profile of each cell line. These show fold changes — how each gene is differentially expressed between cell cultures exposed to mitotane (Group 1) and untreated (Control Group), both group normalized. Each plotted point represents values for $\log_{10} 2^{\wedge}\Delta CT$ for a single gene. Those shown in red represent higher expression and those with green, lower expression.Additional plots on the left hand side present genes expressed with over 2-fold change, and on the right hand side with over 3-fold change. The same rule applies to all cell line charts.

HMEM PCR Array gene groups indicated in Section 1.3 are shown, including respiratory complexes I to V, additional proteins and mitochondrial polycistronic units.

One alternative way of presenting changes of expression in graphical form that represents the array layout are heat maps (axes show the coordinates of the array wells). Heat maps were prepared for duplicate one and duplicate two of the material, enabling comparison between them.Genes on bar charts (Figures: 24,27, 30 & 33) are classified according to the complex they encode, i.e. mitochondrial complexes I, II, III, IV and ATPase, together with mitochondrial function-associated genes. Fold changes shown in red reflect higher expression and in green reflect lower expression, with the colour shades in the bar charts (eg: Fig 24) reflecting the – fold change using the same colours as in the heat maps (eg Fig 23). The vertical axis units represent fold change. This enables visualization of decrease and increase of gene expression following mitotane treatment. Such a method follows the style presented by Zhang *et al.* (2015).

Data presented in the scatter plots and bar charts below are calculated in the *RT² PCR Array Data Analysis version 3.5 software* as an average of the gene expression of duplicates for each cell line respectively. Colouring of bars on charts corresponds to $\log^2$ of the average expression in a similar manner to the heat maps.

81

4.2.1 ACC H295R profile, response to mitotane:

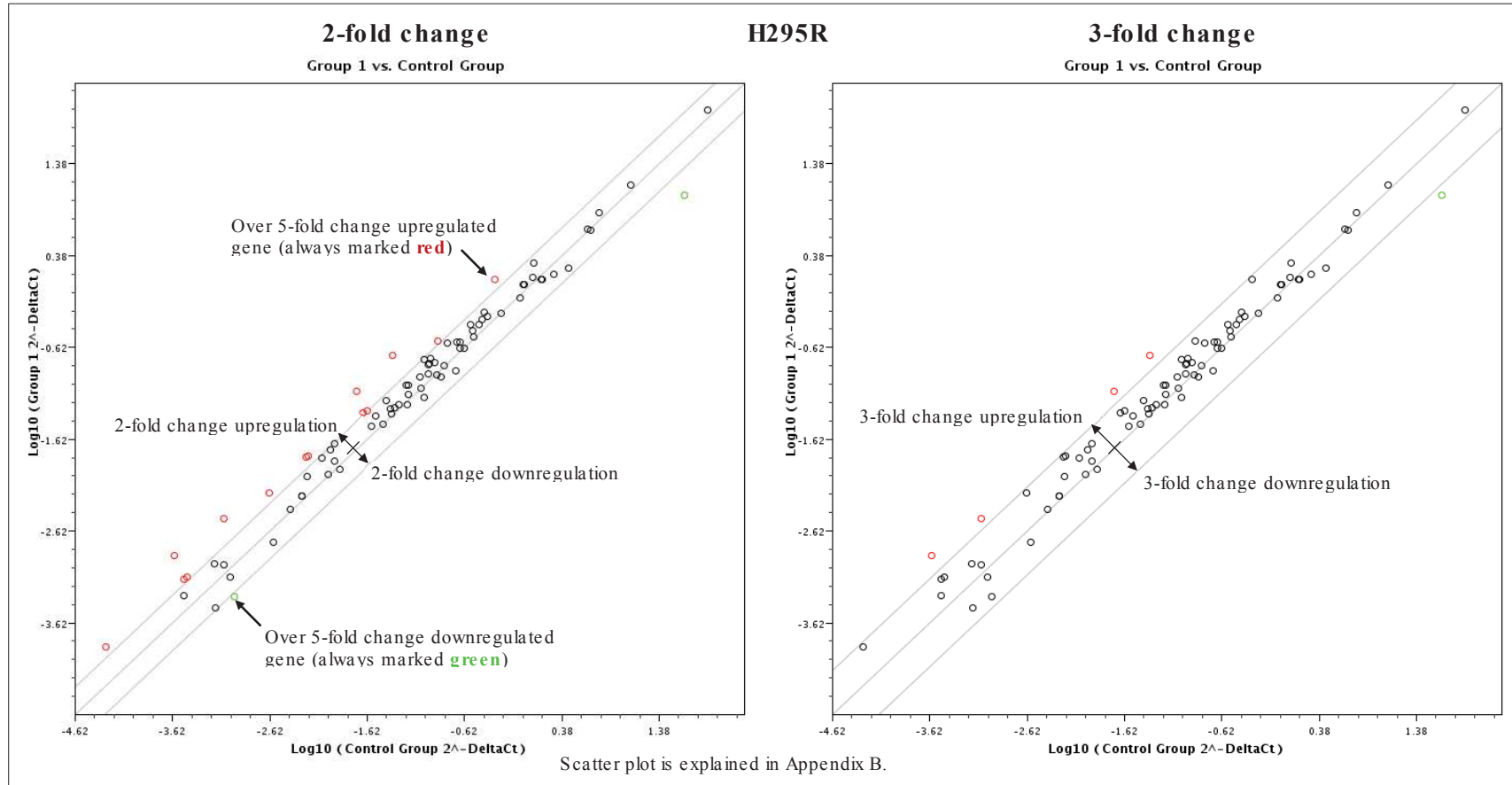**2-fold change**   H295R   **3-fold change**

Figure 22 Fold changes in response to mitotane in the gene expression profile of H295R. Genes expressed with over 2-fold change are shown on the left and 3-fold change on the right.
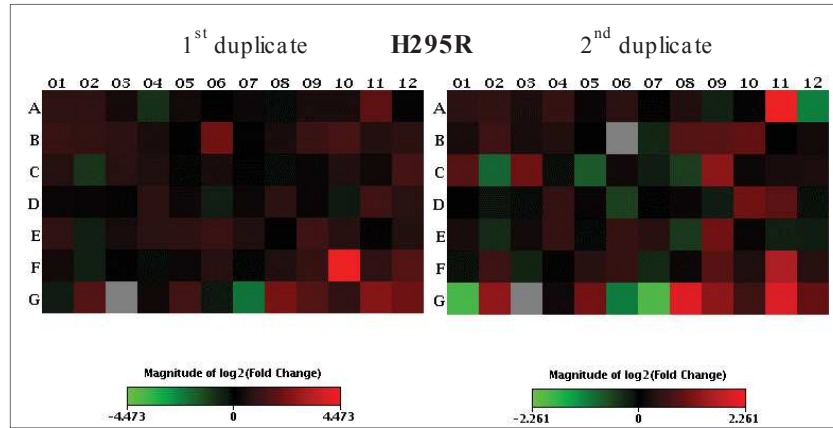
82

Results

Figure 23. *Duplicates one and two shown as heat maps, a graphical representation of similar fold regulation expression data between two groups overlaid onto the PCR array plate layout.*
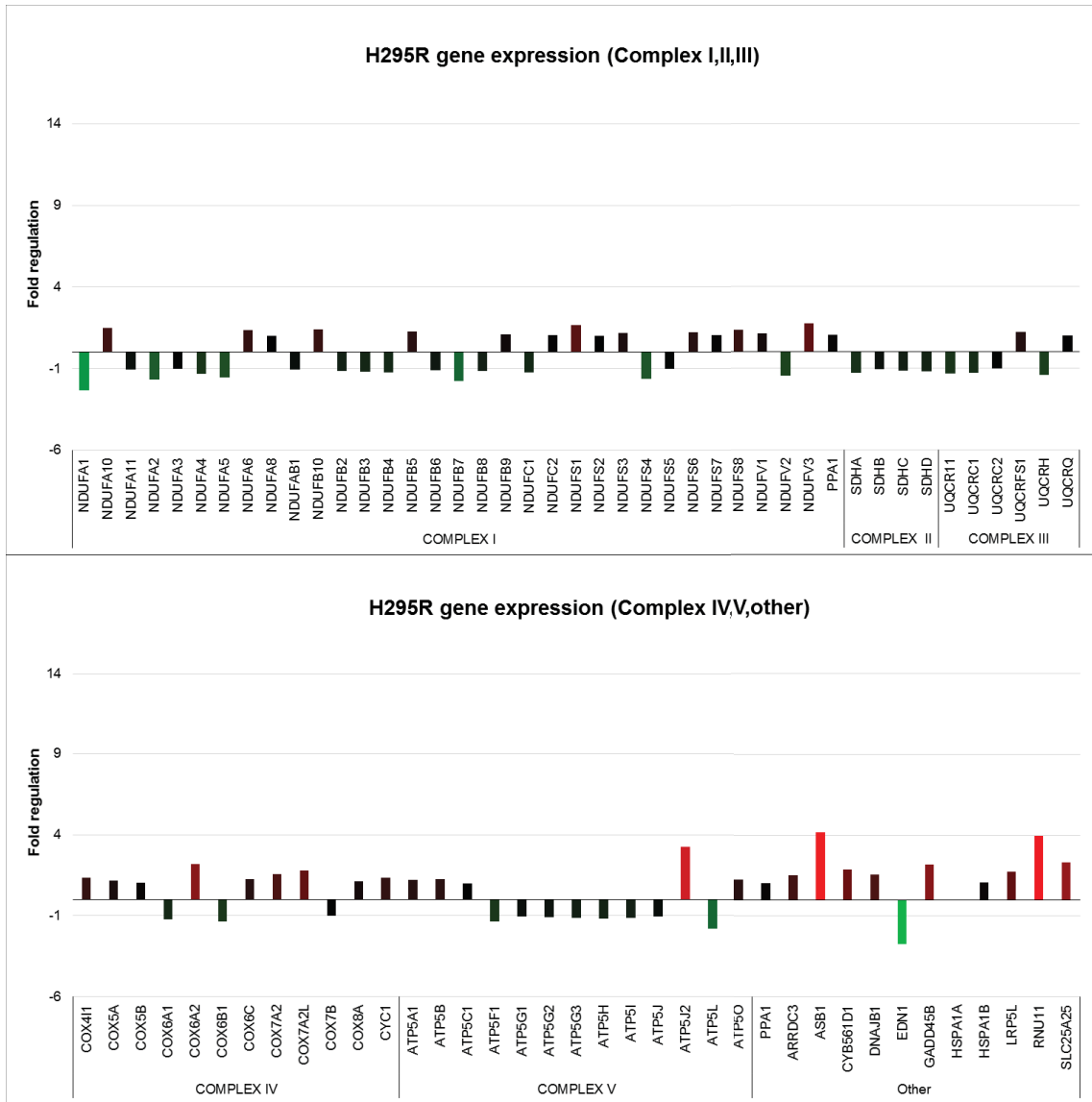

Figure 24. *Expression of individual genes in ACC H295R cells for all the nuclear genes examined.*

83

Results

For the ACC H295R cell line (section 4.2.1), the profile presented above shows that the genes for the respiratory complexes with the most changed expression are ATP6J2 upregulation in complex V, Upregulation of COX subunits, where COX 6A2 & COX7A2L are most strongly upregulated and NDUFA1, which is downregulated.

Considering the other 3 cell line profiles presented below, for HKe-3 (section 4.2.2), the common upregulation of respiratory complexes is visible; the most overexpressed are NDUF6F4, ATPG2 & ATP5I and COX7B. For H1975 (section 4.2.3) examples of the most visible changes are from respiratory complexes and are downregulation of NDUFS5, NDUFB4, ATP5B and upregulation of NDUF A11. For MCF7(4.2.4), most visible is upregulation of COX6A2 and COX7A2L and ATP6G2.

ACC H295R showed visible changes in response to mitotane towards overexpression of genes involved in mitochondrial energy metabolism, even though exposed to a smaller concentration of the agent (10 µM) and for a time of only 24h, in contrast with the other cell lines, which were treated for 3 days with 40 µM mitotane. HKe-3 also showed a strong response, with many over-expressed genes. A response of Lung H1975 to mitotane was visible, but with clear down regulation of some oxidative chain genes. Breast MCF-7, in contrast, showed little change. Common to all cell lines was a significant upregulation of NDUF85 (complex I), SDHA (complex III) and COX7B (complex IV), together with alternative splicing factor RNU11. The last of these is needed for mitochondrial polycistronic unit assembly. The mitochondrial gene precursors did not show a common expression pattern between the different cell lines.

There was a more than 2-fold upregulation of GADD45, a p53-regulated cell growth suppressor, after mitotane only for the ACC cell line; it was unchanged for the HKe-3 cell line and downregulated for the 'LS' cell lines.

SLC25A25 protein (an intermembrane mitochondrial carrier) also showed overexpression exclusively in ACC H295R.

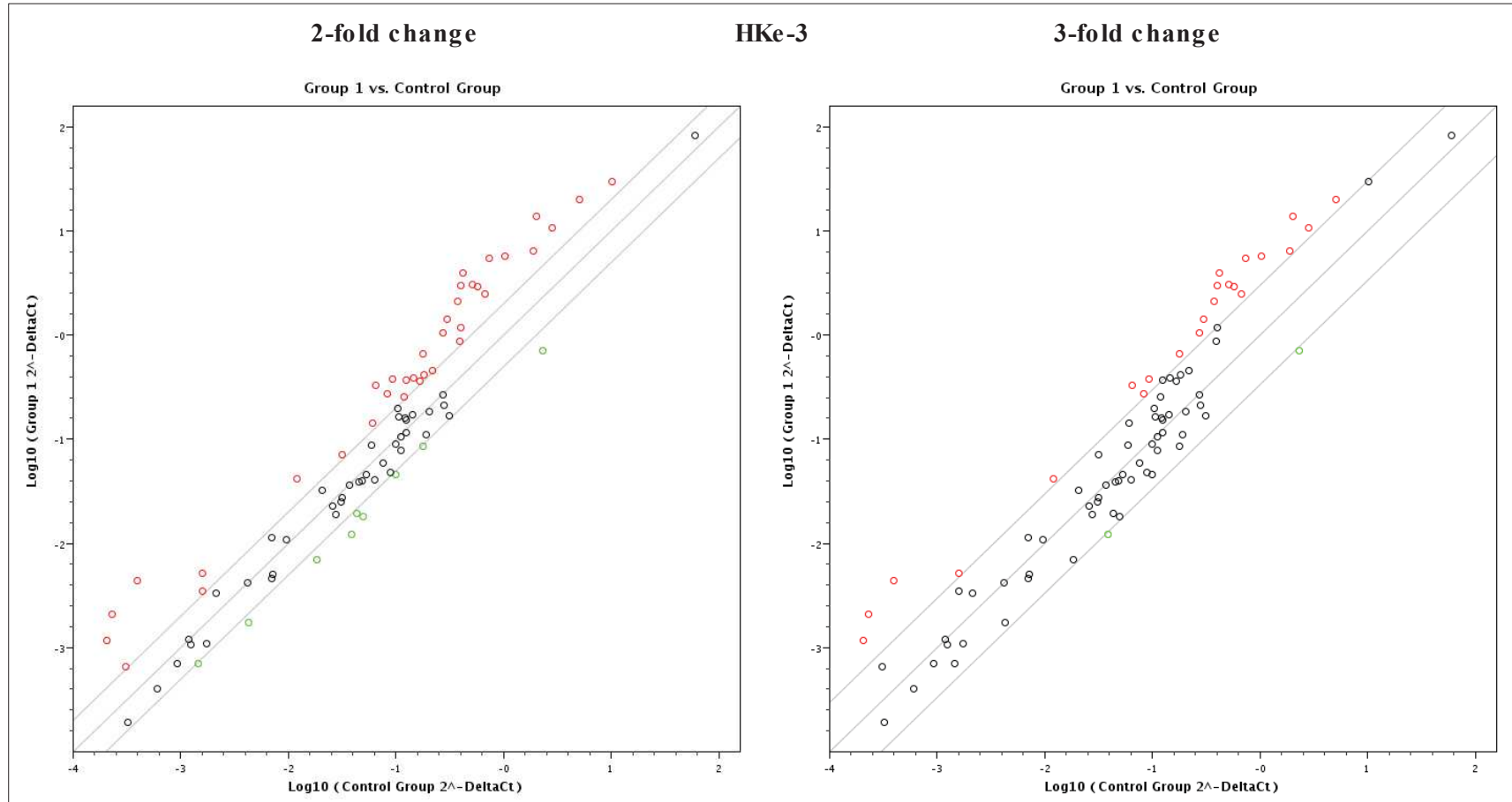## 4.2.2 Colorectal adenocarcinoma HKe-3 profile, response to mitotane:

Figure 25. *Fold changes in response to mitotane in the gene expression profile of HKe-3. Genes expressed with over 2-fold change are shown on the left and 3-fold change on the right*
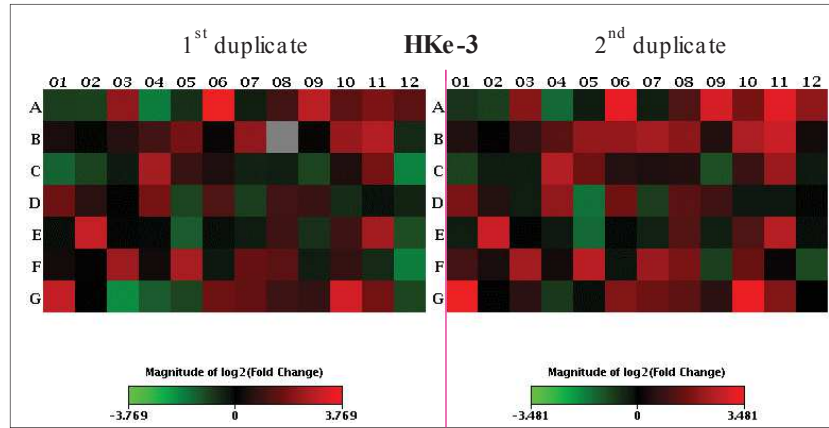
Results

Figure 26. *Duplicates one and two shown as heat maps, a graphical representation of similar fold regulation expression data between two groups overlaid onto the HMEM PCR Array plate layout.*
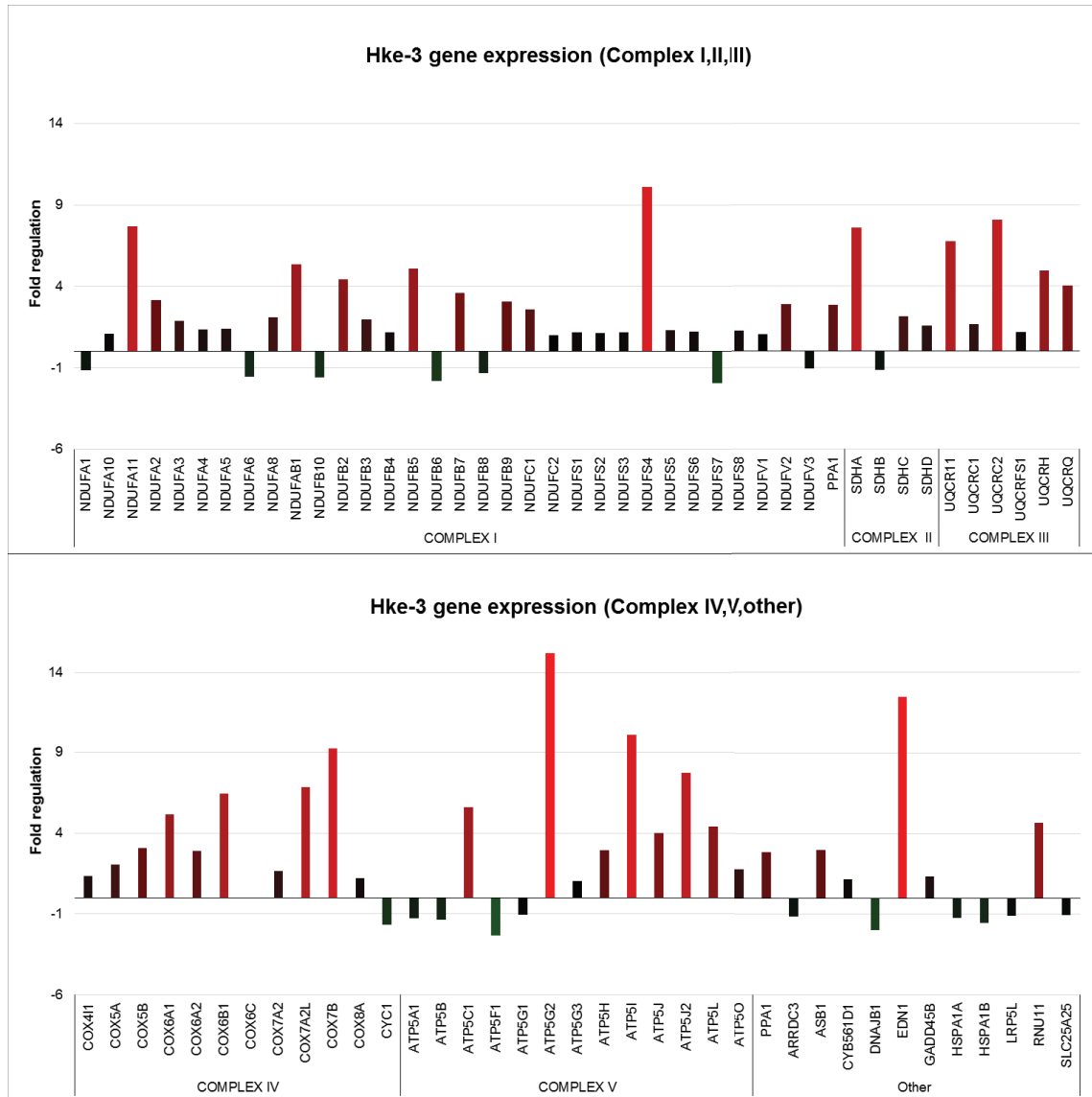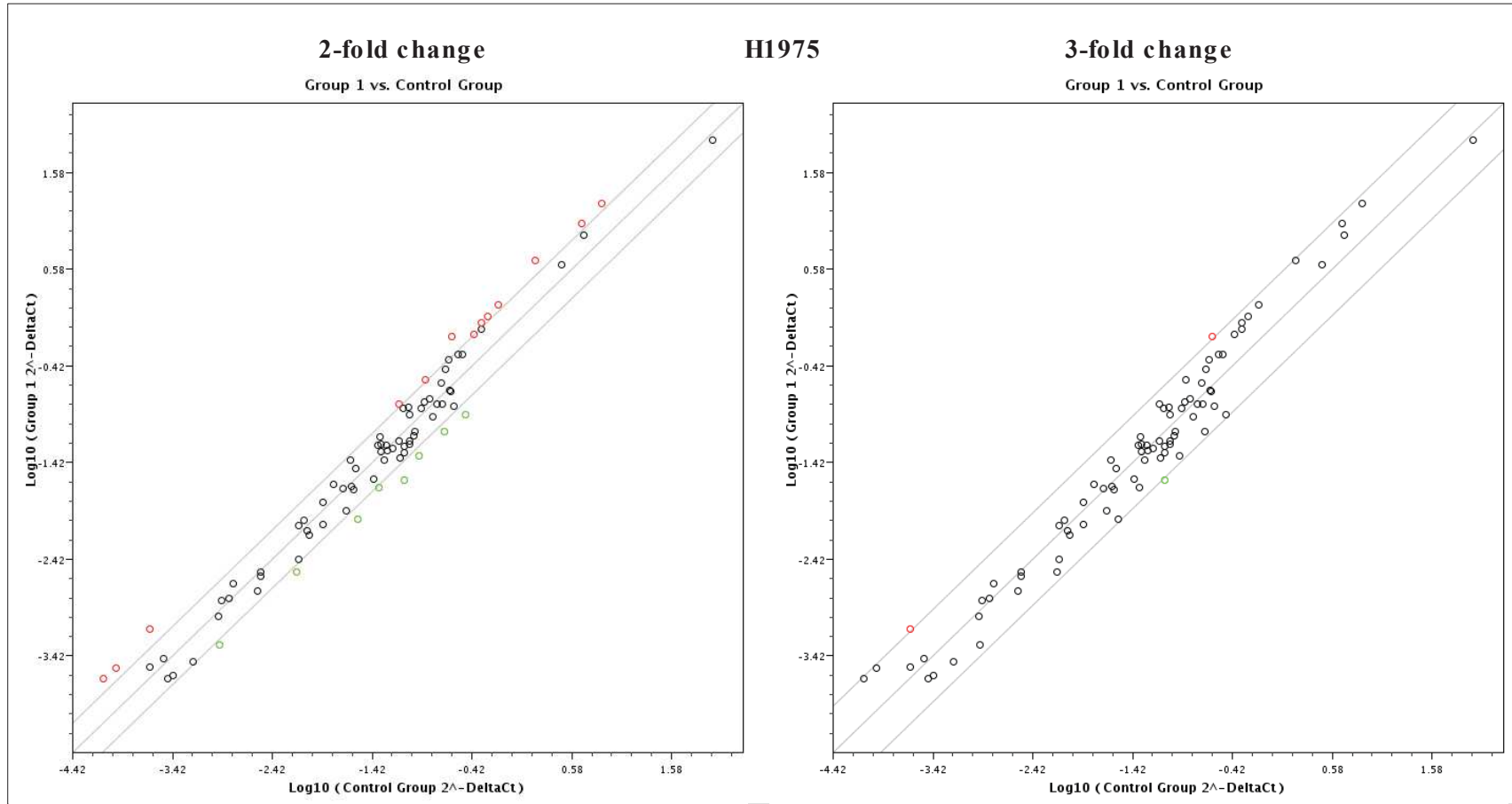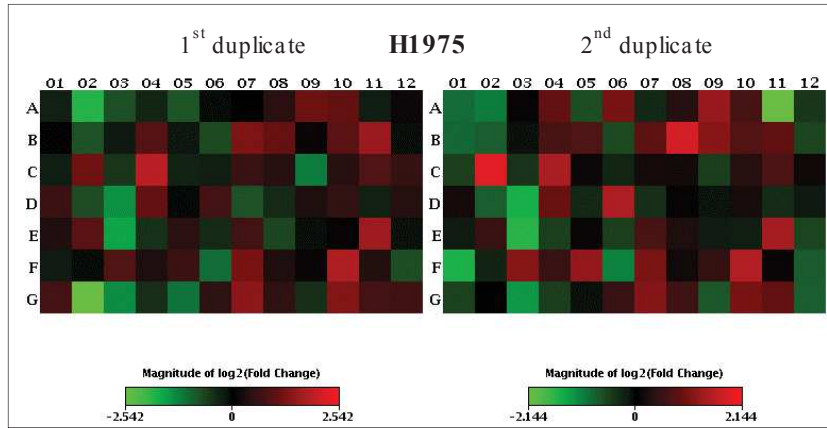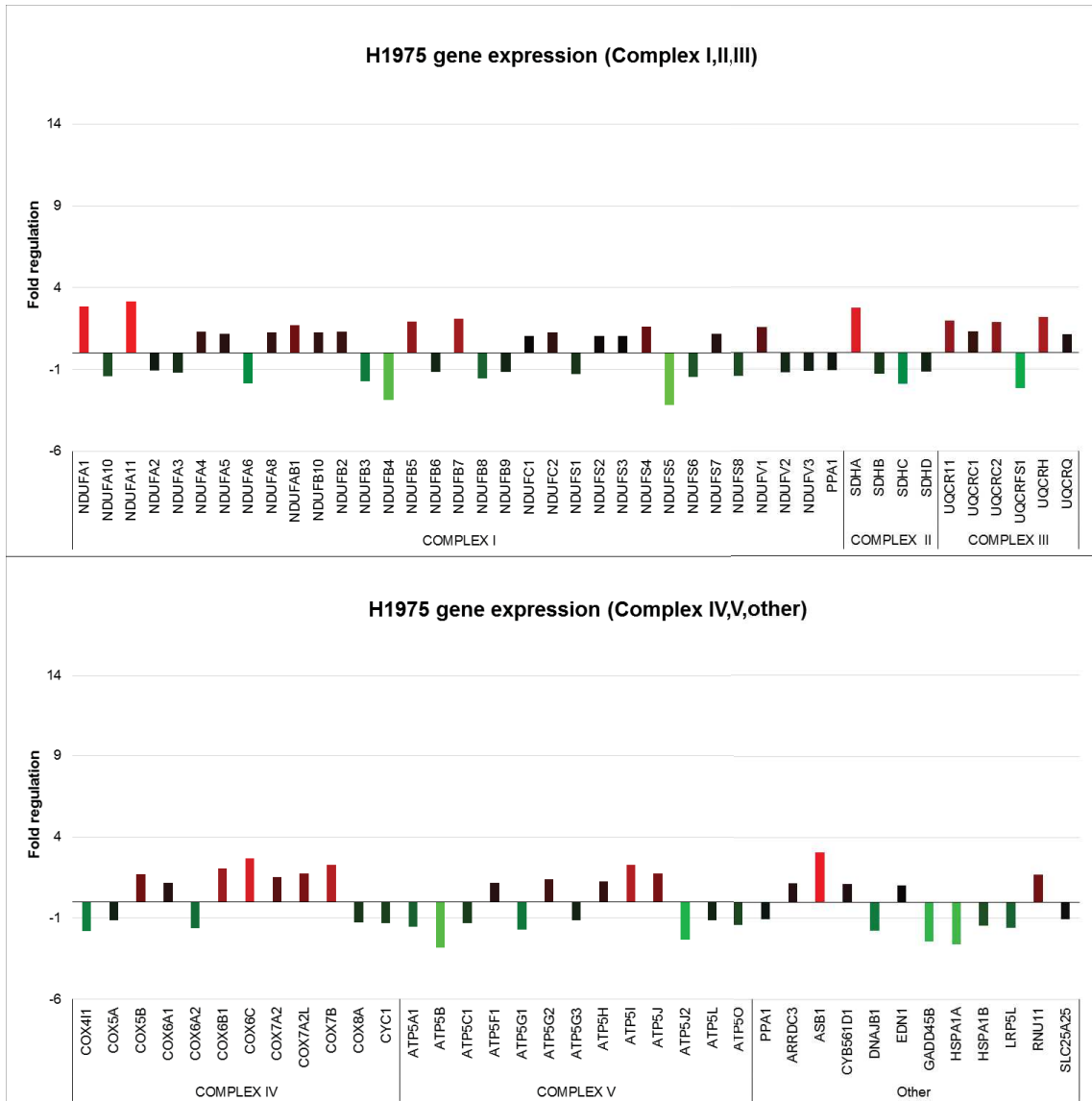

Figure 27. *Expression of individual genes in Hke-3 cells for all the nuclear genes examined.*

4.2.3 Lung adenocarcinoma H1975 profile, response to mitotane:
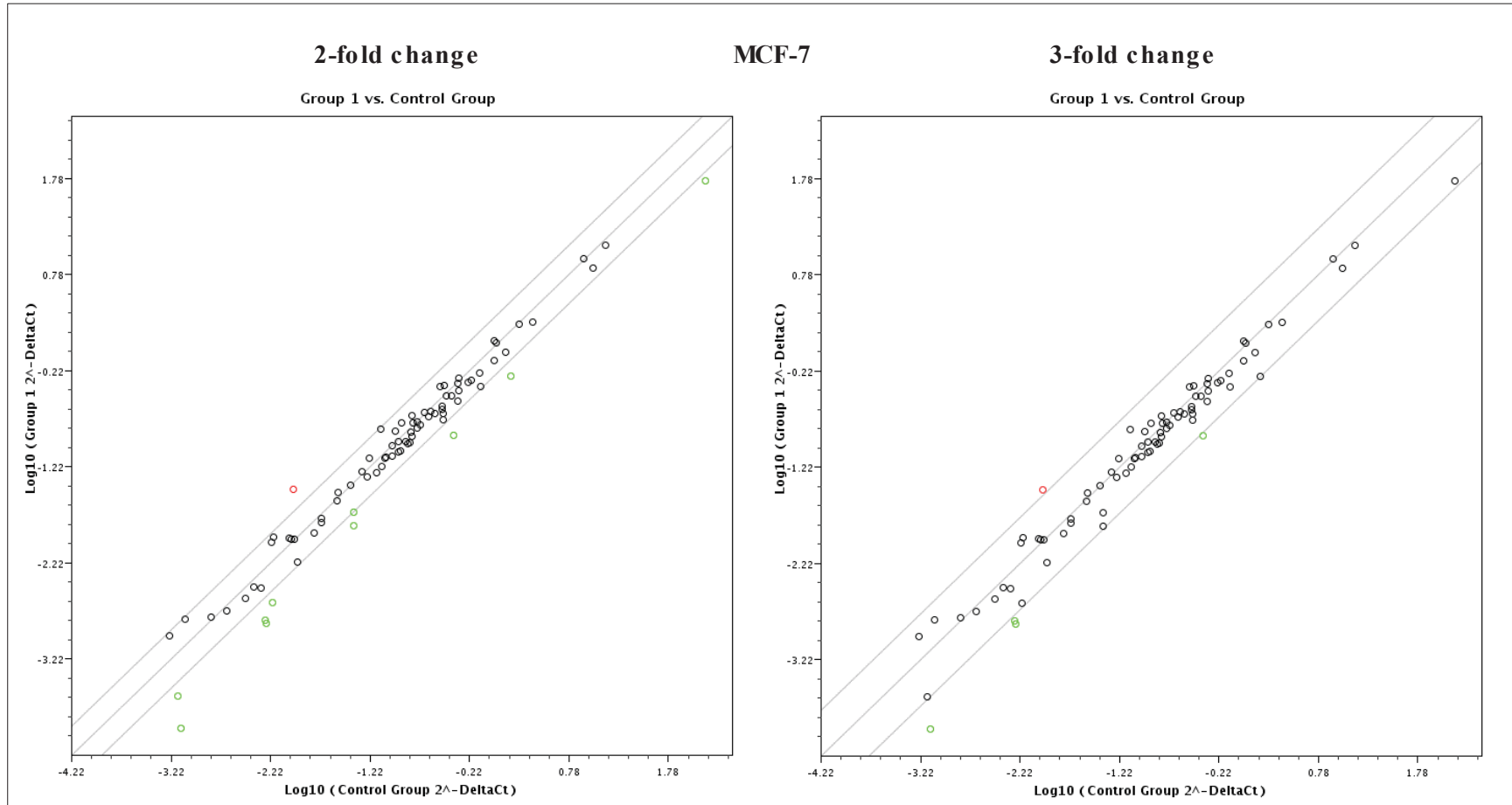

Figure 28. *Fold changes in response to mitotane in the gene expression profile of H1975. Genes expressed with over 2-fold change are shown on the left and 3-fold change on the right*
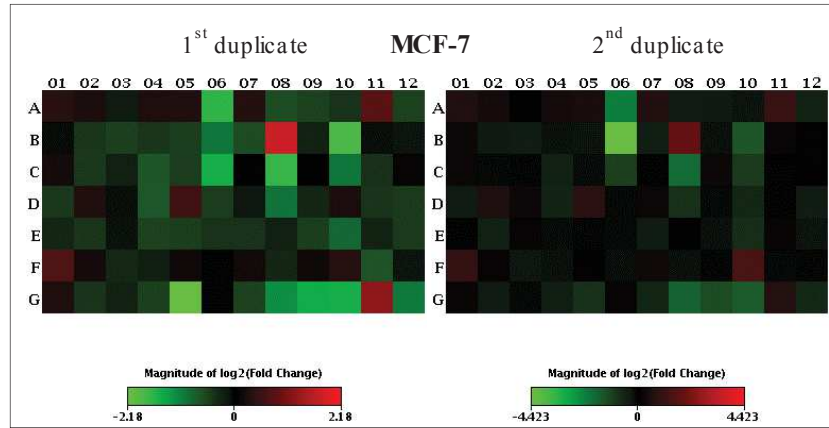
Results

Figure 29. Duplicates one and two shown as heat maps, a graphical representation of similar fold regulation expression data between two groups overlaid onto the HMEM PCR Array plate layout.

Figure 30. Expression of individual genes in H1975 cells for all the <u>nuclear genes</u> examined..

4.2.4 Breast adenocarcinoma MCF-7 profile, response to mitotane:

Figure 31*. Fold changes in response to mitotane in the gene expression profile of MCF-7. Genes expressed with over 2-fold change are shown on the left and 3-fold change on the right.*

Results

Figure 32. *Duplicates one and two shown as heat maps, a graphical representation of similar fold regulation expression data between two groups overlaid onto the HMEM PCR Array plate layout.*
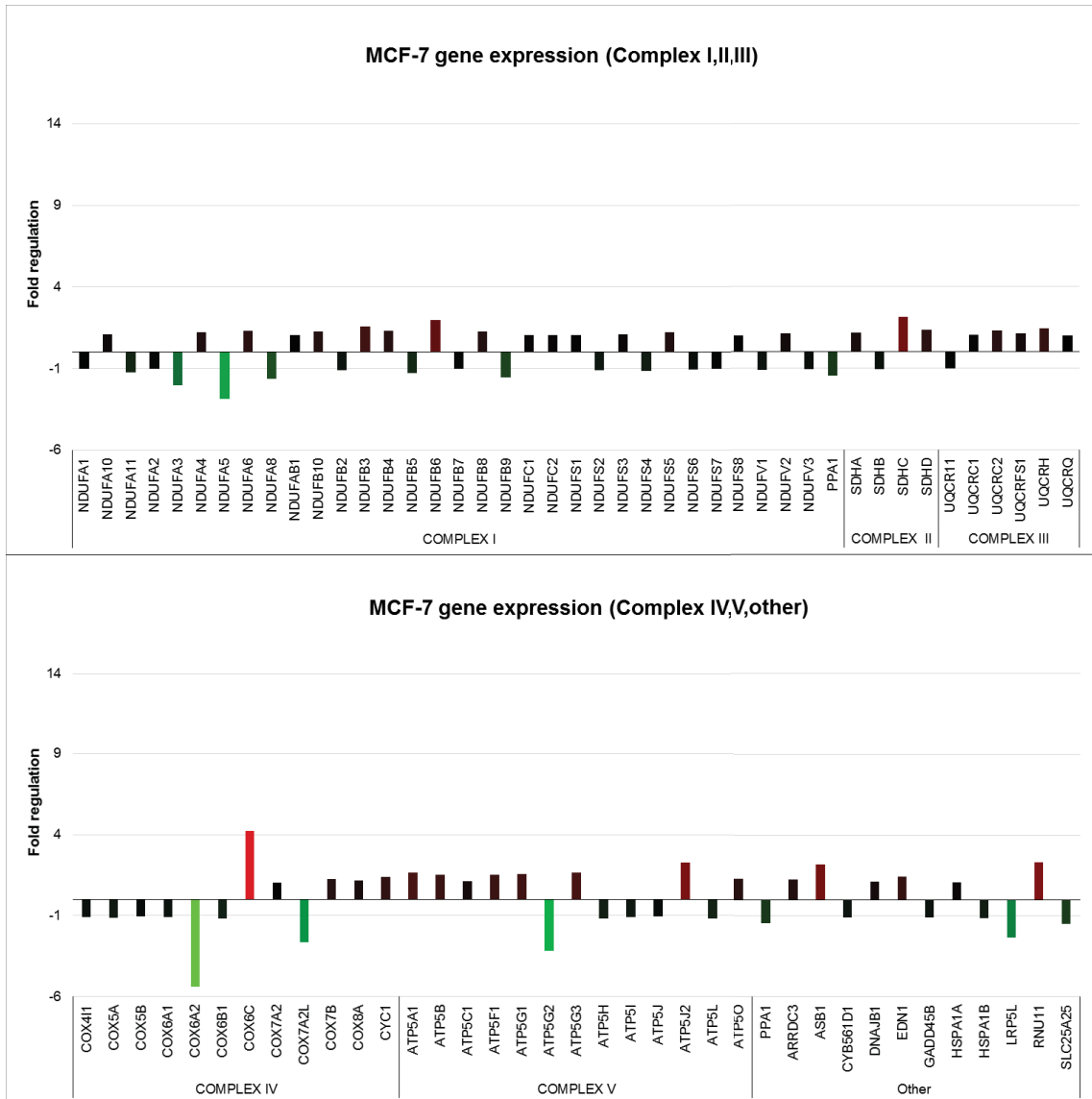

Figure 33. *Expression of individual genes in MCF-7 cells for all the* <u>*nuclear genes*</u> *examined.*

Results

The most important findings for cancer cell lines response to mitotane are summarised below. The growth arrest and DNA-damage-inducible proapoptotic factor (GADD45B) was over 2-fold overexpressed only for H295R. The gene SLC25A2 was also over 2-fold overexpressed only for H295R, with no changes (small overexpression below one) for other cell lines. The SLC25A2 encodes a transport protein essential for import of proteins into the mitochondria that are derived from nuclear gene expression.
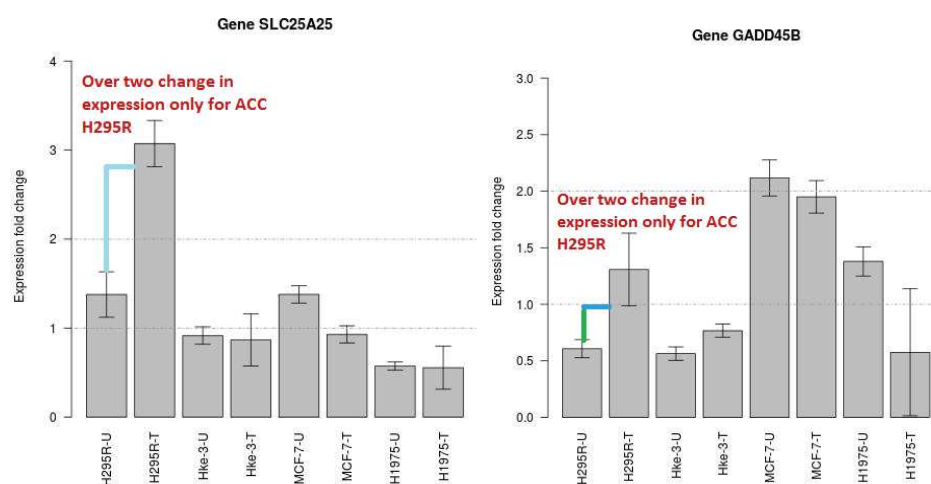

Figure 34 *Relative expression for SLC25A25 and GADD45B, meaning change in expression visible only for H295R. Figure generated in R with computing module ΔΔCT.*

EDN1 was strongly overexpressed for the HKe-3 cell line. This codes for Endothelin-1, which is generated by vascular endothelial cells and is upregulated in response to hypoxia,

Gene RNU11-1 was 3.6x overexpressed in H295R cells and 4.6x overexpressed in HKe-3 cells. This gene codes for RNU11 small nuclear RNA, which activates the alternative splicing mechanism, so this gene product might be needed for the generation of genes from the large H2 transcript.

Although five biological replicates of each cell preparation were pooled together before carrying out gene expression studies, so that the results are representative within the group (Irizarry and Love 2014), the use of fold change is the only valid way of expressing this data, since single comparisons of a pair of duplicates does not provide sufficient data points to enable calculation of significance (p-value). It therefore only provides an indication of mitotane effects and cannot be used to draw reliable conclusions.

Results

4.2.5 Expression profile of the nuclear genes involved in mitochondrial metabolism: comparison between H295R and the other cell lines

The bar charts below show a summary of meaningful (over 2-fold) change in genes required for mitochondrial chain complexes and other nuclear-encoded proteins connected with mitochondrial metabolism, comparing cells exposed to mitotane as described in the chapter introduction versus untreated cells.
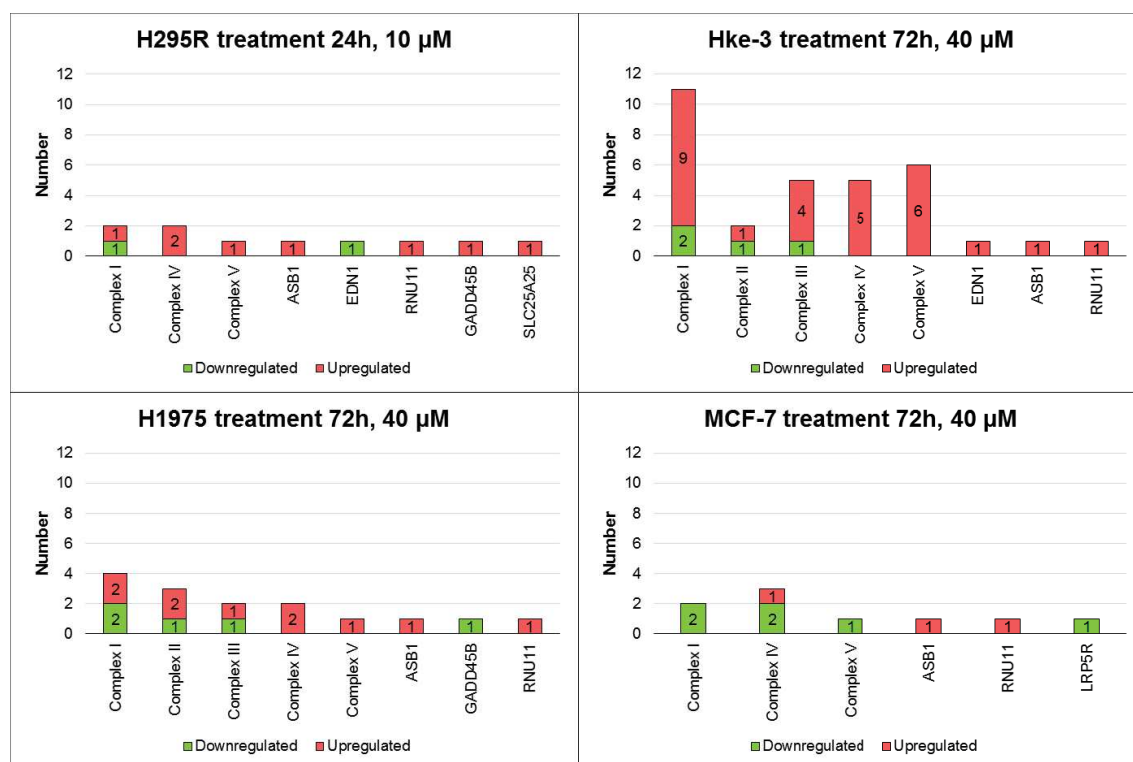

Figure 35. Comparison of the number of genes differentially expressed for the four cell types under study.

The number of genes with over 2-fold change in expression between mitotane treatment and control are shown for mitochondrial complexes I, II, III , IV, ATPase & other proteins, labelled on the x axis. The y axis units are number of genes, with those shown in red having higher expression, and those in green having lower expression.

4.2.6 Mitochondrial genome expression after mitotane treatment for all ACC cell lines

The bar chart below (Figure 36) presents data on genes from the entire mitochondrial mRNA transcript, comprising mitochondrial polycistronic units H1 and H2 (H2 amplified

92

Results

by 4 sets of primers). These comprise precursors of mitochondrial genes, rRNAs and tRNAs, which are then separately generated by endonuclease cleavage.
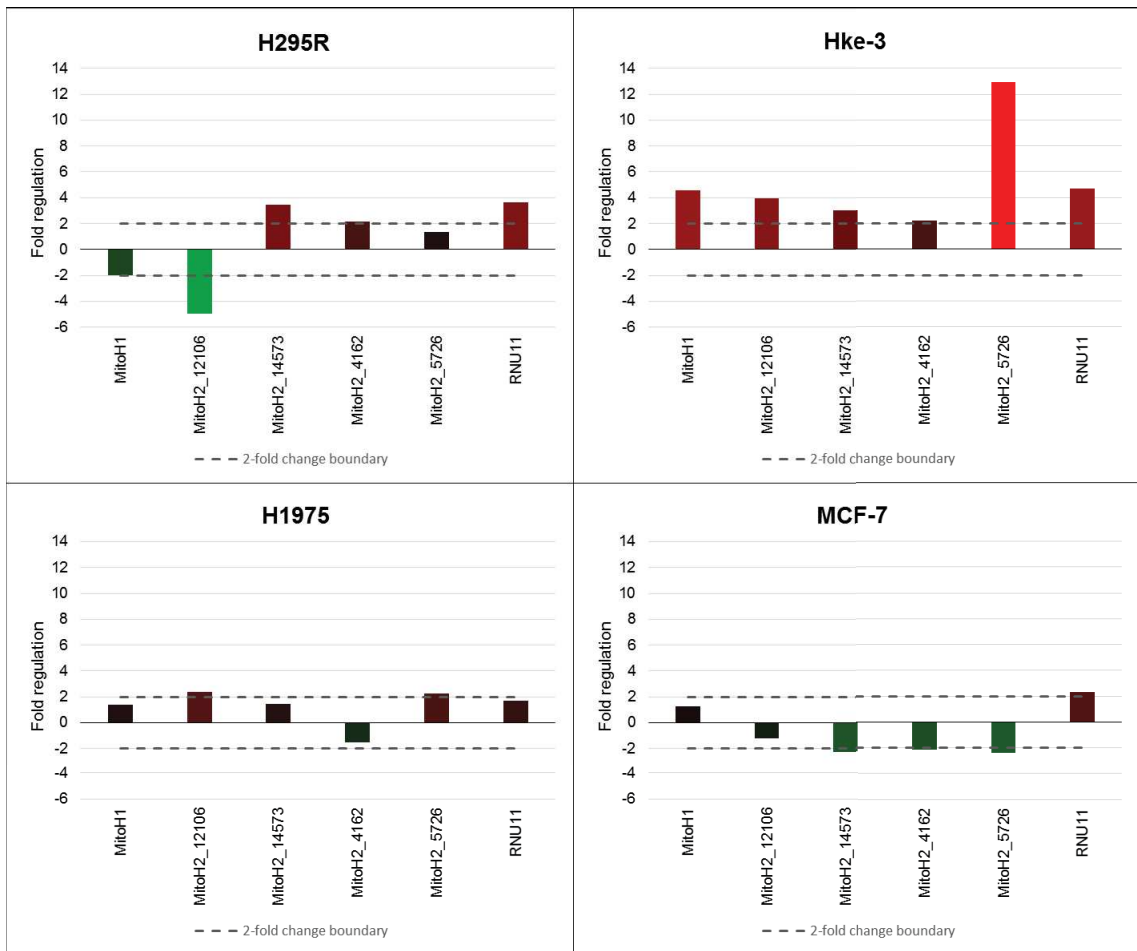

Figure 36. *Expression profile of mitochondrial polycistronic unit expression for four adenocarcinoma cell lines.*

Higher changes in expression occurred selectively for H295R and Hke2

4.2 Comparison of gene expression in all cell lines

The following plot is intended to show action of mitotane on the mitochondrial respiratory chain overall for all cell lines. The gene expression profile is shown below with significant results presented as a histogram of *p*-values, followed by a volcano plot showing significantly downregulated genes (see appendix B for explanation)
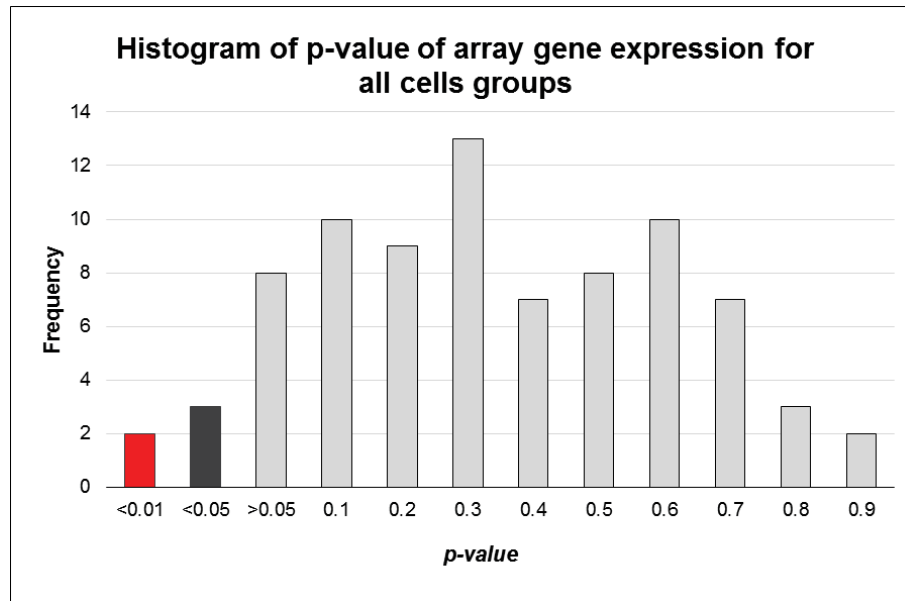
Figure 37. *Histogram of p-values representing a profile of gene expression according to statistical significance for the 84 genes present on the HMEM Array.*

Figure 37 shows samples relating mitotane treatment & control – significant results are those over the 0.05 boundary.

Table 14 identifies the significantly upregulated genes. These comprise NDUF85 (complex I), SDHA (complex III) and COX7B (complex IV), together with RNU11. No results show over two fold change.

Table 14. *Results for mitotane treatment versus control, showing significantly regulated genes above boundary p= 0.05.*

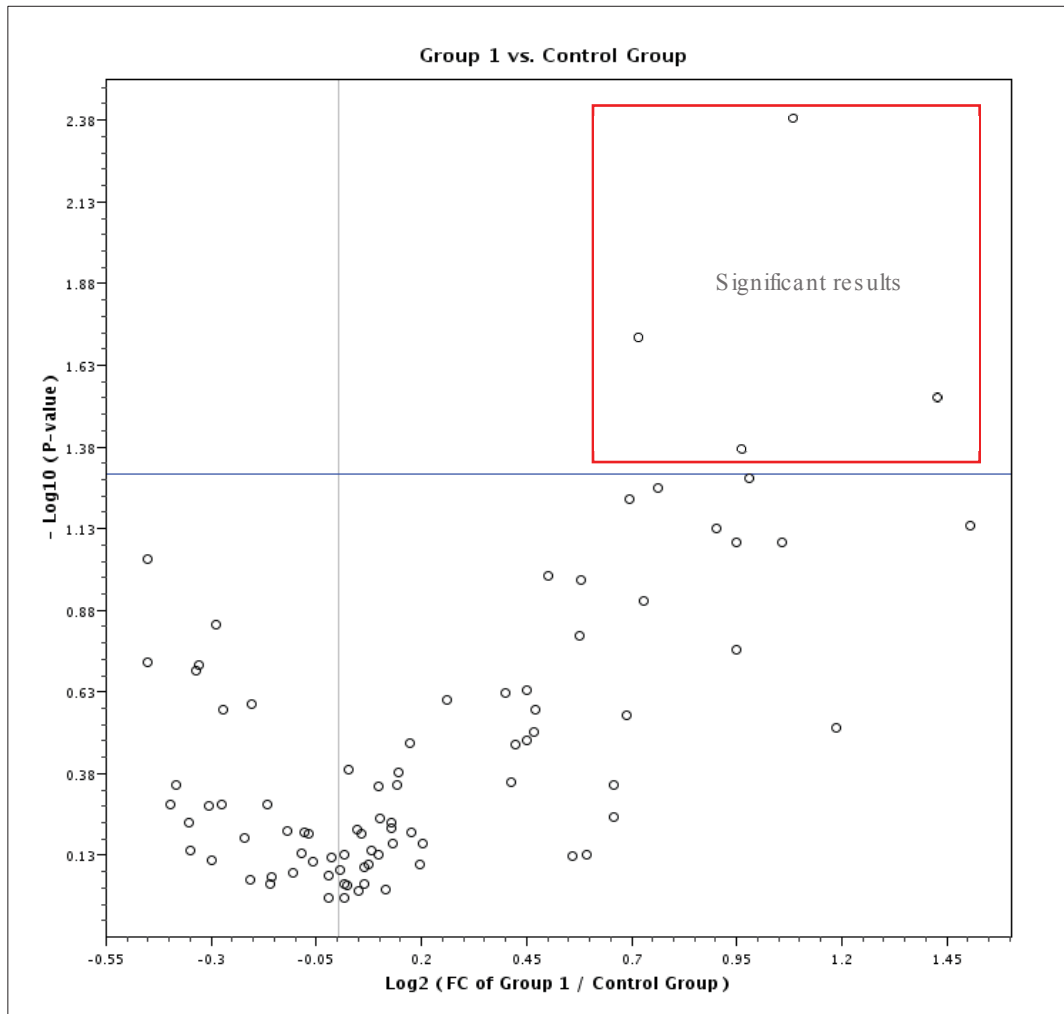| Gene	*p*-value	Fold regulation
COX7B	0.004092	2.12
NDUFB5	0.019120	1.65
SDHA	0.041957	1.95
RNU11	0.029242	2.69

Figure 38. *Volcano plot presenting the expression profile for all four human cell lines.*

4.3 Calculation of significance of expression changes in response to mitotane after grouping the data according to mitotane sensitivity

According to current statistical theory, single or paired observations are insufficient to enable valid comparisons between groups (Livak and Schmittgen 2001) so that the data presented above, expressed as fold change, cannot be used to determine whether a finding is significant, although it provides useful pointers to further work. This could have been done by repeat experiments, but this was not possible within the constraints of this project.

Cytotoxic influence of mitotane was observed for all cell lines (Dworakowska et al. 2015). In order to have more than the minimum of 3 observations per group, the data were classified according to the degree of mitotane response described in the chapter introduction. Based on this, the HKe-3 cells treated with 40 μM mitotane and H295R cells treated with 10 μl mitotane were more susceptible to this agent (27 and 48.5 % respectively) in comparison with MCF-7 and H1975 cells, which were relatively less sensitive (40.2 and 28.6% respectively). Statistical analysis of gene expression thus compared these 'more sensitive', (*MS*, H295R & HKe-3) and 'less sensitive' (*LS*, H1975 & MCF-7) groups. Treatment versus control results for these two groups are presented as plots and tables. The main results for significantly up or down regulated genes with *p*-value < 0.05 are shown. Over 2-fold changes indicating important under- or overexpression of genes are also shown.

4.3.1 Mitotane versus control profile for MS and LS group.

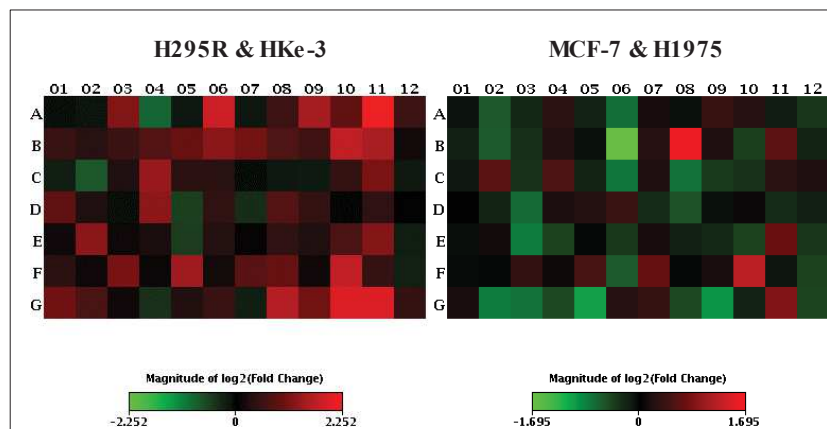Heat maps showing visualization of log$_2$ fold change for both analysed groups.

Figure 39. *Expression magnitude for genes in HMEM Array after mitotane treatment ('MS' group – left, 'LS' group – right).*

Results

Volcano plot: $y = -\log_{10}$ (p-value), Significantly regulated genes $p < 0.05$ over blue boundary; $x = \log_2$ fold change, genes expressed with over two-fold change upregulated and downregulated shown in red and green respectively. Volcano plot is explained in Appendix B.
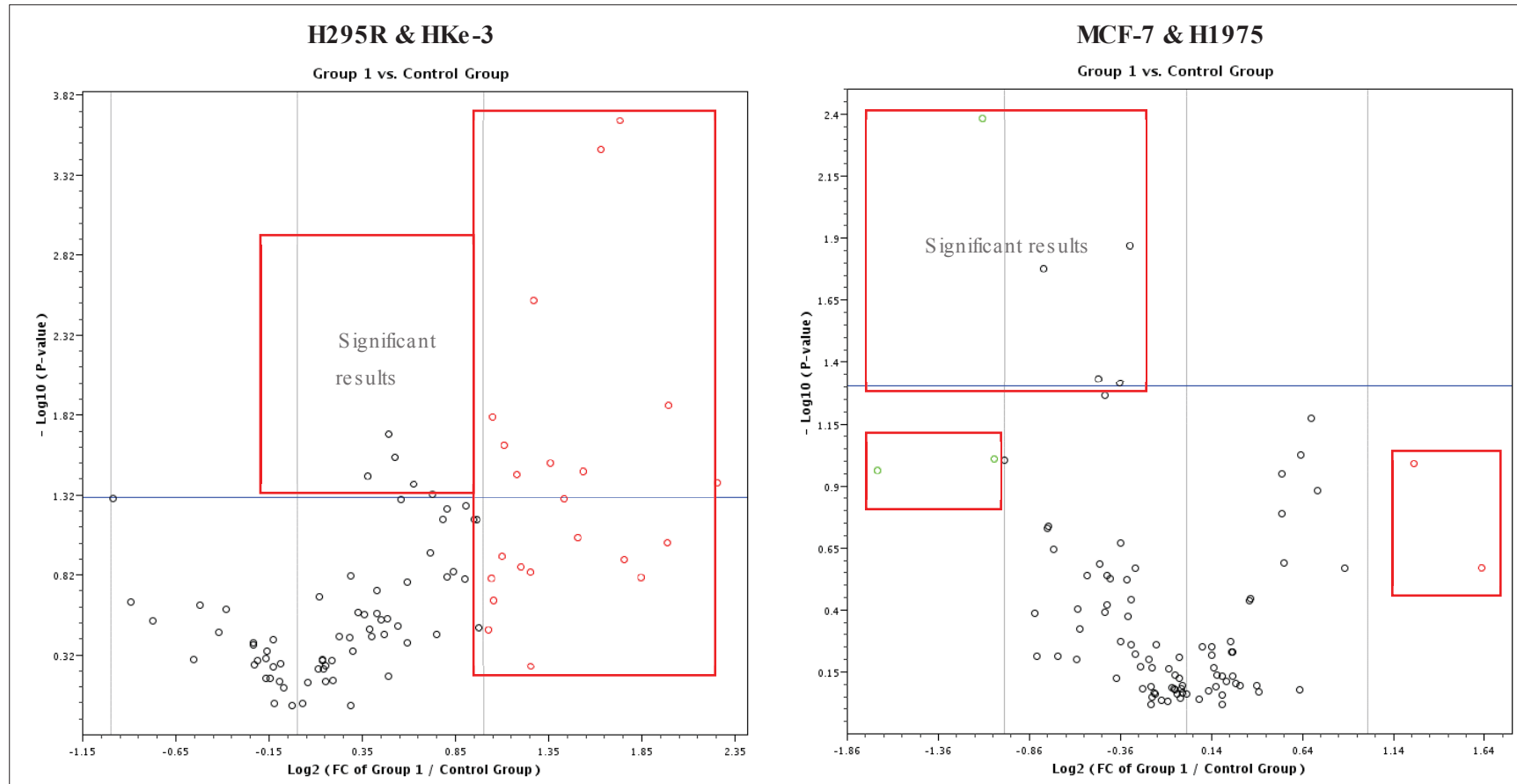

Figure 40*. Results of p-value for gene expression in HMEM Array after mitotane treatment ('MS' group – left, 'LS' group – right).*

Results

Dual-axis bar chart of result significance showing frequency (y) of significant results, results with greater than two-fold change, non-significant results on the x, Fold changes shown in red reflect higher expression and in green reflect lower expression.
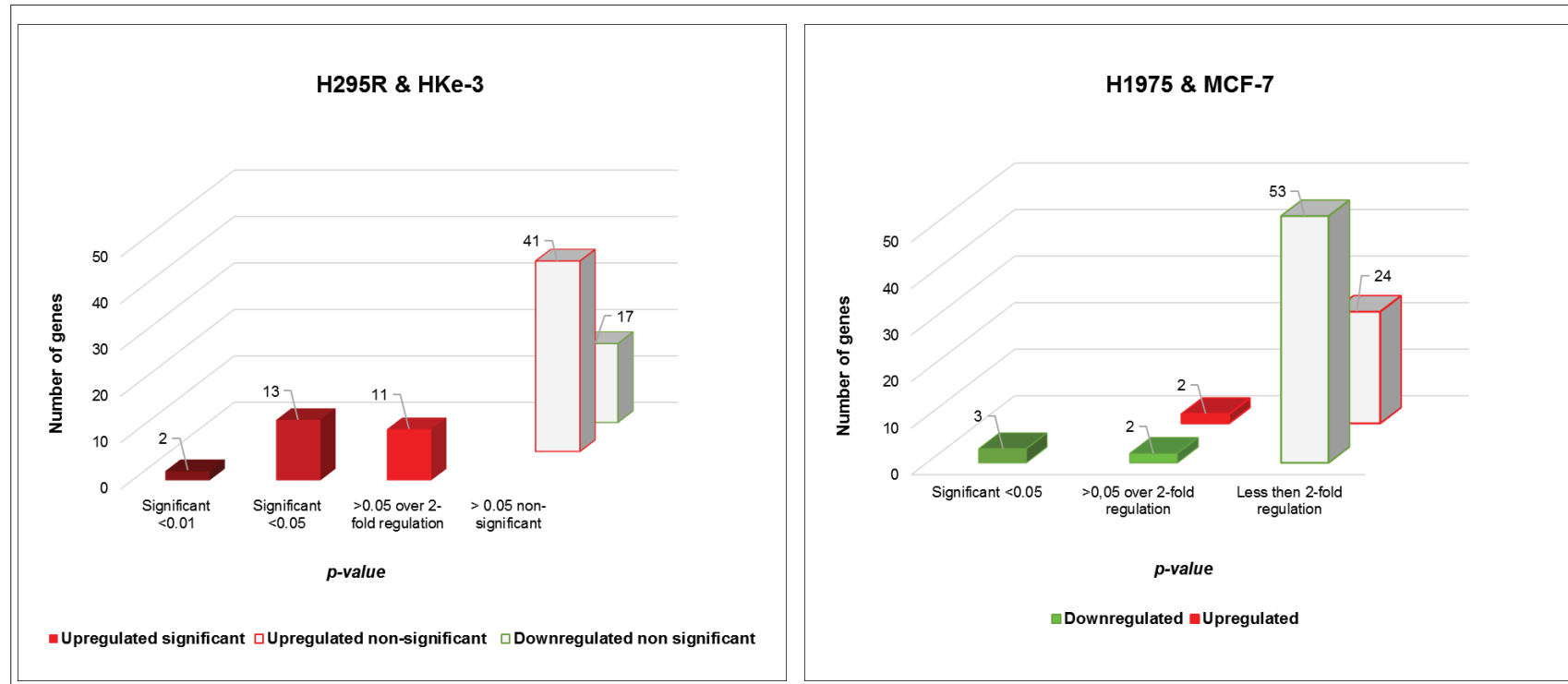

Figure 41. *Distribution of p-value significance and 'over-2-fold change' variables for gene expression in HMEM Array after mitotane treatment ('MS' group – left, 'LS' group – right).*

4.3.2 'Less sensitive' versus 'more sensitive' group summary in the context of the respiratory complexes

The final figures summarise changes in expression of genes belonging to the respiratory chain complexes following mitotane treatment. Figures are based on comparison of the 'more sensitive' (MS) cell lines with the 'less sensitive' (LS) cell lines, which gives sufficient data points to enable calculation of significance. The genes showing significant change in the 'MS' group were all upregulated (Figure 39). Further, genes showing more than 2-fold change but not reaching significance were also all upregulated. For the 'LS' group, there was much less change, with only two genes significantly downregulated and one upregulated (Figure 39). There was important overexpression of ATP genes for the 'MS' group but not for the 'LS' group.

4.3.2.1 'Less sensitive' group

Table 15 and Figure 42 below for the 'LS' group present the significant gene expression profile for oxidative phosphorylation complexes and associated proteins. No mitochondrial gene precursors were found to be significantly or over 2-fold changed in expression.

Table 15. *Summary of changes in expression of genes belonging to respiratory chain complexes I–V following mitotane treatment of the 'LS' group.*

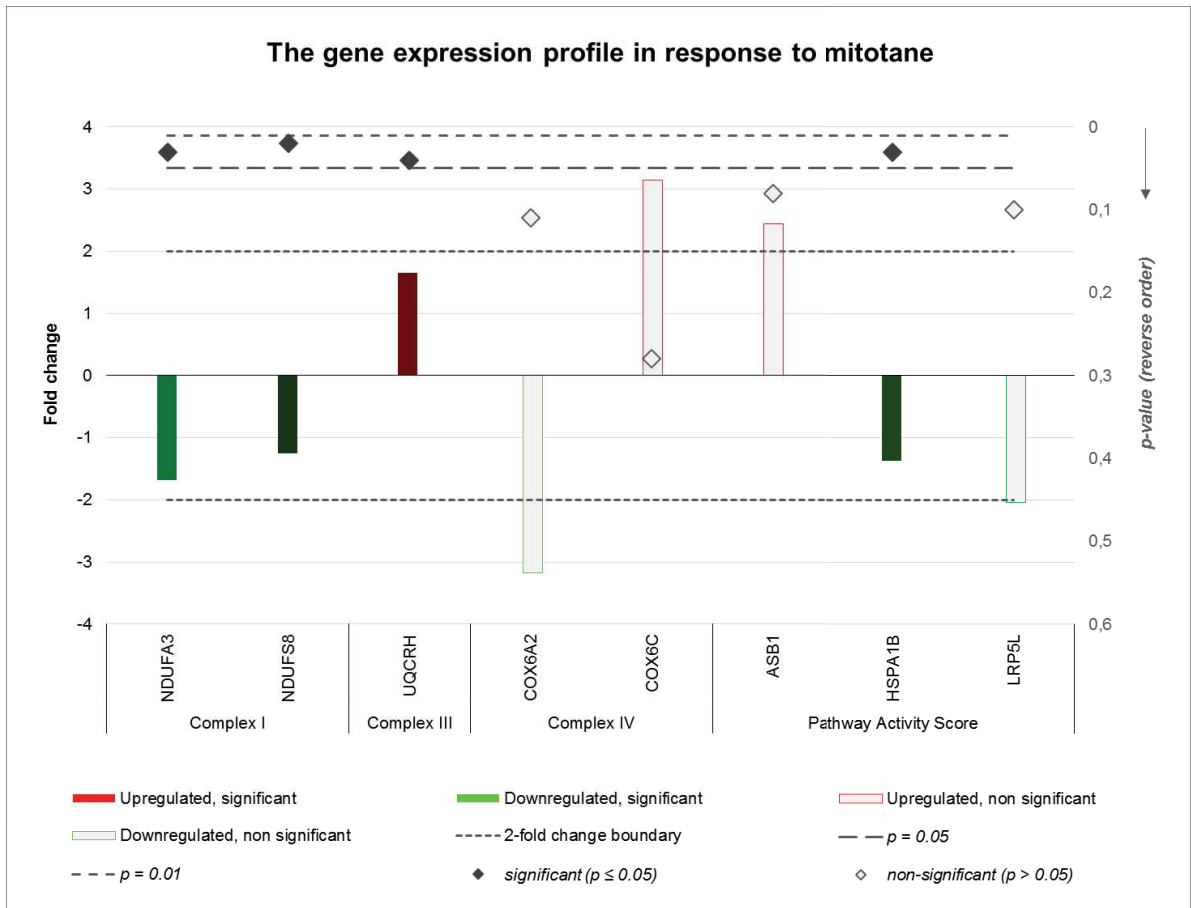| 'LS' group	Fold regulation (**bold** over 2-fold)	p-value (**bold** $p < 0.05$)
Complex I		
NDUFA3	-1.69	**0.03**
NDUFS8	-1.26	**0.02**
Complex III		
UQCRH	1.65	**0.04**
Complex IV		
COX6A2	**-3.17**	0.11
COX6C	**3.15**	0.28
Other proteins		
ASB1	**2.44**	0.08
HSPA1B	1.37	**0.03**
LRP5L	**2.04**	0.10

Figure 42. *The gene expression profile for each oxidation chain complex and additional proteins for the 'LS' group in response to mitotane.*

Two genes of complex I were found to be significantly downregulated, one from complex III was upregulated, one complex IV gene was upregulated and one downregulated over 2-fold (neither was significant). No expression of mitochondrial polycistronic unit was found.

4.3.2.2 *'More sensitive'* **group**

Table 16 and Figure 43 show the significant gene expression profile for oxidative phosphorylation complexes, associated proteins and mitochondrial gene precursors (MitoH2 polycistronic units). Mitochondrial genes are mostly subunits for oxidative phosphorylation (complexes I, III, IV). Results are presented below in tables, followed by bar charts showing the most important results.

Table 16. *Summary of changes in expression of genes belonging to respiratory chain complexes I–V following mitotane treatment for the 'MS' group.*

'MS' group	Fold regulation (**bold** over 2-fold)	*p*-value (**bold** $p < 0.05$, red $p < 0.01$)	'MS' group	Fold regulation (**bold** over 2-fold)	*p*-value (**bold** $p < 0.05$, red $p < 0.01$)
Complex I			**Complex V**		
NDUFB5	**2.4**	**0.003**	ATP5C1	**2.3**	**0.04**
NDUFAB1	**2.2**	**0.024**	ATP5G2	**3.6**	0.16
NDUFA8	1,4	**0.02**	ATP5I	**2.8**	0.09
NDUFA11	**2.6**	**0.03**	ATP5J2	**4.8**	**0.04**
NDUFA3	1.3	**0.04**	ATP5O	1.4	**0.03**
NDUFS4	**2.4**	0.15	PPA1	1.6	**0.05**
Complex II			**Other proteins**		
SDHA	**2.3**	0.13	ASB1	**3.4**	0.12
Complex III			EDN1	**2.0**	0.33
UQCR11	**2.1**	0.11	RNU11	**4.0**	0.09
UQCRC2	**2.7**	**0.05**			
Complex IV			**Mitochondrial genome**		
COX6A2	**2.4**	0.56	MitoH2_14573	**3.1**	**0.00**
COX6B1	**2.1**	0.22	MitoH2_4162	**2.1**	**0.02**
COX7A2	1.5	**0.04**	MitoH2_5726	**4.0**	**0.01**
COX7A2L	**3.3**	**0.0002**			
COX7B	**2.9**	**0.03**			

NADH dehydrogenase (Complex I) has 5 upregulated genes, among the most significant being NDUFB5 (NADH dehydrogenase — ubiquinone, 1 beta subcomplex). Succinate dehydrogenase (Complex II), transfers electron to cyt c reductase (Complex III) — two upregulated genes. Complexes I and III are responsible for ROS production and show 6 significantly upregulated genes. Next, electrons are transferred to cyt c oxidase IV to create the final energy gradient, which ends with energy production at complex V ATPase. Of the 11 important genes that have been found to be upregulated for these complexes, the most significant are COX 7AL2 (Cytochrome c oxidase subunit VIIa polypeptide 2 like) and ATP5O (ATP synthase, H+ transporting, mitochondrial F1 complex, O subunit). ATPase with inorganic pyrophosphate can contribute to increase of mitochondrial membrane permeability, resulting in cyt c leakage to promote apoptosis induction. Three from five polycistronic RNA units were found to be significantly upregulated. The bar chart used to visualize the expression as fold change of target genes is adapted from Zhang *et al.* (2015).
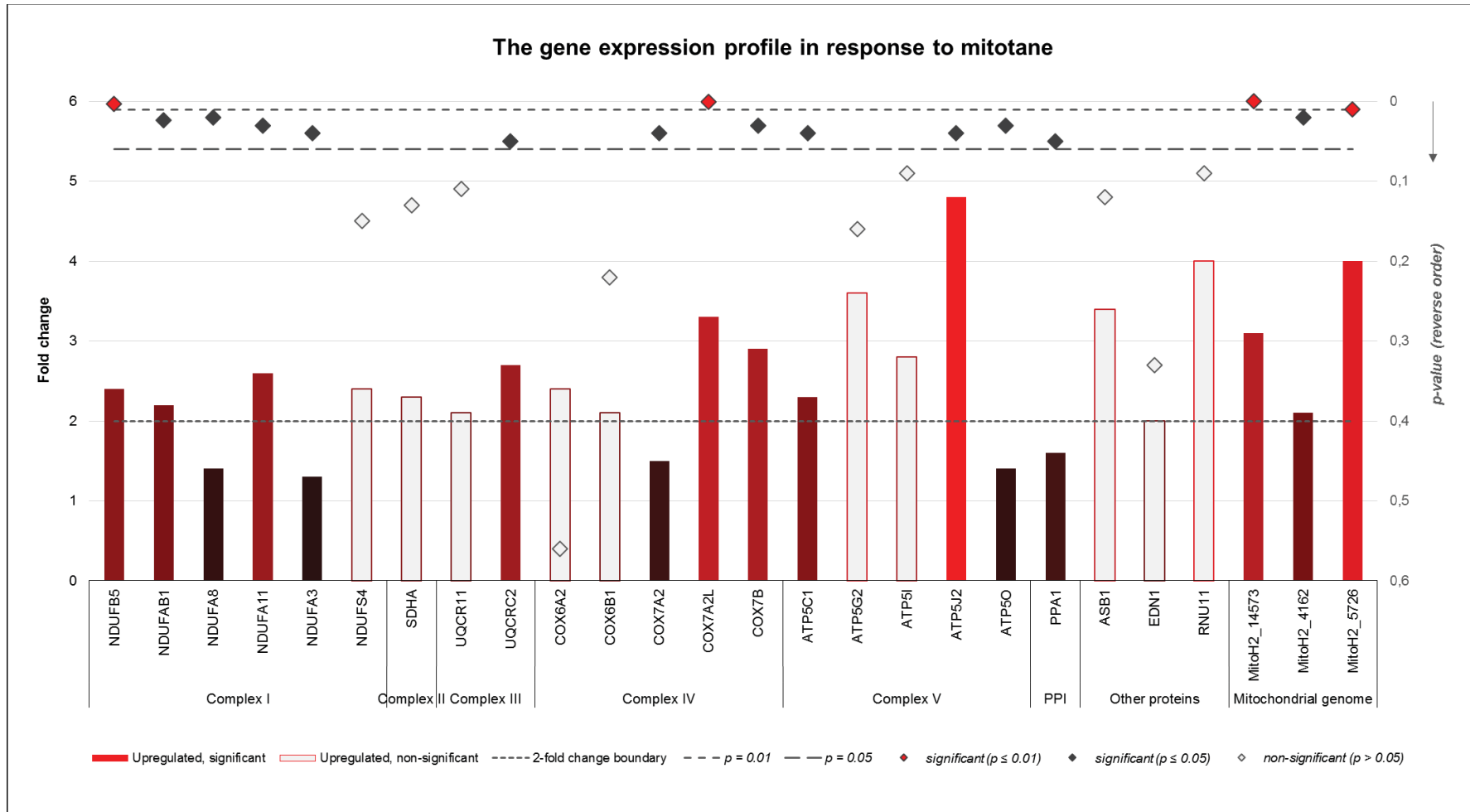
Figure 43. *The gene expression profile for each oxidation chain complex, additional proteins and mitochondrial polycistronic unit for the 'MS' group in response to mitotane.*

Results

Statistical analysis of gene expression in adrenal H295R and adolescent colorectal HKe-3, classified as the 'more sensitive' group (4.3.2), showed six genes belonging to respiratory complexes I and III to be significantly upregulated, with four genes expressed with over 2-fold change. Since complexes I and III are responsible for ROS production, this offers one mechanism for promotion of apoptosis by mitotane. Six genes of complex V with the PPA1 gene were significantly upregulated, with tree showing over 2-fold change. Tree genes of COX (complex IV) were significantly upregulated.

Cell lines found to be 'less sensitive'(4.3.1) to mitotane (breast MCF-7 and lung H1975), showed two significantly downregulated genes in complex I, one upregulated gene from complex II, all results below 2 fold-change.

PPA1 significant upregulation suggests this as an additional proapoptotic factor, since increase of high-energy phosphates can induce apoptosis. Oxidants have been reported to increase the release of calcium from mitochondria, which was suggested to be a trigger for apoptosis. Mitotane has also been shown to enhance calcium flux in different tissues and cause ROS production. Upregulation of complex I and III genes offers a mechanism for this process. The relatively lower sensitivity of MCF- 7 cells to mitotane may thus relate to lower rates of oxidant generation. Mitotane has been interpeted as having a strong impact on energy metabolism connected with mitochondrial membrane permeability and inner mitochondrial space stress, initiating the death of the cell independent of the c-Myc-dependent mechanism by which cyt c promotes the activation of the initiator, with BAX proteins.

COX 7 was found to be significantly overexpressed when all cell lines were considered together (p = 0.004). ACC H295R cells showed greater than 2-fold overexpression for COX7A2L and COX6A2, while most other COX subunits showed increased expression in HKe-3 cells, COX6C among them. COX6A2 was over 2-fold underexpressed and COX7B overexpressed in H1975 cells. For MCF-7, there was very strong underexpression of COXA62, and overexpression of COX6C. COX subunit overexpression has been described as responsible for cell death. Overexpression of at least one form in all cell lines thus offers one common mechanism for mitotane toxicity.

4.5 Summary of RNA purification and *mTOR PCR Array* experiments from FFPE tumour sections as a methodological contribution

An important concern when developing a protocol for gene expression from FFPE is to determine what quantity of material from five 7 mm slide sections might be needed to generate sufficient cDNA for *mTOR PCR Array* or for other reactions. Inquiries with the company and literature searching did not provide any information.

The study carried out has established that on average, this material yields 300 ng/µl of RNA in 15 µl after proper nucleic acid extraction and concentration measurement. Three microlitres of such a solution is needed for one array.

It was considered desirable to examine different regions of the tumour, since they are heterogeneous and frequently show visible differences. If separating two regions, 50 to 300 ng/µl of RNA can still be obtained. Another problem is of RNA modification and quality. FFPE RNA will never provide as efficient a template as RNA from a fresh tissue sample or cultured cells, as has been pointed out by QIAGEN. Following full optimisation of the reactions, it was considered that between 500 ng to 1 µg of starting material would be required.

In practice, having an approximately 4 mm × 4 mm area of FFPE tumours is sufficient from slides with 7 µm thickness, providing enough RNA to enable 4 runs on a 368 well plate format. These can be in singlicate on different array types (e.g. for the mechanistic target of rapamycin (mTOR) pathway, energy metabolism etc.), or two types in duplicate. The protocol used takes into account the need to include the preamplification reaction and also enables 14 qPCR validation reactions to be run.

Although the array did not provide Ct values for all samples (because not enough template was used), results for most genes were obtained. All results were normalized to the most stable array gene.

The scatter plot below presents the results with the boundary set at 5. Those exceeding this were considered as showing significant change, in contrast to cellular material where the boundary was set at two. It was considered necessary to set the boundary wider for FFPE, because there is a greater risk of false positive results, due to the material being of lower quality.
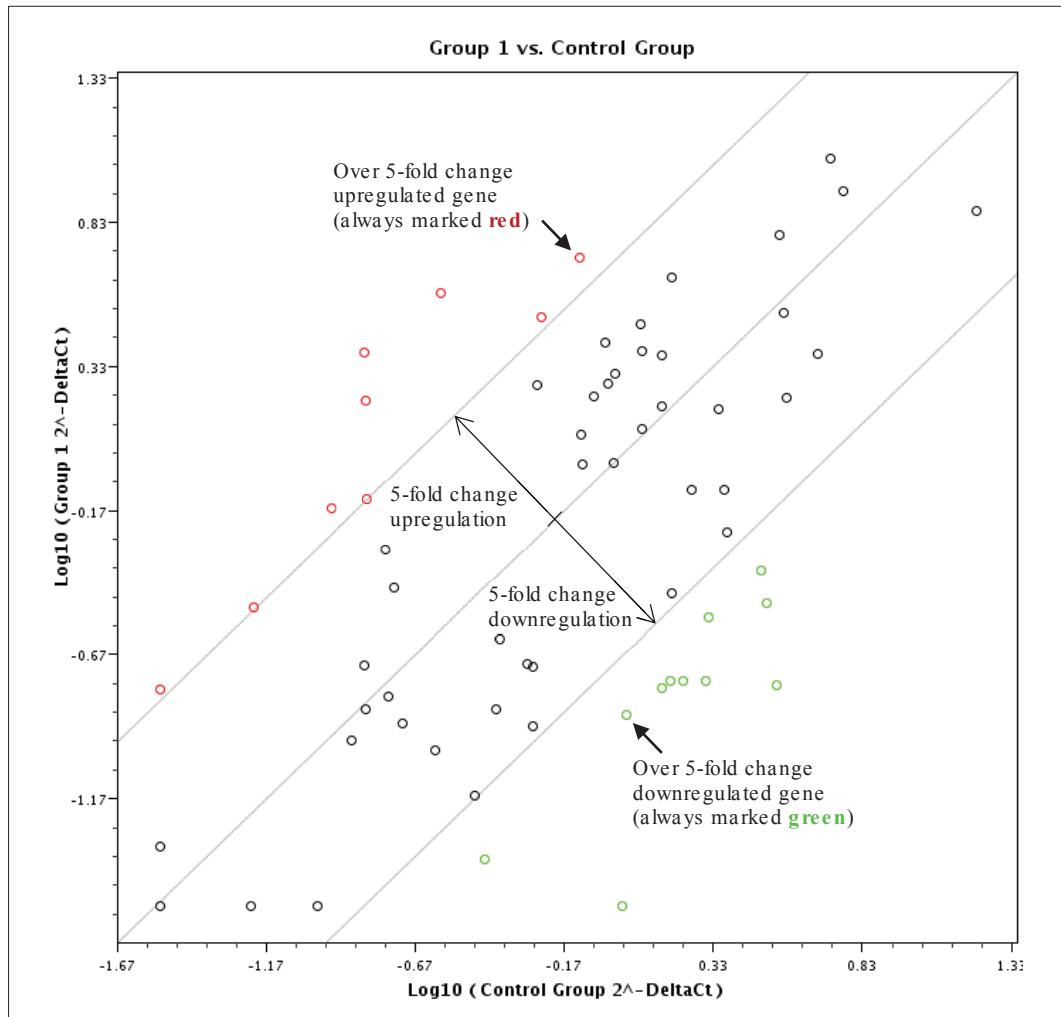
Results

Figure 44. *Results of relative gene expression for peripheral ACC versus normal cortex in the mTOR PCR Array.*

The scatter plot is explained in Appendix C.

The results above show how strongly (in terms of fold change) the genes are altered in tumour in comparison to normal cortex. The following table shows regulation of genes in figures.

The table below summarizes regulation and functions of genes showing over 5-fold change.

Table 17. *mTOR functions of 'over-5-fold change' regulated genes.*

mTOR function	Gene	Fold regulation
mTORC1 Positive Regulation	EIF4E	**-8.8**
mTORC2 Positive Regulation	GSK3B	**-7.1**
mTORC1 Positive Regulation, Growth Factor Response	IGF1	**-11.7**
mTORC1 Positive Regulation, Insulin Signalling	INSR	**5.1**

Results

mTORC1 Positive Regulation	MAPK3	5.6
mTORC2 Positive Regulation	MYO1C	-20.6
mTORC1 Positive Regulation, mTORC2 Positive Regulation, Insulin Signalling	PIK3CD	-36.6
mTORC1 Positive Regulation	PLD1	5.0
mTORC1 Positive Regulation	PLD2	-8.8
mTORC1 Negative Regulation	PRKAB2	-8.9
mTORC1 Negative Regulation, Energy Stress, mTORC2 Negative Regulation	PRKAG3	-7.4
mTORC2 Positive Regulation, Cytoskeletal Organization	PRKCG	-8.3
mTORC1 Positive Regulation	RHOA	6.1
mTORC1 Positive Regulation, mTORC2 Positive Regulation, Translation	RPS6KB1	-10.0
mTORC1 Positive Regulation, Amino Acid Response	RRAGA	11.1
mTORC1 Negative Regulation, mTORC2 Negative Regulation	STK11	5.5
mTORC1 Positive Regulation	TELO2	-9.7
mTORC1 Positive Regulation, Angiogenesis	VEGFA	6.7
mTORC1 Positive Regulation, Angiogenesis	VEGFB	14.8
mTORC1 Positive Regulation, Angiogenesis	VEGFC	16.6

The most significantly overexpressed genes in tumour tissue in comparison to normal were the angiogenesis-enhancing genes VEGF C and VEGF B; VEGFA was also upregulated. Several mTORC1 positive regulators were upregulated, including TELO, RHOA, MAPK3 and RRAGA, which is important for cellular amino acid response, whereas others such as IGF mTORC1 positive regulators were strongly decreased, most notably MYO1C, which encodes a member of the unconventional myosin protein family. This gene provides the instruction for an enzyme that is important for proper interaction of immune cells in the tissues. Other important findings were several-fold over-expression of VEGFs and strong downregulation of PIK3CD, a gene connected with immunology interaction in tissue, as well as upregulation of some important downstream effectors of the TRK receptor.

.

V. Discussion

5.1 The effect of mitotane on non adrenal tissues.

While most literature reports have concentrated on the selective actions of mitotane on adrenal tissue, the findings presented here show that it has toxic actions on a variety of cell types at higher threshold concentrations. A review of published non adrenal effects shows that these are widespread. One field of study has been of side effects of mitotane when used clinically. Concern has also been raised about effects of residues of this and related chlorinated pesticides in the environment, especially on reproductive function of fish and other wildlife.

Most in vitro studies of the actions of mitotane and related compounds on non-adrenal cells show they do not involve the mitochondria and frequently mimic non-genomic actions of steroids. For example, the analogue o'p-DDE has been found to rapidly increase intracellular Ca^{2+} concentration in cultured human granulosa-lutein cells. This mimics the response to androstenedione of luteinizing human granulosa cells, in which there is a rapid increase in intracellular Ca^{2+} via an influx of these cations from the extracellular fluid through voltage - dependent Ca^{2+} channels. An increase in intracellular calcium is one of the earliest events in the non-genomic action of steroids. Such ligands act through G- protein receptors, inducing the formation of IP3 (inositol triphosphate), which in turns activates the endoplasmic reticulum Ca^{2+} pump, which in turn may stimulate calcium channel-mediated influx. Mitotane thus has an influence on this rapid highly localized Ca^{2+} surge, which acts as an intracellular messenger controlling many cellular processes. (Wu, Foster, and Younglai 2006). The mitochondria are also responsive to Ca^{2+} elevations, with ATP formation, loss of cytochrome c and onset of apoptosis, but these occur at abnormally high elevations (Leo et al 2005), so may be only be relevant when high concentrations of mitotane are used in vitro (quoted by Wu). Mitotane and related compounds also appear to have steroid receptor-mediated affects when at high concentrations, for example, behaving as an androgen antagonist at concentrations above 10^{-6} M in a human hepatoma cell line transiently transfected with the human androgen receptor (Maness et al 1998, quoted by Wu).

Discussion

Similar effects on Ca^{2+} mobilization have been observed in other cells. Mitotane increases Ca^{2+} in myometrial smooth muscle cells, while the unsaturated mitotane isomer o'p-DDE stimulates Ca^{2+} uptake and a concentration-dependent prolactin release in GH3 /B6 pituitary tumour cells and has been shown to enhance prolactin secretion by breast tissue. It has a high binding affinity for the membrane estradiol receptor of SKBR3 breast cancer cells and mimics the action of estradiol.

The prostatic cell line PALM has been shown to respond to the organochlorine pesticides DDT and o'pDDT, among others, acting in competition for the nuclear androgen receptor with the synthetic androgen compound R1881 (Wu, Foster, and Younglai 2006). Also o'p-DDT was found to inhibit the L type calcium channel in vascular smooth muscle cells and evoke a rapid endothelium - independent relaxation of the coronary vasculature similar to that induced by estradiol (Wu, Foster, and Younglai 2006). These changes in Ca^{2+} flux caused by pesticide exposure may affect calcium-binding proteins and gene expression, as shown in trophoblast cells, inhibiting cell proliferation and inducing apoptosis via several trophoblast differentiation genes (Wu, Foster, and Younglai 2006)

Environmental effects of organochlorine pesticides may not be simply dose-related, because these agents accumulate in fat tissue and so may circulate at high concentrations after fat mobilization in times of calorie deficit. Mitotane binds to the plasma membrane receptor for progestogens in the ovaries of spotted sea trout, while O'p DDE blocks the progesterone-induced stimulation of sperm motility in Atlantic croaker (Wu, Foster, and Younglai 2006).

Mitotane has an oestrogenic effect on sex hormone- binding globulin and corticosteroid-binding globulin in humans. It has been shown to promote release of these globulins in a hepatoma cell line stably transfected with human oestrogen receptor-α but not in a cell line that was not, indicating an oestrogen-dependent effect (Nader et al. 2006). Most male patients under mitotane treatment at a dose ranging from 4 to 6.5 g daily show dose-dependent increase in these globulin levels. This might explain the common finding of gynaecomastia in these patients, although direct reduction of testicular androgen production and inhibition of testosterone to dihydrotestosterone conversion (Ghataore *et al.* 2013) may also be factors.

Mitotane causes serious neurological and neuropsychological side-effects in some patients. The lipophilic nature of this agent enables it to cross the blood-brain barrier to a certain extent. Interestingly, one affected patient receiving 2 years of treatment with

108

Discussion

mitotane for adrenal carcinoma showed complete recovery after discontinuation of the drug. These effects appear to involve cerebral cortex as well as cerebellum. A peripheral neuropathy has also been reported. In the studied case, side effects were severe at serum levels above 15 mg/l. Since other causes of reversible dementia could be excluded, o,p'-DDD (or one of its metabolites) appeared to be the responsible agent. The underlying mechanism of these effects has not been elucidated. Besides particular impairment of performance IQs, disturbances of memory, language, calculation and constructional abilities were found. The authors concluded that investigation of patients before, during and after o,p'-DDD treatment was warranted, which might enable high dose o,p'-DDD therapy to be continued for a longer period. (Bollen and Lanser 1992).

The manufacturer of Lysodren (mitotane) reports as side effects leucopenia, skin rash, neuromuscular dysfunction and psychiatric symptoms, serious gastro-intestinal side effects, increased blood levels of liver enzymes, cholesterol and triglycerides (European Medicines Agency, 2013). Hypercholesterolemia is a common consequence of mitotane therapy and was first described in a cohort of 69 patients treated for Cushing's disease, who showed an average increase in serum cholesterol of 30 % which was not associated with any change in triglycerides and was reversible on withdrawal of the drug [5]. This may be explained by the marked increase in HMG CoA reductase activity induced by mitotane. A similar effect was observed in vitro when the drug was added to isolated hepatocytes (Maher et al. 1992). Mitotane induces hepatic microsomal enzymes, notably Cyp 34A1 and also inhibits 5a-reductase 2 and 20B-hydroxysteroid dehydrogenase and thus markedly affects hepatic metabolism of cortisol administered simultaneously with mitotane (Ghataore et al 2013).

5.2 Mitotane action on mitochondrial energy metabolism

The striking effects of mitotane on mitochondria (above) may be predicted to radically effect cellular energy metabolism. It is therefore useful to first consider what is known about changes that occur in cancer before considering those that may be specific to the adrenals.

5.2.1 Mitochondrial metabolism in tumours

Mitochondrial defects have been associated with many types of cancers. Warburg classically described how most cancer cells predominantly produce energy by a high rate

109

of glycolysis followed by lactic acid fermentation in the cytosol, rather than by a comparatively low rate of glycolysis followed by oxidation of pyruvate in mitochondria, as in most normal cells. An enhanced rate of glucose utilisation by many cancer cells enables them to be distinguished by increased fluorodeoxyglucose uptake, detected by positron emission tomography (PET). This phenomenon, commonly known as the 'Warburg effect' led to the assumption that mitochondrial function was unimportant in cancer cells, and this appeared to be supported by down-regulation of gene expression being a commonly observed feature of cancer (Wei et al. 2015), (Hebe, Blackburn, and Miller 2011), (Cairns 2015).

Today, however, it is known that different types of tumours show a wide range of changes in the balance between glycolysis and oxidative phosphorylation and that this can also depend on the developmental state of the neoplastic cell. Tumours with low glycolytic activity such as adenomas, bronchoalveolar carcinomas, carcinoid tumours, low grade lymphomas and small sized tumours have shown false negative findings on PET scan (Chang et al. 2006).

Mitochondrial function is indispensable for cancer cells. Mutations of genes associated with mitochondrial structure and metabolism are known that enhance cell survival or promote cell proliferation and invasion (Wallace 2012). Measurements of absolute rates of mitochondrial oxidative metabolism often show that they are not lower than in normal cells and levels of ATP production are not impaired.

When malignant cells are growing *in vivo*, they may have important interactions with adjacent tissue, both signalling to them and capturing intermediates from them to utilise for growth. The well-known phenomenon of cancer cachexia shows that capture of nutrients in favour of growth of the cancer is widespread. An illustrative example of how cell-cell interaction can provide a very different interpretation of the energy budget of cancer cells has been well described for breast cancer and has been termed the '*reverse Warburg effect*'. Co-culture of MCF-7 cells with fibroblasts showed decrease of mitochondrial mass in the fibroblasts but *increase* in the MCF-7 cells. The mechanism is interpreted as oxidative stress within the cancer cells resulting in activation of the transcription factors HIF1 (hypoxia inducible factor 1) and NFκB (nuclear factor kappa-light-chain-enhancer) in the fibroblasts, resulting in autophagy and mitophagy, which generates nutrients, including lactate and pyruvate, which are then utilised by the cancer cells. Hypoxic damage within cancer cells has been postulated to be a key driver of DNA mutagenesis, which may provide positive survival benefit for the cells (Sotgia et al. 2011).

110

Discussion

The diverse mechanisms behind the neoplastic processes that are related to changes in mitochondrial regulation are summarised below. These have been comprehensively reviewed by Wallace (2012).

Firstly, mitochondrial function is affected by changes of signalling pathways and oncogenes that are known to be crucial for tumour and cancer origin. One of most important and common alterations found in cancer cell bioenergetic metabolism concerns the PI3K (phosphoinositide 3-kinase) - *PTEN*- Akt (protein kinase B) signalling route, because it shifts metabolism from oxidative to hypoxic. Changes in this transduction pathway not only promote a higher level of glucose utilisation, but enhance expression of genes for glycolysis and lipogenesis, to allow conversion of up 90% of the pyruvate into lactate and operate both glycolysis and pentose phosphate pathways in an unrestrained way. Furthermore, the FOXO (forkhead transcription) protein, which normally decreases mitochondrial function and oxidation phosphorylation after activation by the PI3K pathway, may have the opposite effect in the presence of hypoxia by arresting stabilisation of HIF1, which is a factor that strongly represses mitochondrial biogenesis.

Another example is that of an increased expression level of c-Myc, which is common to many cancers. It has been found to boost mitochondrial oxygen consumption and mitogenesis by activation of many genes such as those for mitochondrial membrane proteins for subunits of complex I, uncoupling proteins and genes engaged in intermediary metabolism.

An important factor related to mitochondria is the well-known tumour suppressor gene p53. Usually in the case of DNA damage or metabolic stresses such as hypoxia, this acts with other cytokines to mediate growth arrest and induce apoptosis (Maclaine and Hupp 2009). However, in response to energy limitation it becomes phosphorylated by AMP-activated protein kinase, which activates cell cycle checkpoints that can stimulate tumourigenesis. Additionally the activity of p53 supports ATP production by oxidative phosphorylation, and a decrease of cellular ROS production, due to action of the TIGAR regulator. This regulator is responsible for negative regulation of hypoxia by transferring carbon flow away from glycolysis into the pentose phosphate pathway, which increases NADPH production. Also, inhibition of glycolysis and enhancement of expression of oxidative phosphorylation in complex IV occurs as a result of negative regulation of phosphoglycerase mutase and Akt by this tumour suppressor. Inactivation of p53 could increase hypoxia, decreasing oxidative phosphorylation and inhibiting apoptosis.

Discussion

However, under other circumstances, p53 can activate processes that result in reduction of mitochondrial function, and impairment of their ability to divide (Wallace 2012).

Acetyl-CoA can be hydrolysed by mitochondria to generate ATP. This regulator takes part in the reaction of protein acetylation to modulate the signal transduction pathway and epigenome. Acetyl-CoA is also produced within mitochondria from pyruvate and by fatty acid oxidation. Fatty acetyl-CoA particles are imported into mitochondria by carnitine. A carnitine transferase isoform was found to be unregulated in lung cancer, which may indicate an important role in energy metabolism and precursor production in tumourigenesis.

The transcription factor HIF1 is one of the most important regulation agents. Under low oxygen tension, HIF1 induces glycolysis, stimulating expression of genes for glucose transporters, glycolytic proteins and angiogenesis factors (VEGF and erythropoietin). HIF1 factor inhibits mitochondria or can activate mitophagy in a number of ways, the most important of which is down-regulation of mitochondrial metabolism by blocking expression of proteins involved in iron-sulphur centre synthesis and genes for subunits of complexes I, II and IV.

Mutations in genes for citric acid cycle enzymes form an important group of mitochondrial causes of tumourigenesis. Those in subunits of the respiratory complex II protein (succinate dehydrogenase) have been observed in gangliomas and pheochromocytomas. Accumulation of succinate results, which exits the mitochondria via a carrier and inhibits HIF1 hydroxylases, resulting in an induction of a hypoxic response under normoxic conditions — *pseudo hypoxia*. HIF1 thus escapes degradation and, on transfer from cytosol to nucleus, activates expression of genes engaged in angiogenesis, proliferation, cell survival and glycolysis. Mutations of fumarate hydratase and isocitrate dehydrogenase have also been associated with tumour formation, causing a shift of energy metabolism from oxidative to glycolytic, which leads in turn to oxidative stress and epigenetic deregulation via changes in a large number of histones and DNA methylation. The enzyme fumarate hydratase converts fumarate to malate. Overproduction has been found in uterine leiomyoma and malignant renal cancer due to a homozygous null mutation, leading to a 100-fold increase in fumarate. An increased fumarate level activates the stress response pathway regulated by Nrf2. This turns on the endonuclear DNA stress-response genes. One of these is haem oxidase, which is suspected to be important for tumourigenesis.

Discussion

Mitochondria regulate ROS production in complex III, which stabilises HIF1α, mediated by sirtuin-3 protein. Additional factors that stabilise HIF1α include cyt c interaction with complex IV and mitochondrial disulphide proteins.

Mitochondrial activity is strongly regulated by calcium. The calcium uniporter, which is energised by an electrochemical gradient, is located in the mitochondria-associated endoplasmic reticulum (ER) membrane. Inactivation of this protein may reduce induction of apoptosis and thus could promote neoplasms.

It is interesting to note that when mitochondrial ROS are overproduced, they can induce apoptosis or necrosis. However when apoptosis is inhibited in cancer, they can become potential mitogens and thus mitochondrial ROS production may contribute to transformation towards cancer.

It can thus be seen that many control factors such as HIF1 work in an ambivalent way, either promoting tumours, or acting as a suppressor. Similarly, other oncogenes such as FOXO and c-Myc can enhance or decrease mitochondrial biogenesis and p53 can activate the coenzyme respiratory chain in cancer or have the opposite effect.

In spite of the wealth of observations summarised above, many aspects of mitochondrial biology are poorly understood, such as the significance of protein structural components and the regulation of mitochondrial genes coded in the nucleus in relation to the bioenergetics of the epigenome. The processes of regulation by which mitochondrial membrane potential and calcium concentration have influence on the nucleus and cytosol still require clarification.

Finally, the mutations that directly change mtDNA may be summarised as damaging oxidation phosphorylation, stimulating neoplastic transformation and allowing cancer cell adaptation to a changing bioenergetic environment.

5.2.2 Bioenergetics of adrenocortical cancer

As for many cancers, ACCs appear to exhibit the Warburg effect, since PET scanning shows they tend to preferentially take up 18-fluoredeoxyglucose. This is enhanced by mitotane and has been suggested as a means of directly monitoring response to treatment. Uptake may also be enhanced in the contralateral adrenal (Mpanaka et al. 2011) supporting a deleterious effect of mitotane on oxidative phosphorylation, although these authors could not exclude an effect of enhanced ACTH stimulation secondary to

113

Discussion

diminution of serum cortisol.

ACCs often show areas of necrosis, perhaps indicating that they have outgrown their blood supply and so must have developed in a relatively hypoxic environment. Given that they are very diverse in their steroid biochemistry and have areas within them of different cell types, it may be predicted that detailed bioenergetic studies of ACC will uncover a large diversity of mutations related to energy metabolism. The use of one culture of the cell line (H295R) does offer a model for an ACC cell type that is sensitive to mitotane. However this may not reflect the diversity of mutations and changes in gene expression in energy pathways that might be found across the range of ACC.

Whether or not mitochondria in ACC tissue have defective energy metabolism, it may be that, given the requirement of molecular oxygen for steroid metabolism in mitochondria and the overall tendency to hypoxia in these tumours, mitotane may differentially affect ACC mitochondria by promoting energy metabolism and thus oxygen utilisation in an organelle which is already poised at the limit of its minimum oxygen requirements.

5.2.3 Mitotane influence on mitochondrial energy metabolism

Proteomic studies of Stigliano *et al.* (2008) have shown that mitotane disrupts activity of D-3-PGDH isoforms, enzymes involved in a key process of maintaining redox potential. They are involved in electron transfer from ferredoxin, which in sequence gives electrons to P450s. This results in changed electron flow in CYP11A1 and CYP11B1.

Direct studies of the respiratory complexes using spectrophotometry (Hescot et al. 2013) shows mitotane inhibition, but in a selective manner. At a concentration of 50 μM after 48 hours, inhibition of complex IV was observed, which was then shown to be dose dependent, with an IC_{50} of 67 μM. The mRNA transcripts for complex I and complex IV, as well as protein expression of the whole COX complex, measured by blue light polyacrylamide gel electrophoresis, were strongly decreased on treatment of H295R and also the non secreting ACC cell line SW13, whereas for complex II and III there were no such changes. There was also increased expression of mitochondrial DNA content and peroxisome proliferator–activated receptor alpha (PGC1a) in response to mitotane. This apparently paradoxical finding may mirror mitochondrial proliferation in adrenocortical tumours with oncocytic change, which may be a response to a hypoxic insult (Mearini et al. 2013). In the work described here, use of a mitochondrial energy metabolism gene

114

Discussion

expression panel has demonstrated changed expression of many genes in H295R cells and three cell lines derived from other cancer types (Dworakowska et al. 2015). Moreover, mitochondria are quantitatively the most significant source of intracellular reactive oxygen species and leakage from the respiratory chain is the main entry point (Pinton et al. 2008), (Waszut, Szyszka, and Dworakowska 2017).

There is some evidence that mitochondrial energy deficit alone could explain diminished 11β-hydroxylase activity. In Lesch-Nyan disease, a relative increase of urinary excretion of 11-deoxycortisol metabolites after ACTH stimulation indicated a partial block of 11β-hydroxylation. Since this is a disorder of the purine salvage pathway, it was speculated that lack of supply of purine nucleotides was compromising mitochondrial energy metabolism (Watts et al. 1987).

5.3 A mitochondrial basis for mitotane specificity

Comparing studies describing mitotane actions on different tissue types, it is clear that, although mitotane exerts toxic effects in many of them, adrenocortical tissue is much the most sensitive. One recently identified element of this is the high expression in adrenal tissue of SOAT1, reflecting the quantitatively important management of cholesterol for steroid synthesis. Sbiera et al., (2015), suggest that this is the main determinant of mitotane sensitivity, but given the near ubiquitous occurrence of this enzyme in mammalian cells, this appears unlikely. Another factor, FATE 1, which influences ER-mitochiondrial distance at the MAM, is more highly expressed in ACCs resistant to mitotane (Doghman-Boughuerra *et al.,* (2016) and these authors have suggested that the ER-mitochondrial interaction in adrenal cells has special characteristics related to the need to traffic cholesterol and steroids during the process of hormonal steroid biosynthesis (Doghman-Boughuerra and Lalli, 2017). Specificity may otherwise be more closely related to the particular configuration of the mitochondria, which expresses at least three mitochondrial cytochrome P450s required for steroid synthesis.

There is no evidence that mitotane acts in this way in other tissues, although there is some clinical evidence, supported by studies of the mouse pituitary cell line TalphaT1, for a deleterious effect on pituitary thyrotrophes, and induction of apoptosis in the mouse cell line TαT1. Mitotane influenced cell survival and function of ACTH-secreting cells derived from human pituitary adenomas in primary culture of and in the mouse pituitary

Discussion

cell line AtT20/D16v-F2 (Zatelli et al. 2010),(Gentilin et al. 2013) . Since the gonads are also sites of steroidogenesis, they may also be sensitive to mitotane, but no studies were found of gross or ultrastructual effects in this tissue or in isolated cells. Some features of mitochondrial ultrastructure, such as presence of lamellar cristae, are common to adrenal and gonadal tissue (Vafai and Mootha 2012). A number of case reports show response of testicular tumours to mitotane (Bertram et al. 1991), but women receiving mitotane continue to cycle and may achieve pregnancy (Tripto-Shkolnik et al. 2013). Both men and women show marked decreases in urinary androgen metabolite excretion during mitotane (Ghataore et al. 2012), (Gentilin et al. 2013). Only one of the identified mitochondrial steroidogenic cytochrome P450s, CYP11A1, functions in this tissue, but as suggested above for adrenal tissue, an alternative cytochrome that is responsible for activation of mitotane may be present.

Adrenal mitochondria employ adrenal ferredoxin, also called ferredoxin-1, to transfer electrons from NADPH to cytochrome P450. This was thought initially to be a source of mitotane specificity, but this same ferredoxin has also been detected in mitochondria in a number of other tissues, including the testes, ovaries, placenta, kidney, liver and brain, being involved in P450-dependent hydroxylation (Redick et al. 1977).

Studies of mitotane effects on expression of both mitochondrial and nuclear genes, show that these are extensive (Dworakowska et al. 2015), (Sbiera et al. 2015). There are clearly opportunities to develop this field and to further characterise the proteomic profile of this sensitive tissue. Recent developments in the understanding of the epigenetic control of nuclear DNA gene expression, such as the complex regulation by NRF-1 (section 1.2, 6.2.1) may point to secondary mechanisms that are initiated by mitotane. (Whelan and Zuckerbraun 2013).

The cancer-testis antigen FATE1 is localised to the MAM and decreases calcium flux by widening the ER-mitochondrial distance and is overexpressed in some cancers. Doghman-Boughuerra (2016) developed H295/TR SF-1 cells, in which overexpression of SF-1 was deoxycycline dependent and was found to induce high FATE1 expression. Using this model, they demonstrated a decreased apoptoptotic response to mitotane, but when FATE1 was knocked down, it was increased. Patients with adrenocortical tumours and receiving mitotane who had relatively high tumour expression of FATE1 had worse outcomes than those in whom it was low (Doghman-Bouguerra et al. 2016).

Discussion

5.4 Mitotane influence on mitochondrial energy metabolism and role in promoting apoptosis

There is much evidence, described in this thesis that mitochondria are the structures that mediate cell responses induced by mitotane. There are gross effects on mitochondrial structure, which lead to loss of mitochondrial membrane potential and also on other processes that increase mitochondrial membrane permeability, which in turn may lead to apoptosis.

Mitochondrial oxidative stress has been shown to result in excess production of ROS. Superoxide is a messenger between mitochondria, leading to a wave of mitochondrial membrane depolarisation and further ROS release. This change can be reversible until a critical threshold is reached, leading to global depolarisation (Whelan and Zuckerbraun 2013). Generation of ROS following exposure to mitotane is likely to be highly significant. A variable capacity for ROS production may help explain the variable sensitivity to mitotane exhibited by adrenal tumours (Kufe et al. 2010)(Schteingart 2000).

Active forms of mitotane may react with specific targets. Covalent linkage with proteins may result in adducts that then accumulate in the intermediate space (IMS). One plausible mechanism is by formation of disulphides, with a damaging accumulation being associated with ROS production (Wey et al. 1997).

IMS stress causes an accumulation of misfolded proteins, activating an 'unfolded protein response', within the endoplasmic reticulum (ER), resulting in release of ER calcium stores and transmission of calcium into the mitochondrial lumen, primarily via voltage-gated anion channels (VDAC), as a major initiator of the apoptotic cascade (Pinton et al. 2008).

Interestingly, it has been shown that during IMS stress, associated processes take place. An accumulation of protein increases proteasome activity and activates oestrogen receptors and lysosomal protease cathepsin D, is increased by mitotane. ROS production leads to further upregulation of proteases required for mitochondrial homeostasis. The trA2/Omi protease can also be released into the cytosol where it contributes to apoptosis through caspase-dependent and -independent pathways. Stress also leads to increase of NRF-1, which regulates the expression three mitochondrial-encoded COX subunits. A stress reaction in the ER and IMS and increased ROS production can be regarded as inner membrane space stress responses. Further accumulation of these agents leads to

117

Discussion

apoptosis, when the capacity to protect stability is overcome. It is possible that mitotane activates this process via the oestrogen receptor. (Papa and Germain 2011), (Poli et al. 2013), (Lalli 2015) The most recent studies indicate that this process is caused by mitotane-induced lipid accumulation (Kroiss and Fassnacht 2016)

The role of ROS in both promotion and prevention of apoptosis has been reviewed (Simon, Haj-Yehia, and Levi-Schaffer 2000). They are products of oxidative phosphorylation and are increased by oxidative stress. Their precursors are transported through VDAC. Mitochondria produce ROS by direct donation of excess electrons, primarily from complex I to O_2, giving rise to superoxide anions that generate H_2O_2 by catalysis by Mn superoxide dismutase, which is mostly found in complex III. In the presence of reduced transitionmetals, H_2O_2 can be the most reactive of hydroxyl radicals (Wallace 2012) (Waszut, Szyszka, and Dworakowska 2017). Initial release of ROS by mitochondria may be mediated by the adaptor protein p66shc, which translocates to the mitochondria and acts to strip electrons from the coenzyme respiratory chain (Pinton et al. 2008). ROS directly or indirectly increase the gating potential of the permeability transition pore, so that mitochondria would be both source and target of ROS. (Kufe et al. 2010), (Germano 2010), (Waszut, Szyszka, and Dworakowska 2017).

While calcium is essential for mitochondrial function, being an activator of three Kreb's cycle enzymes, excess is deleterious. The described effects on mitochondrial morphology of calcium loading closely resemble effects of mitotane. There is also ample evidence for direct actions of mitotane on the mitochondria (Pinton et al. 2008), (Alberts et al. 2002). An increase in the release of calcium to mitochondria by oxidants stimulates calcium-dependent enzymes such as proteases, nucleases, and phospholipases, which subsequently trigger apoptosis of the cells. Calcium can leave mitochondria by a number of different ways. Once calcium efflux has been triggered, a series of common pathways of apoptosis are initiated, each of which may be sufficient to destroy the cell. (Chakraborti et al. 1999) (Waszut, Szyszka, and Dworakowska 2017). The mitochondrial permeability transition pore can be activated by factors which include a decreased membrane potential, high-energy phosphates such as ATP, a more oxidised redox status, increased ROS production and increased Ca^{2+} level (Singh and Costello 2009), (Tait and Green 2012), (Waszut, Szyszka, and Dworakowska 2017).

The findings in this project are consistent with an increase of outer membrane permeability following matrix injury and membrane rupture after mitotane treatment, with increased expression of genes encoding for the subunit complexes I, III, IV & V.

118

Discussion

Complexes I and III are responsible for ROS production, while PPA1 and ATPase generate high energy phosphates which can induce increase of mitochondrial membrane permeability. Catalytic activity of inorganic pyrophosphatase 1 (PPA1), in the presence of Mn^{2+}, is responsible for generation of high energy phosphates: diphosphate $+ H_2O = 2$ phosphates. This enzyme quite possibly resides in the cytoplasm. The PPA1 enzyme has been found to be upregulated for the 'MS' group. A high energy phosphate requirement is connected with highly energetic processes within cells; their increase is also connected with induction of apoptosis. The ATP level could explain the observed gradation of the mitochondrial damage induced by mitotane in cultured cells and *in vivo*, which variously include apoptosis, extensive apoptosis (atrophy), or necrosis.

Other similar studies on the role of the respiratory complexes provide support for the studies described in this thesis. Experiments with pancreatic cancer cells have shown a role for the respiratory chain in cathepsin-induced oxidative stress, leading to apoptosis (Pramanik, Boreddy, and Srivastava 2011).

Another potentially crucial aspect is that it has been shown that induction of cyt c oxidase unit gene expression has itself proapoptotic effects (Othumpangat, Noti, and Beezhold 2014). In their study, COX6C was significantly overexpressed 2-fold, with an additional non-significant increase in COX6A2 expression, whereas other COX subunits were unchanged, resulting in increased caspase-9 protein release, leading to apoptosis. COX subunit overexpression was induced by viral miRNA, initiating an apoptotic pathway. This leads to the important conclusion that even one COX subunit can act as a cell death trigger, supporting the findings presented in this thesis. COX overexpression is a good candidate for further analysis, especially COX6C, with aim of achieving statistical significance.

Exactly how this respiratory chain complex induction and enhancement of apoptosis signalling is reflected in expression of other energy metabolism genes has been barely described. The most significant clue may be the observation that cancer cell death caused by experimental exposure to interferon beta and retinoic acid was associated with a complex upregulation of the respiratory complexes with a postulated key role in apoptosis initiation by two genes of complex I. This clearly suggested that overproduction of ROS by upregulation of mitochondrial respiratory chain activity had contributed to treatment-triggered cell death. Drug-induced apoptosis may be a prolonged process that leads to initiation of respiratory complex regulatory events. This is another example in which mitochondrial physiology plays a direct role in apoptotic cell death (G. Huang et al. 2007).

119

Discussion

The scenario of mitochondrial respiratory chain-mediated apoptosis, and its gene expression, together with ROS signal mediation is presented in the scheme below.
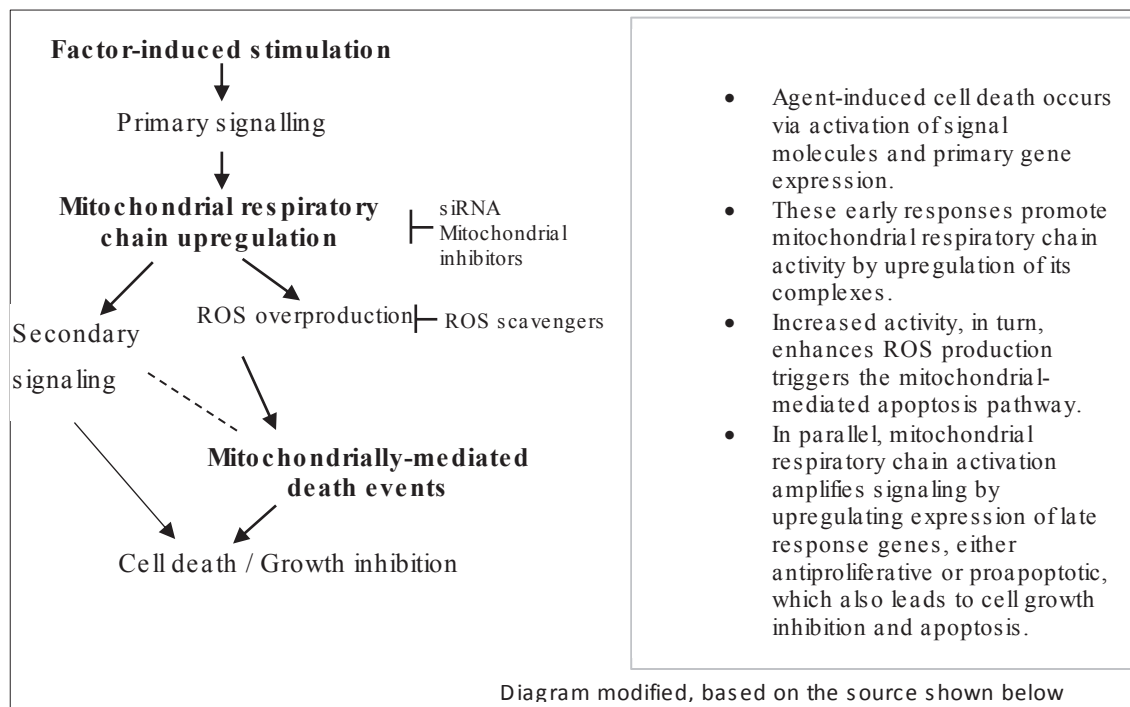

Factor-induced stimulation

Primary signalling

Mitochondrial respiratory chain upregulation — siRNA Mitochondrial inhibitors

Secondary signaling   ROS overproduction — ROS scavengers

Mitochondrially-mediated death events

Cell death / Growth inhibition

- Agent-induced cell death occurs via activation of signal molecules and primary gene expression.
- These early responses promote mitochondrial respiratory chain activity by upregulation of its complexes.
- Increased activity, in turn, enhances ROS production triggers the mitochondrial-mediated apoptosis pathway.
- In parallel, mitochondrial respiratory chain activation amplifies signaling by upregulating expression of late response genes, either antiproliferative or proapoptotic, which also leads to cell growth inhibition and apoptosis.

Diagram modified, based on the source shown below

Figure 45. Diagram showing mitochondria-mediated death events with a central role of the mitochondrial respiratory chain, adapted from a model of Huang et al. (2007).

Additionally there are two facts that should be mentioned

The SLC25A25 belongs to a family of calcium-binding mitochondrial carriers, characteristic to the inner membranes of mitochondria. They shuttle metabolites, nucleotides and cofactors through the mitochondrial membrane and thereby connect and/or regulate cytoplasm and matrix functions. SLC25A25 protein may serve as an ATP-Mg/Pi carrier that mediates the transport of Mg-ATP in exchange for phosphate, and is probably responsible for the net uptake or efflux of adenine nucleotides into or from the mitochondria ("NCBI GENE RESOURCES" 2015). This overexpression might by connected with interactions Calcium flux at the MAM transition between ER and mitochondria is one of the most important factor triggering cell death (Alberts et al. 2002).

The GADD45B gene belongs to a family that produces GADD45 proteins, which interact with Cdc2 protein and inhibit Cdc2 kinase activity, causing growth arrest and exposure to DNA-damaging agents. This factor has been shown to associate with an upstream component of JKN Kinase, which can trigger JNK stress-activated kinase-

120

dependent apoptosis. This is supported by work showing that overexpression of GADD45 in human fibroblasts causes cell arrest in an early mitotic state (Cerquetti et al. 2008), (Stigliano et al. 2008). To sum up, GADDD45 may have a key role in the control of cell progression, regulation of signalling pathways, DNA repair and apoptosis, and may be responsible for mitotane-induced cell death.

5.5 Discussion of findings on response to mitotane in cultured cell lines in relation to effects *in vivo*

The concentration of mitotane in this study was relatively small and within the serum therapeutic range, in contrast to another study (quoted in Section 1.2.7), in which a higher dose of mitotane and a longer exposure time for ACC cell lines was used. That study reported that mitochondrial respiratory chain gene expression changes took place in an uncoordinated way, including underexpression (Hescot *et al.* 2013). However, only one gene per complex was targeted, rather than the comprehensive approach used in the current study. Use of the Affymetrix method, which provides a high throughput, but less sensitive, array analysis has shown mitotane-induced underexpression of steroidogenic enzyme genes, and overexpression of aldehyde dehydrogenase and serpins, which are proteins involved in the intercellular matrix (Zsippai et al., 2012).

The study of mitotane effects using a cell line model does have controversial aspects. Some researchers have not confirmed that it has anticancer ability (section1.3.3); some have shown that it does have effects on other cells. However, these results do fit with the selective susceptibility of the specific adrenocortical cell line, H295R, towards mitotane.

The results reported here do require repetition to enable statistically significant confirmation before it is possible to draw very solid and unambivalent conclusions. They represent a useful initial study, offering an incremental contribution to the very complex problem of the mechanisms of the mitotane effect.

It should be emphasised that the current findings have been established on isolated cells, whereas there is much evidence that the growth of cancer cells frequently depends on interaction with adjacent cell types, such as fibroblasts. While low levels of mitochondrial function within the cancer cell *in situ* may be sustained by these interactions, it might be predicted that fully functioning cell lines in culture would not exhibit this feature. Nevertheless, there may be differences between the cell lines in their mitochondrial number and function and these may directly influence the calculated

Discussion

expression of energy metabolism genes. What it has been possible to show is that for the adrenocortical cell line, which may have more mitochondria in comparison with the two cell lines that are resistant to mitotane, there are observed changes. Those changes embrace mainly gene overexpression of mitochondrial chain complexes and this may be a useful contribution given that mitotane-induced apoptosis occurs through mitochondrial pathways.

Current technologies, including those in the present study, enable changes in expression of large panels of genes to be quantified, but interpretation of the data generated is challenging. Increase or decrease of gene expression may reflect response of an established cell signalling mechanism or may be much less easily interpreted. It may reflect action of an unknown signalling pathway or be a secondary consequence of a toxic effect that has not been recognised. As has been described in results, chapter 4, , more upregulation than downregulation of energy metabolism genes occurs in response to mitotane, so it is tempting to speculate that these do represent organised responses rather than nonspecific toxic effects, which might have been expected to cause decrease of gene expression. As indicated in the review of mitochondrial signalling by Whelen and Zuckerbraun (2013), most studies have been carried out in unicellular organisms, so that any understanding of these processes in the human remains at an early stage.

The bioenergetics of cancer *in vivo* may be different from cancer cell lines, so the features described may not represent the clinical condition. These findings do offer important pointers to the development of protocols for gene expression analysis from FFPE.

5.6 Methodological contribution of mRNA preparation from FFPE; discussion of *mTOR PCR Array* results

In the only retrieved study of gene expression in FFPE material prepared from ACC positive results for RT-PCR for β-actin were obtained in only four out of 14 preparations, two ACCs and two ACAs (Lombardi et al. 2006). In contrast, in the present study, all samples gave positive results for RT-PCR for β-actin. The published study discussed the potential for confusion caused by the presence of non neoplastic tissue in the tumour samples and advised microdissection but pointed out that laser microdissection causes further degradation. The painstaking approach adopted in the present study, in which a

Discussion

scalpel was used under a binocular microscope, therefore appears worthwhile. The single case report of Fonseca et al., (2012) illustrates that comparing benign and malignant areas of the same tumour is important. As pointed out by Lombardi *et al.* (2006), the use of archival FFPEs for the evaluation of the genetic profile of adrenal tumours greatly expands the potential for study, because of the rarity of malignant ACC. The current results, similarly to their presented study, is only a pilot, mainly aimed to set up and validate the methodology, but represents an important technical contribution that suggests that further development towards larger scale analysis would be worthwhile.

The FFPE material has revealed interesting differences in gene expression profiles. In the course of these studies, the FFPE-originated templates were confirmed as a sufficient for gene expression analysis on the PCR array.

The mTOR pathway plays a role as a key regulator of cell growth and proliferation, in response to environmental and nutritional conditions. This pathway may be crucial for cancerogenesis because it acts as a specific switcher, allowing accumulated mRNA to be translated. Signalling through mTOR modulates several downstream pathways that control cell-cycle progression, translation initiation, transcriptional stress responses, protein stability, and survival of cells. Growth factors, amino acids, and ATP and O_2 levels regulate the mTOR signalling pathway (Pópulo, Lopes, and Soares 2012).

Considering the most striking results in this study, referring to their actual biological role in promoting or inhibiting mTOR signaling, VEGFs were found to be strongly overexpressed in ACC tumour in comparison to normal cortex, suggesting a typical picture of an invasive tumour which strongly stimulates angiogenesis. TRKs activate several downstream signals including small GTPases, PKC, and PI3K. Akt activates the protein kinase mTOR, by phosphorylation, promoting cell growth and proliferation (Pópulo, Lopes, and Soares 2012). Other very important results suggest there is blocking of the AMPK pathway main inhibitor of mTOR in the ACC tumour.

A Plan for future experiments should take into consideration a wider scale of research material. Three donors of biological replicates of tumour tissue in comparison to normal cortex would be the minimum requirement for assignment of statistical significance. A scheme of these experiments is shown below.

Discussion
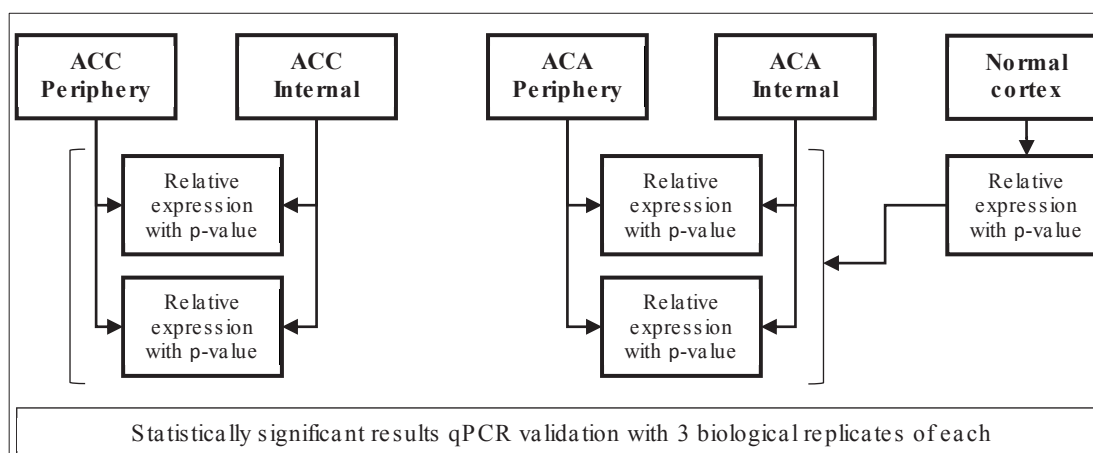
Figure 46. Projected scheme of further research on FFPE derived tumorous material.

ACCs often show areas of necrosis, perhaps indicating that they have outgrown their blood supply and so must have developed in a relatively hypoxic environment. Their patterns of steroidogenesis frequently indicate relative deficit of the enzyme activities that are mitochondrial, especially of 11β-hydroxylase, which may reflect hypoxia or specific mutations that affect mitochondrial function. Although tumours are known to secrete angiogenic factors and so are adept at ensuring their own blood supply, it may be that a capacity to endure hypoxia is a common feature of tumour tissue that is critical to their survival and proliferation. It may be predicted that cancer cell survival mirrors an evolutionary process: only those with useful mutations will be selected to grow. The observation that glycolysis is enhanced and oxidative phosphorylation is diminished in many cancers, together with increase of lactate fermentation (the Warburg effect) may reflect a capacity to cope with hypoxia but also has importance for the supply of glycolysis pathway intermediates that are utilised for cell growth and differentiation.

Growth of malignant tissue may require cooperation with adjacent non-malignant tissue. Observations on lactate production or utilisation may reflect more the activity of adjacent cell types such as fibroblasts than the cancer cells (Section 2.2.1).

Given that ACCs are very diverse in their steroid biochemistry and have areas within them of different cell types, it may be predicted that detailed bioenergetic studies of ACC will uncover a large diversity of mutations related to energy metabolism. The use of one culture of the cell line (H295R) in the current study offers a model for an ACC cell type that is sensitive to mitotane. However this model may not reflect the diversity of mutations and changes in gene expression in energy pathways that might be found across the range of ACC. Even small changes in incubation conditions for the cells under study

124

Discussion

were found to result in changes in the pattern of steroid accumulation in the medium (Paulina Szyszka personal communication).

Whether or not mitochondria in ACC tissue have defective energy metabolism, it may be that, given the requirement of molecular oxygen for steroid metabolism in mitochondria and the overall tendency to hypoxia in these tumours, mitotane may differentially affect ACC mitochondria by promoting energy metabolism and thus oxygen utilisation in an organelle which is already poised at the limit of its minimum oxygen requirements. The observation that 11β-hydroxylation is inhibited by mitotane offers support for such a conclusion.

Conclusions

To Aim 1:

Following a process of optimization using an array for mTOR, quantification of cDNA transcripts obtained by qPCR amplification was achieved for the mitochondrial energy metabolism array, expressed as CT values for the control and mitotane-treated groups for each of the four cancer cell types.

To Aim 2:

The calculation of -fold difference between cell types and treatment by the delta delta CT method enabled comparison of the expression of energy metabolism genes between the cell lines under study. Under basal conditions, there was a range of activities of mitochondrial energy metabolism genes in the ascending order: MCF-7, H295R, H1975, HKe-3. The higher expression in HKe-3 was dominated by genes in complex 1 when compared with H1975 and H295R but not in comparison with H1975. Considering the adrenal H295R cells, there were no clear trends in comparison with the other cell lines, with genes of all complexes represented and no single group dominating. Alteration of mitochondrial energy metabolism was shown to take place in response to mitotane, mostly in a non unified manner.

To Aim 3:

The finding of increased expression of GADD45 only in the H295R cells confirms earlier reports that mitotane suppresses cell growth in the G2-M phase, where growth arrest mediated by this p53 effector is a major mechanism. This factor can trigger JNK stress-activated kinase-dependent apoptosis, suggesting that it is one mediator of the adrenolytic action of mitotane.

ACC H295R showed visible changes in response to mitotane towards overexpression of genes involved in mitochondrial energy metabolism, even though exposed to a smaller concentration of the agent (10 μM) and for a time of only 24h, in contrast with the other cell lines, which were treated for 3 days with 40 μM mitotane. This does suggest that these are involved in the processes of cell stasis and death via generation of ROS and promotion of apoptosis. However, it should be noted that the changes will have taken

126

Conclusions

place in intact cells that have not yet undergone apoptosis, so may not reflect the later phases of cell destruction. Studies published since this work was planned indicate that effects of mitotane on calcium signalling at the MAM are likely to be key to understanding mitotane specificity, but, given the multifactorial nature of the processes outlined in this thesis, changes in energy metabolism genes that this study has characterised may be contributory.

To Aim 4.

Yield and quality of RNA following optimisation was found to be sufficient for the requirements of microarray-based methods of examining gene expression. A preliminary check using an mTOR array on 2 preparations gave good results. This is substantially better than published findings and provides an encouraging indication that different portions of an adrenal tumour preserved as an FFPE block can be compared.

Overall conclusions

Alteration of mitochondrial energy metabolism in response to mitotane does not take place in a unified manner, with these results suggesting upregulation in both respiratory complexes and other proapoptotic proteins related to a variety of mechanisms which may play a key role in the processes of cell stasis and death.

The wider significance of these findings is difficult to judge, since published gene expression studies in the area of mitochondrial energy metabolism are limited and changes may represent the resultant of more than one process. However, after combining results into groups of 'more' and 'less' sensitive cell lines, the more sensitive show significantly increased expression of more genes than the less sensitive cell lines, suggesting that these increases either contribute to cell death via promotion of damaging processes such as formation of ROS and/or represent an enhanced protective response secondary to the greater toxic effects in this group. Direct, non genomic effects of mitotane are also likely.

The results reported here cannot be said to to convey definitive information until they are confirmed by larger studies. However, these preliminary indications of changes of energy metabolism genes are capable of further testing, since the cultured cells used are

127

Conclusions

standardised, homogeneous groups. However, use of cell culture findings to develop models of mitotane action in vivo requires caution, since the controlled environment in which cells proliferate *in vitro* is very different to the circumstances of cell-cell interaction within living tissue.

The encouraging preliminary results on preparation of mRNA from FFPE material from adrenocortical carcinomas does show that careful preparation, with optimisation of each step, is a productive approach, potentially opening the way to understanding structure-function relationships within this highly heterogeneous tumour and perhaps improving assessment of prognosis in individual patients.

Appendix

Appendix A: QIAGEN Human Mitochondrial Energy Metabolism Plus *RT² Profiler PCR Array.*

This list of incorporates information supplied by the manufacturer (QIAGEN) in the *Human Mitochondrial Energy Metabolism Plus RT² Profiler PCR Array*. together with names of complexes, grouping genes of the array in order to keep the integrity of classification used across the document.

Complex I (NADH-Coenzyme Q Reductase: NDUFA1, NDUFA10, NDUFA11, NDUFA2, NDUFA3, NDUFA4, NDUFA5, NDUFA6, NDUFA8, NDUFAB1, NDUFB10, NDUFB2, NDUFB3, NDUFB4, NDUFB5, NDUFB6, NDUFB7, NDUFB8, NDUFB9, NDUFC1, NDUFC2, NDUFS1, NDUFS2, NDUFS3, NDUFS4, NDUFS5, NDUFS6, NDUFS7, NDUFS8, NDUFV1, NDUFV2, NDUFV3);

Complex II (Succinate-Coenzyme Q Reductase: SDHA, SDHB, SDHC, SDHD);

Complex III (Coenzyme Q-Cytochrome c Reductase: CYC1, UQCR11, UQCRC1, UQCRC2, UQCRFS1, UQCRH, UQCRQ);

Note: In the table below complex III is split into two parts.

Complex IV (Cytochrome c Oxidase: COX4I1, COX5A, COX5B, COX6A1, COX6A2, COX6B1, COX6C, COX7A2, COX7A2L, COX7B; COX8A);

Complex V (ATP Synthase: ATP5A1, ATP5B, ATP5C1, ATP5F1, ATP5G1, ATP5G2, ATP5G3, ATP5H, ATP5I, ATP5J, ATP5J2, ATP5L, ATP5O, PPA1);

Note: In the table below complex V is split into two parts.

Pathway Activity Score (ARRDC3, ASB1, CYB561D1, DNAJB1, EDN1, GADD45B, HSPA1A, HSPA1B, LRP5L, MitoH1, MitoH2_12106, MitoH2_14573, MitoH2_4162, MitoH2_5726, RNU11, SLC25A25);

Reference and control genes (ACTB, B2M, GAPDH, HPRT1, RPLP0, HGDC, RTC, RTC, RTC, PPC, PPC, PPC).

Position	UniGene	GeneBank	Symbol	Description	Gene Name
Complex V (ATP Synthase) – part 1					
A01	Hs.298280	NM_004046	ATP5A1	ATP synthase, H+ transporting, mitochondrial F1 complex, alpha subunit 1, cardiac muscle	ATP5A, ATP5AL2, ATPM, HEL-S-123m, MC5DN4, MOM2, OMR, ORM, hATP1
A02	Hs.406510	NM_001686	ATP5B	ATP synthase, H+ transporting, mitochondrial F1 complex, beta polypeptide	ATPMB, ATPSB, HEL-S-271
A03	Hs.271135	NM_005174	ATP5C1	ATP synthase, H+ transporting, mitochondrial F1 complex, gamma polypeptide 1	ATP5C, ATP5CL1

129

Position	UniGene	GeneBank	Symbol	Description	Gene Name
A04	Hs.514870	NM_001688	ATP5F1	ATP synthase, H+ transporting, mitochondrial Fo complex, subunit B1	PIG47
A05	Hs.80986	NM_005175	ATP5G1	ATP synthase, H+ transporting, mitochondrial Fo complex, subunit C1 (subunit 9)	ATP5A, ATP5G
A06	Hs.524464	NM_001002031	ATP5G2	ATP synthase, H+ transporting, mitochondrial Fo complex, subunit C2 (subunit 9)	ATP5A
A07	Hs.429	NM_001689	ATP5G3	ATP synthase, H+ transporting, mitochondrial Fo complex, subunit C3 (subunit 9)	P3
A08	Hs.514465	NM_006356	ATP5H	ATP synthase, H+ transporting, mitochondrial Fo complex, subunit d	ATPQ
A09	Hs.85539	NM_007100	ATP5I	ATP synthase, H+ transporting, mitochondrial Fo complex, subunit E	ATP5K
A10	Hs.246310	NM_001685	ATP5J	ATP synthase, H+ transporting, mitochondrial Fo complex, subunit F6	ATP5, ATP5A, ATPM, CF6, F6
A11	Hs.656515	NM_004889	ATP5J2	ATP synthase, H+ transporting, mitochondrial Fo complex, subunit F2	ATP5JL
A12	Hs.486360	NM_006476	ATP5L	ATP synthase, H+ transporting, mitochondrial Fo complex, subunit G	ATP5JG
B01	Hs.409140	NM_001697	ATP5O	ATP synthase, H+ transporting, mitochondrial F1 complex, O subunit	ATPO, OSCP

Complex IV (Cytochrome c Oxidase)

Position	UniGene	GeneBank	Symbol	Description	Gene Name
B02	Hs.433419	NM_001861	COX4I1	Cytochrome c oxidase subunit IV isoform 1	COX4, COX4-1, COXIV
B03	Hs.401903	NM_004255	COX5A	Cytochrome c oxidase subunit Va	COX, COX-VA, VA
B04	Hs.1342	NM_001862	COX5B	Cytochrome c oxidase subunit Vb	COXVB
B05	Hs.706889	NM_004373	COX6A1	Cytochrome c oxidase subunit VIa polypeptide 1	COX6A, COX6AL
B06	Hs.250760	NM_005205	COX6A2	Cytochrome c oxidase subunit VIa polypeptide 2	COX6AH, COXVIAH
B07	Hs.431668	NM_001863	COX6B1	Cytochrome c oxidase subunit Vib polypeptide 1 (ubiquitous)	COX6B, COXG, COXVIb1
B08	Hs.351875	NM_004374	COX6C	Cytochrome c oxidase subunit VIc	-
B09	Hs.70312	NM_001865	COX7A2	Cytochrome c oxidase subunit VIIa polypeptide 2 (liver)	COX7AL, COX7AL1, COXVIIAL, COXVIIa-L, VIIAL
B10	Hs.744101	NM_004718	COX7A2L	Cytochrome c oxidase subunit VIIa polypeptide 2 like	COX7AR, COX7RP, EB1, SIG81
B11	Hs.522699	NM_001866	COX7B	Cytochrome c oxidase subunit VIIb	APLCC
B12	Hs.743989	NM_004074	COX8A	Cytochrome c oxidase subunit VIIIA (ubiquitous)	COX, COX8, COX8-2, COX8L, VIII, VIII-L

Appendix

Position	UniGene	GeneBank	Symbol	Description	Gene Name
Complex III (Coenzyme Q-Cytochrome c Reductase) – part 1					
C01	Hs.289271	NM_001916	CYC1	Cytochrome c-1	MC3DN6, UQCR4
Complex I (NADH-Coenzyme Q Reductase)					
C02	Hs.534168	NM_004541	NDUFA1	NADH dehydrogenase (ubiquinone) 1 alpha subcomplex, 1, 7.5kDa	CI-MWFE, MWFE, ZNF183
C03	Hs.277677	NM_004544	NDUFA10	NADH dehydrogenase (ubiquinone) 1 alpha subcomplex, 10, 42kDa	CI-42KD, CI-42k
C04	Hs.406062	NM_175614	NDUFA11	NADH dehydrogenase (ubiquinone) 1 alpha subcomplex, 11, 14.7kDa	B14.7, CI-B14.7
C05	Hs.75914	NM_002488	NDUFA2	NADH dehydrogenase (ubiquinone) 1 alpha subcomplex, 2, 8kDa	B8, CD14, CIB8
C06	Hs.198269	NM_004542	NDUFA3	NADH dehydrogenase (ubiquinone) 1 alpha subcomplex, 3, 9kDa	B9, CI-B9
C07	Hs.50098	NM_002489	NDUFA4	NADH dehydrogenase (ubiquinone) 1 alpha subcomplex, 4, 9kDa	CI-9k, CI-MLRQ, MLRQ
C08	Hs.651219	NM_005000	NDUFA5	NADH dehydrogenase (ubiquinone) 1 alpha subcomplex, 5, 13kDa	B13, CI-13KD-B, CI-13kB, NUFM, UQOR13
C09	Hs.274416	NM_002490	NDUFA6	NADH dehydrogenase (ubiquinone) 1 alpha subcomplex, 6, 14kDa	B14, CI-B14, LYRM6, NADHB14
C10	Hs.495039	NM_014222	NDUFA8	NADH dehydrogenase (ubiquinone) 1 alpha subcomplex, 8, 19kDa	CI-19KD, CI-PGIV, PGIV
C11	Hs.189716	NM_005003	NDUFAB1	NADH dehydrogenase (ubiquinone) 1, alpha/beta subcomplex, 1, 8kDa	ACP, FASN2A, SDAP
C12	Hs.513266	NM_004548	NDUFB10	NADH dehydrogenase (ubiquinone) 1 beta subcomplex, 10, 22kDa	PDSW
D01	Hs.655788	NM_004546	NDUFB2	NADH dehydrogenase (ubiquinone) 1 beta subcomplex, 2, 8kDa	AGGG, CI-AGGG
D02	Hs.109760	NM_002491	NDUFB3	NADH dehydrogenase (ubiquinone) 1 beta subcomplex, 3, 12kDa	B12, CI-B12
D03	Hs.304613	NM_004547	NDUFB4	NADH dehydrogenase (ubiquinone) 1 beta subcomplex, 4, 15kDa	B15, CI-B15
D04	Hs.730674	NM_002492	NDUFB5	NADH dehydrogenase (ubiquinone) 1 beta subcomplex, 5, 16kDa	CISGDH, SGDH

Appendix

Position	UniGene	GeneBank	Symbol	Description	Gene Name
D05	Hs.493668	NM_182739	NDUFB6	NADH dehydrogenase (ubiquinone) 1 beta subcomplex, 6, 17kDa	B17, CI
D06	Hs.532853	NM_004146	NDUFB7	NADH dehydrogenase (ubiquinone) 1 beta subcomplex, 7, 18kDa	B18, CI-B18
D07	Hs.523215	NM_005004	NDUFB8	NADH dehydrogenase (ubiquinone) 1 beta subcomplex, 8, 19kDa	ASHI, CI-ASHI
D08	Hs.15977	NM_005005	NDUFB9	NADH dehydrogenase (ubiquinone) 1 beta subcomplex, 9, 22kDa	B22, CI-B22, LYRM3, UQOR22
D09	Hs.84549	NM_002494	NDUFC1	NADH dehydrogenase (ubiquinone) 1, subcomplex unknown, 1, 6kDa	KFYI
D10	Hs.407860	NM_004549	NDUFC2	NADH dehydrogenase (ubiquinone) 1, subcomplex unknown, 2, 14.5kDa	B14.5b, CI-B14.5b, HLC-1, NADHDH2
D11	Hs.598436	NM_005006	NDUFS1	NADH dehydrogenase (ubiquinone) Fe-S protein 1, 75kDa (NADH-coenzyme Q reductase)	CI-75Kd, CI-75k, PRO1304
D12	Hs.173611	NM_004550	NDUFS2	NADH dehydrogenase (ubiquinone) Fe-S protein 2, 49kDa (NADH-coenzyme Q reductase)	CI-49
E01	Hs.502528	NM_004551	NDUFS3	NADH dehydrogenase (ubiquinone) Fe-S protein 3, 30kDa (NADH-coenzyme Q reductase)	CI-30
E02	Hs.528222	NM_002495	NDUFS4	NADH dehydrogenase (ubiquinone) Fe-S protein 4, 18kDa (NADH-coenzyme Q reductase)	AQDQ, CI-18
E03	Hs.632385	NM_004552	NDUFS5	NADH dehydrogenase (ubiquinone) Fe-S protein 5, 15kDa (NADH-coenzyme Q reductase)	CI-15k, CI15K
E04	Hs.408257	NM_004553	NDUFS6	NADH dehydrogenase (ubiquinone) Fe-S protein 6, 13kDa (NADH-coenzyme Q reductase)	CI-13kA, CI-13kD-A, CI13KDA
E05	Hs.211914	NM_024407	NDUFS7	NADH dehydrogenase (ubiquinone) Fe-S protein 7, 20kDa (NADH-coenzyme Q reductase)	CI-20, CI-20KD, MY017, PSST
E06	Hs.90443	NM_002496	NDUFS8	NADH dehydrogenase (ubiquinone) Fe-S protein 8, 23kDa (NADH-coenzyme Q reductase)	CI-23k, CI23KD, TYKY
E07	Hs.7744	NM_007103	NDUFV1	NADH dehydrogenase (ubiquinone) flavoprotein 1, 51kDa	CI-51K, CI51KD, UQOR1
E08	Hs.464572	NM_021074	NDUFV2	NADH dehydrogenase (ubiquinone) flavoprotein 2, 24kDa	CI-24k
E09	Hs.473937	NM_021075	NDUFV3	NADH dehydrogenase (ubiquinone) flavoprotein 3, 10kDa	CI-10k, CI-9KD

Complex V (ATP Synthase) – part 2

Position	UniGene	GeneBank	Symbol	Description	Gene Name
E10	Hs.437403	NM_021129	PPA1	Pyrophosphatase (inorganic) 1	HEL-S-66p, IOPPP, PP, PP1, SID6-8061

Appendix

Position	UniGene	GeneBank	Symbol	Description	Gene Name
Complex II (Succinate-Coenzyme Q Reductase)					
E11	Hs.440475	NM_004168	SDHA	Succinate dehydrogenase complex, subunit A, flavoprotein (Fp)	CMD1GG, FP, PGL5, SDH1, SDH2, SDHF
E12	Hs.465924	NM_003000	SDHB	Succinate dehydrogenase complex, subunit B, iron sulfur (Ip)	CWS2, IP, PGL4, SDH, SDH1, SDH2, SDHIP
F01	Hs.444472	NM_003001	SDHC	Succinate dehydrogenase complex, subunit C, integral membrane protein, 15kDa	CYB560, CYBL, PGL3, QPS1, SDH3
F02	Hs.744039	NM_003002	SDHD	Succinate dehydrogenase complex, subunit D, integral membrane protein	CBT1, CII-4, CWS3, PGL, PGL1, QPs3, SDH4, cybS
Complex III (Coenzyme Q-Cytochrome c Reductase) – part 2					
F03	Hs.8372	NM_006830	UQCR11	Ubiquinol-cytochrome c reductase, complex III subunit XI	0710008D09Rik, QCR10, UQCR
F04	Hs.119251	NM_003365	UQCRC1	Ubiquinol-cytochrome c reductase core protein I	D3S3191, QCR1, UQCR1
F05	Hs.528803	NM_003366	UQCRC2	Ubiquinol-cytochrome c reductase core protein II	MC3DN5, QCR2, UQCR2
F06	Hs.743307	NM_006003	UQCRFS1	Ubiquinol-cytochrome c reductase, Rieske iron-sulfur polypeptide 1	RIP1, RIS1, RISP, UQCR5
F07	Hs.481571	NM_006004	UQCRH	Ubiquinol-cytochrome c reductase hinge protein	QCR6, UQCR8
F08	Hs.146602	NM_014402	UQCRQ	Ubiquinol-cytochrome c reductase, complex III subunit VII, 9.5kDa	MC3DN4, QCR8, QP-C, QPC, UQCR7
Complex VI (Pathway Activity Score)					
F09	Hs.24684	NM_020801	ARRDC3	Arrestin domain containing 3	TLIMP
F10	Hs.516788	NM_001040445	ASB1	Ankyrin repeat and SOCS box containing 1	ASB-1
F11	Hs.514682	NM_182580	CYB561D1	Cytochrome b-561 domain containing 1	-
F12	Hs.515210	NM_006145	DNAJB1	DnaJ (Hsp40) homolog, subfamily B, member 1	HSPF1, Hdj1, Hsp40, RSPH16B, Sis1
G01	Hs.713645	NM_001955	EDN1	Endothelin 1	ET1, HDLCQ7, PPET1
G02	Hs.110571	NM_015675	GADD45B	Growth arrest and DNA-damage-inducible, beta	GADD45BETA, MYD118
G03	Hs.702139	NM_005345	HSPA1A	Heat shock 70kDa protein 1A	HEL-S-103, HSP70-1, HSP70-1A, HSP70I, HSP72, HSPA1
G04	Hs.719966	NM_005346	HSPA1B	Heat shock 70kDa protein 1B	HSP70-1B, HSP70-2
G05	Hs.634058	NM_182492	LRP5L	Low density lipoprotein receptor-related protein 5-like	-
G06	N/A	r4_NC_012920	MitoH1	Polycistronic_H1_3	
G07	N/A	r3_NC_012920	MitoH2_12106	Polycistronic_H2_200_12106_1	
G08	N/A	r2_NC_012920	MitoH2_14573	Polycistronic_H2_200_14573_3	
G09	N/A	r1_NC_012920	MitoH2_4162	Polycistronic_H2_200_4162_1	

Appendix

Position	UniGene	GeneBank	Symbol	Description	Gene Name
G10	N/A	r5_NC_012920	MitoH2_5726	Polycistronic_H2_200_5726_3	
G11	Hs.640266	NR_004407	RNU11	RNU11	RNU11-1, U11
G12	Hs.729700	NM_052901	SLC25A25	Solute carrier family 25 (mitochondrial carrier; phosphate carrier), member 25	MCSC, PCSCL, RP11-395P17.4, SCAMC-2
Reference and control genes					
H01	Hs.520640	NM_001101	ACTB	Actin, beta	BRWS1, PS1TP5BP1
H02	Hs.534255	NM_004048	B2M	Beta-2-microglobulin	-
H03	Hs.544577	NM_002046	GAPDH	Glyceraldehyde-3-phosphate dehydrogenase	G3PD, GAPD
H04	Hs.412707	NM_000194	HPRT1	Hypoxanthine phosphoribosyltransferase 1	HGPRT, HPRT
H05	Hs.546285	NM_001002	RPLP0	Ribosomal protein, large, P0	L10E, LP0, P0, PRLP0, RPP0
H06	N/A	SA_00105	HGDC	Human Genomic DNA Contamination	HIGX1A
H07	N/A	SA_00104	RTC	Reverse Transcription Control	RTC
H08	N/A	SA_00104	RTC	Reverse Transcription Control	RTC
H09	N/A	SA_00104	RTC	Reverse Transcription Control	RTC
H10	N/A	SA_00103	PPC	Positive PCR Control	PPC
H11	N/A	SA_00103	PPC	Positive PCR Control	PPC
H12	N/A	SA_00103	PPC	Positive PCR Control	PPC

Appendix

Appendix B: *Described effects of mitotane, a summary of the references*

Mitotane effects on:	Cellular material	Reference
Gross morphology and cell growth		
Inhibition of cell growth and proliferation	H295R	(Schteingart et al. 1993) (Dworakowska et al. 2015) (Cerquetti et al. 2008) (De Martino et al. 2015)
Blockage of cell division, growth and function in a dose-related, reversible manner	H295R	(Fang 1979)* (Schteingart et al. 1993) (Schteingart et al. 1993)
G2 arrest	H295R	(Lehmann, Wrzesinski, and Jagodzinski 2013) (Cerquetti et al. 2008)
Cytotoxicity, with more than half cells undergoing apoptosis in the therapeutic range	H295R	(Fang 1979)*(Poli et al. 2013)
Cell death	Adrenal primary culture	(Morishita et al. 2001)
Growth arrest of tumour deposits, prevention of recurrence and improvement of overall survival rates, when maintained in therapeutic range	clinical research	(Terzolo et al. 2007), (Hescot et al. 2013), (Takeshita et al. 2013), (Else et al. 2014).
Higher toxicity for adrenal cell lines than other cell lines	H295R	(Poli et al. 2013) (Dworakowska et al. 2015)
Higher toxicity for adrenal cell lines when combined with IGF-1R antagonists	H295R mouse xenograft	(Barlaskar et al. 2009)
Apoptosis	H295R	(Fang 1979)* (Poli et al. 2013) (Stigliano et al. 2008) (Lehmann, Wrzesinski, and Jagodzinski 2013) (Schteingart et al. 1993) (Hescot et al. 2014) (Germano et al. 2014) (Barlaskar et al. 2009)
Caspase cascade-mediated apoptosis	H295R	(Lehmann, Wrzesinski, and Jagodzinski 2013)

Apoptosis not acting by the P53 c-Myc pathway	H295R	(Lehmann, Wrzesinski, and Jagodzinski 2013) (Cerquetti et al. 2008)
Suppression of tumour necrosis factor alpha (TNF)-induced apoptosis	ER-positive MCF-7 human breast carcinoma cells	(Burow et al. 1999)
Combined stronger inhibition of cell growth with sirolimus	H295R	(De Martino et al. 2015)
Combined stronger inhibition of cell growth with gemcitabine	SW13	(Martz and Straw 1980)
Combined weaker inhibition of cell growth with gemcitabine	H295R	(Martz and Straw 1980)
Adrenal damage observed by light microscopy, including haemorrhage and necrosis	Animal tissue preps	(Breuner et al. 2000) (Schteingart et al. 1993) (Martz and Straw 1977) (Martz and Straw 1980) (Cai, Counsell, et al. 1995)
Similarity of effects across animal species	Animal tissue preps	(Cai et al. 1997) (Martz and Straw 1980) (Cai, Counsell, et al. 1995)
Mitochondrial structure		
Visible evidence of cytotoxicity on adrenal cells on electron microscopy	H295R	(Fang 1979)* (Poli et al. 2013) (A Zsippai et al. 2012) (Schteingart et al. 1993)
Visible evidence of a toxic reaction on electron microscopy	Animal tissue preps	(Hart, Reagan, and Adamson 1973)
Swelling or defragmentation of mitochondria with dissolution of the inner matrix.	H295R	(Fang 1979)* (Poli et al. 2013) (Hescot et al. 2013)
Swelling or defragmentation of mitochondria	Animal tissue preps	(Hart, Reagan, and Adamson 1973) (Martz and Straw 1977) (Martz and Straw 1980) (Cai, Counsell, et al. 1995)
Mitochondrial function		

Appendix

Enhancement of mitochondrial biogenesis	H295R	(Hescot et al. 2014)
Mitochondrial membrane depolarisation and permeability	H295R	(Poli et al. 2013) (Hescot et al. 2013) (Stigliano et al. 2008)
Decrease of net oxygen consumption	H295R	(Poli et al. 2013)
Effects on mitochondrial respiratory chain enzyme activity, oxidative stress, ROS production	H295R	(Poli et al. 2013) (Hescot et al. 2013) (Stigliano et al. 2008) (Schteingart et al. 1993) (Hescot et al. 2014)
Mitochondria associated ER membranes		
ER stress, with a key role of inhibition of SOAT1 enzyme complex, resulting in reduction of cholesterol ester and increase of free cholesterol, transducing signal through transciption factors, with final CHOP triggering intrinsic pathway by interaction with Bax and Bcl-2. Action mimics Sandoz 58-035 (SOAT1 inhibitor)	H295R	(Sbiera et al. 2015)
FATE1 expression decreases apoptosis on exposure to mitotane; FATE1 knockdown increases it	Dox – treated H295RTR SF-1	(Doghman-Bouguerra et al. 2016)
Mechanism of action is similar to ATR-101 (SOAT1 inhibitor) [23], inducing caspase-dependent apoptosis	H295R	(Kroiss and Fassnacht 2016)
Cell biochemistry – interaction with steroidogenesis		
Loss of steroidogenesis, steroid inhibitory effects	H295R	(Hescot et al. 2013) (Stigliano et al. 2008) (A Zsippai et al. 2012) (Schteingart et al. 1993) (Hescot et al. 2014) (A Zsippai et al. 2012)
Loss of steroidogenesis, steroid inhibitory effects	Adrenal primary culture	(Morishita et al. 2001) (Touitou, Bogdan, and Luton 1978)
Non effectiveness of unchanged mitotane; activation involves cytochrome P450(s)	Adrenal primary culture	(Touitou, Bogdan, and Luton 1978) (Touitou, Bogdan, and Luton 1978) (Nelson and Woodard 1949)

Appendix

Induction of *CYP3A4* expression trought activation of the steroid and xenobiotic receptor in the liver and intestine	human hepatocyte-derived cells culture	(Takeshita et al. 2013)
Activation via cytochrome P450(s)	Animal tissue preps	(Schteingart et al. 1993) (Martz and Straw 1977) (Cai et al. 1997) (Martz and Straw 1980) (Cai, Counsell, et al. 1995)
Steroid inhibitory effects or loss of steroidogenesis	Animal tissue preps	(Breuner et al. 2000) (Young et al. 1973)
Androgen receptor antagonism	Animal tissue preps	(Breuner et al. 2000)
Posible decrease aldosterone production	Clinical study	(Fukushima, Bradlow, and Hellman 1971), (Fassnacht and Allolio 2009), (Schteingart et al. 1980)
Decrease of cortisol secretion	Clinical study	(Schteingart et al. 1980) (Howlett, Rees, and Besser 1985), (Ghataore et al. 2012), (Takeshita et al. 2013)
Proteome		
Intracellular formation and irreversible binding of protein adducts	H295R	(Poli et al. 2013) (Schteingart et al. 1993) (Schteingart et al. 1993)
Modulation of proteins playing roles in: tumourigenesis, respiratory chain enzyme activity, oxidative stress, cytoskeletal structure, growth, ageing, transcription, RNA splicing	H295R	(Stigliano et al. 2008)
Mitochondrial protein macromolecule formation	Animal tissue preps	(Martz and Straw 1980)
Irreversible formation and binding of protein adducts, covalent bound of mitotane metabolites to proteins, and binding to phospholipids	Animal tissue preps	(Martz and Straw 1980) (Cai, Counsell, et al. 1995) (Schteingart 2000)
Genome		
Suppression of complex IX (COX) gene expression but not complex II or III	H295R	(Hescot et al. 2013)

138

Appendix

Expression change in 567/1967 genes: of 30 most downregulated, 8 involved in lipid metabolism & steroidogenesis; of 30 most upregulated, 6 relate to apoptosis; activation of 22/53 ER stress response genes	H295R	(Sbiera et al. 2015)
Suppression of genes coding for steroidogenic enzymes	H295R	(Hescot et al. 2013) (Adrienn Zsippai et al. 2012) (Lehmann, Wrzesinski, and Jagodzinski 2013)[36] (Lin, Chang, and Pu 2012)
Oestrogenic effect via induction of gene expression for SHBG and CBG	Human hepatoma cells	(Nader et al. 2006)

Appendix

Appendix C: *Description of QIAGEN Human mTOR Signaling RT² Profiler PCR Array*.

The mTORC1 complex controls biosynthetic cellular processes such as protein synthesis, cell cycle progression, cell growth and proliferation, whereas the mTORC2 response is AKT activation, important for cell proliferation, migration and survival (apoptosis and autophagy inhibition). The first generation of mTOR inhibitors e.g. rapamycin failed to inhibit all its functions, because the kinase forms two distinct protein complexes, mTORC1 and mTORC2. The current *mTOR PCR Array* includes members of the mTORC1 and mTORC2 complexes as well as upstream regulators of many mTOR responses, and downstream genes from the many cellular processes regulated by mTOR complex activation (QIAGEN 2015).

Appendix
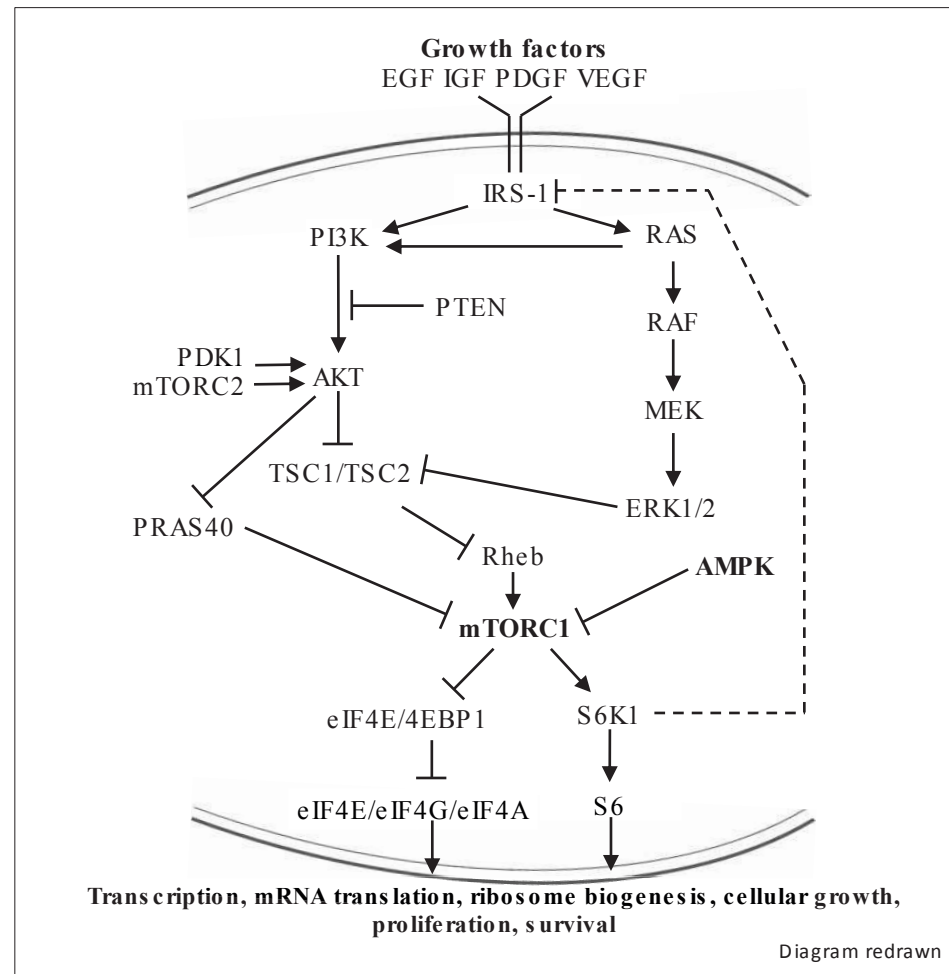
Figure 47. Diagram of mTOR signalling with TRK receptor (Y-shaped on the image) (taken from (Pópulo, Lopes, and Soares 2012))*).*
On the Figure 8, arrows indicate activation and T-shaped connectors indicate inhibition. The Y-shape on the top of the image symbolises the

TRK receptor, the role of which is described later in the Section 5.3.

141

Appendix

The Complexes and regulative functions of the *mTOR PCR Array* and their members are listed below.

mTOR Complexes

mTORC1 Complex: MLST8, MTOR, RPTOR.

mTORC2 Complex: MLST8, MAPKAP1, MTOR, RICTOR.

mTOR Upstream Regulators

mTORC1 Positive Regulation: AKT1, AKT2, AKT3, HRAS, IGF1, IKBKB (IKKβ), INS, INSR, IRS1, MAPK1 (ERK2), MAPK3(ERK1), PDPK1, PIK3C3 (Vps34), PIK3CA (p110-alpha), PIK3CB, PIK3CD, PIK3CG, PLD1, PLD2, RHEB, RPS6KA1,RPS6KA2, RPS6KA5, RRAGA, RRAGB, RRAGC, RRAGD, TELO2.

mTORC2 Positive Regulation: AKT1, AKT2, AKT3, MAPK1 (ERK2), MAPK3 (ERK1), PDPK1, PIK3C3 (Vps34), PIK3CA(p110-alpha), PIK3CB, PIK3CD, PIK3CG, RHEB, RPS6KA1, RPS6KA2, RPS6KA5.

mTORC1 Negative Regulation: AKT1S1 (PRAS40), CAB39, CAB39L, DDIT4 (REDD1), DDIT4L (REDD2), DEPTOR(DEPDC6), FKBP1A (FKBP12), FKBP8, IGFBP3, PRKAA1 (AMPK), PRKAA2, PRKAB1, PRKAB2, PRKAG1, PRKAG2,PRKAG3, PTEN, STK11 (LKB1), STRADB, TP53 (p53), TSC1, TSC2, YWHAQ (14-3-3θ).

mTORC2 Negative Regulation: CAB39, CAB39L, DDIT4 (REDD1), DDIT4L (REDD2), DEPTOR (DEPDC6), PRKAA1(AMPK), PRKAA2, PRKAB1, PRKAB2, PRKAG1, PRKAG2, PRKAG3, STK11 (LKB1), STRADB, TSC1, TSC2.

mTOR Downstream Effectors

mTORC1 Positive Regulation: CHUK (IKKα), EIF4B, EIF4E, HIF1A, IKBKB (IKKβ), RPS6, RPS6KB1, RPS6KB2, TP53 (p53),VEGFA, VEGFB, VEGFC.

mTORC2 Positive Regulation: AKT1, CDC42, GSK3B, HSPA4 (hsp70), ILK, MYO1C, PRKCA, PRKCB, PRKCE, PRKCG,RHOA, RPS6KB1, SGK1.

mTORC1 Negative Regulation: EIF4EBP1 (4E-BP1), EIF4EBP2, PPP2CA, PPP2R2B, PPP2R4, TP53 (p53), ULK1, ULK2.

Cellular Processes Regulated by mTOR Signaling

Amino Acid Response: PIK3C3 (Vps34), RRAGA, RRAGB, RRAGC, RRAGD.

Angiogenesis: CHUK (IKKα), DDIT4 (REDD1), DDIT4L (REDD2), HIF1A, IKBKB (IKKβ), VEGFA, VEGFB, VEGFC.

Autophagy: PIK3C3 (Vps34), ULK1, ULK2.

Cytoskeletal Organization: CDC42, PRKCA, PRKCB, PRKCE, PRKCG, RHOA.

Growth Factor Response: HRAS, IGF1, IGFBP3, MAPK1 (ERK2), MAPK3 (ERK1), RPS6KA1, RPS6KA2, RPS6KA5.

Energy Stress: PRKAA1 (AMPK), PRKAA2, PRKAB1, PRKAB2, PRKAG1, PRKAG2, PRKAG3.

Insulin Signaling: AKT1, AKT2, AKT3, INS, INSR, IRS1, PDPK1, PIK3CA (p110-alpha), PIK3CB, PIK3CD, PIK3CG, TP53(p53).
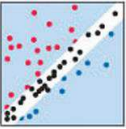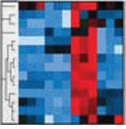
Lipid Metabolism: PLD1, PLD2.

Appendix

Appendix D: Explanation of plot types

All descriptions in this table are cited *in extenso* from the *RT² PCR Array Data Analysis version 3.5 software* manufacturer site:

http://pcrdataanalysis.sabiosciences.com/pcr/arrayanalysis.php?target=plothome

Plot type	Description
Scatter Plot	**The scatter** plot compares the normalized expression of every gene on the array between two groups by plotting them against one another to quickly visualize large gene expression changes. The central line indicates unchanged gene expression. Set the boundary (fold regulation cut-off) and the experimental groups to compare. Then, export the lists of genes whose expression changes are greater than the selected boundary.
Clustergram	**The clustergram** performs non-supervised hierarchical clustering of the entire dataset to display a heat map with dendrograms indicating co-regulated genes across groups or individual samples.
Heat Map	**A heat map** provides a graphical representation of fold regulation expression data between two groups overlaid onto the PCR Array plate layout. Simply select the experimental and control groups to display.
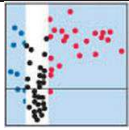
Volcano Plot

The volcano plot helps quickly identify significant gene expression changes. The volcano plot displays statistical significance versus fold-change on the y- and x-axes, respectively. The volcano plot combines a p-value statistical test with the fold regulation change enabling identification of genes with both large and small expression changes that are statistically significant. Select the experimental groups and the boundaries or the fold regulation cutoffs and p-value cutoff values. Then, export the lists of genes whose expression changes and p-values are beyond the selected boundaries.

* NOTE: This plot requires three or more replicates in each group.

Table of figures:

145

146

147

Table of tables:

148

References

Alberts, B., A. Johnson, J. Lewis, M. Raff, K. Roberts, and P. Walter. 2002. "Molecular Biology of the Cell." In *Chapter 17. The Cell Cycle and Programmed Cell Death*, 4th ed. Garland Science. doi:10.1002/bmb.20192.

Allolio, Bruno, and Martin Fassnacht. 2006. "Clinical Review: Adrenocortical Carcinoma: Clinical Update." *The Journal of Clinical Endocrinology and Metabolism* 91 (6). United States: 2027–37. doi:10.1210/jc.2005-2639.

Asin-Cayuela, Jordi, and Claes M Gustafsson. 2007. "Mitochondrial Transcription and Its Regulation in Mammalian Cells." *Trends in Biochemical Sciences* 32 (3). England: 111–17. doi:10.1016/j.tibs.2007.01.003.

Asp, Vendela, Erik Ullerås, Veronica Lindström, Ulrika Bergström, Agneta Oskarsson, and Ingvar Brandt. 2010. "Biphasic Hormonal Responses to the Adrenocorticolytic DDT Metabolite 3-Methylsulfonyl-DDE in Human Cells." *Toxicology and Applied Pharmacology* 242 (3): 281–89. doi:10.1016/j.taap.2009.10.018.

Assié, Guillaume, Anne Jouinot, and Jérôme Bertherat. 2014. "The 'Omics' of Adrenocortical Tumours for Personalized Medicine." *Nature Reviews Endocrinology* 10 (4). Nature Publishing Group: 215–28. doi:10.1038/nrendo.2013.272.

Azizan, Elena A B, Brian Y H Lam, Stephen J Newhouse, Junhua Zhou, Rhoda E Kuc, Jennifer Clarke, Lisa Happerfield, Alison Marker, Gary J Hoffman, and Morris J Brown. 2012. "Microarray, qPCR, and KCNJ5 Sequencing of Aldosterone-Producing Adenomas Reveal Differences in Genotype and Phenotype between Zona Glomerulosa- and Zona Fasciculata-like Tumors." *The Journal of Clinical Endocrinology and Metabolism* 97 (5). United States: E819-29. doi:10.1210/jc.2011-2965.

Barlaskar, Ferdous M, Aaron C Spalding, Joanne H Heaton, Rork Kuick, Alex C Kim, Dafydd G Thomas, Thomas J Giordano, Edgar Ben-Josef, and Gary D Hammer. 2009. "Preclinical Targeting of the Type I Insulin-like Growth Factor Receptor in Adrenocortical Carcinoma." *The Journal of Clinical Endocrinology and Metabolism* 94 (1): 204–12. doi:10.1210/jc.2008-1456.

Bernard, Marie Hélène, Stan Sidhu, Nicole Berger, Jean Louis Peix, Deborah J. Marsh, Bruce G. Robinson, Véronique Gaston, Yves Le Bouc, and Christine Gicquel. 2003.

"Clinical Case Seminar: A Case Report in Favor of a Multistep Adrenocortical Tumorigenesis." *Journal of Clinical Endocrinology and Metabolism* 88 (3): 998–1001. doi:10.1210/jc.2002-021117.

Bertram, K A, B Bratloff, G F Hodges, and H Davidson. 1991. "Treatment of Malignant Leydig Cell Tumor." *Cancer* 68 (10). United States: 2324–29.

Bollen, E, and J B Lanser. 1992. "Reversible Mental Deterioration and Neurological Disturbances with o,p'-DDD Therapy." *Clinical Neurology and Neurosurgery* 94 Suppl: S49–51. doi:10.1016/0303-8467(92)90020-4.

Breuner, C W, D H Jennings, M C Moore, and M Orchinik. 2000. "Pharmacological Adrenalectomy with Mitotane." *General and Comparative Endocrinology* 120 (1): 27–34. doi:10.1006/gcen.2000.7537.

Burow, M E, Y Tang, B M Collins-Burow, S Krajewski, J C Reed, J A McLachlan, and B S Beckman. 1999. "Effects of Environmental Estrogens on Tumor Necrosis Factor Alpha-Mediated Apoptosis in MCF-7 Cells." *Carcinogenesis* 20 (11): 2057–61.

Cai, W, R Benitez, R E Counsell, T Djanegara, D E Schteingart, J E Sinsheimer, and L L Wotring. 1995. "Bovine Adrenal Cortex Transformations of Mitotane [1-(2-Chlorophenyl)-1-(4-Chlorophenyl)-2,2-Dichloroethane; o,p'-DDD] and Its P,p'- and M,p'-isomers." *Biochemical Pharmacology* 49 (10): 1483–89.

Cai, W, R E Counsell, T Djanegara, D E Schteingart, J E Sinsheimer, and L L Wotring. 1995. "Metabolic Activation and Binding of Mitotane in Adrenal Cortex Homogenates." *Journal of Pharmaceutical Sciences* 84 (2): 134–38.

Cai, W, R E Counsell, D E Schteingart, J E Sinsheimer, A D Vaz, and L L Wotring. 1997. "Adrenal Proteins Bound by a Reactive Intermediate of Mitotane." *Cancer Chemotherapy and Pharmacology* 39 (6): 537–40. doi:10.1007/s002800050610.

Cairns, Rob A. 2015. "Drivers of the Warburg Phenotype." *Cancer Journal (Sudbury, Mass.)* 21 (2). United States: 56–61. doi:10.1097/PPO.0000000000000106.

Cerquetti, L., B. Bucci, R. Marchese, S. Misiti, U. De Paula, R. Miceli, a. Muleti, et al. 2008. "Mitotane Increases the Radiotherapy Inhibitory Effect and Induces G 2-Arrest in Combined Treatment on Both H295R and SW13 Adrenocortical Cell Lines." *Endocrine-Related Cancer* 15: 623–34. doi:10.1677/erc.1.1315.

Chakraborti, T, S Das, M Mondal, S Roychoudhury, and S Chakraborti. 1999. "Oxidant, Mitochondria and Calcium: An Overview." *Cellular Signalling* 11 (2): 77–85.

Chang, Jung Min, Hyun Ju Lee, Jin Mo Goo, Ho-Young Lee, Jong Jin Lee, June-Key Chung, and Jung-Gi Im. 2006. "False Positive and False Negative FDG-PET Scans
150

in Various Thoracic Diseases." *Korean Journal of Radiology* 7 (1). The Korean Radiological Society: 57–69. doi:10.3348/kjr.2006.7.1.57.

Coope, M Geoffrey, and Robert E. Hausman. 2006. "The Cell: A Molecular Approach." In , 4thed., 433–39. Sunderland (MA): Sinauer Associates;

D'haene, Barbara. 2013. "Four Tips for RT-qPCR Data Normalization Using Reference Genes." *Biogazzele*. https://www.biogazelle.com/four-tips-rt-qpcr-data-normalization-using-reference-genes.

Ditzhuijsen, C I M van, R van de Weijer, and H R Haak. 2007. "Adrenocortical Carcinoma." *The Netherlands Journal of Medicine* 65 (2): 55–60.

Doghman-Bouguerra, Mabrouka, Veronica Granatiero, Silviu Sbiera, Iuliu Sbiera, Sandra Lacas-Gervais, Frédéric Brau, Martin Fassnacht, Rosario Rizzuto, and Enzo Lalli. 2016. "FATE1 Antagonizes Calcium- and Drug-Induced Apoptosis by Uncoupling ER and Mitochondria." *EMBO Reports* 17 (9): 1264–80. doi:10.15252/embr.201541504.

Dworakowska, Dorota, Paulina Szyszka, Urszula Waszut, Gregory Weitsman, Melvyn Smith, Salvador J Diaz-Cano, Jane Moorhead, et al. 2015. "Mitotane Inhibits Proliferation and Affects Mitochondrial Metabolism in Human Breast, Lung and Colon Cancer Cell Lines." In *Endocrine Society's 97th Annual Meeting and Expo*. San Diego, USA; 03/2015.

Else, Tobias, Alex C. Kim, Aaron Sabolch, Victoria M. Raymond, Asha Kandathil, Elaine M. Caoili, Shruti Jolly, Barbra S. Miller, Thomas J. Giordano, and Gary D. Hammer. 2014. "Adrenocortical Carcinoma." *Endocrine Reviews* 35 (2): 282–326. doi:10.1210/er.2013-1029.

Escandell, José M, Pawan Kaler, M Carmen Recio, Takehiko Sasazuki, Senji Shirasawa, Leonard Augenlicht, José-Luis Ríos, and Lidija Klampfer. 2008. "Activated kRas Protects Colon Cancer Cells from Cucurbitacin-Induced Apoptosis; the Role of p53 and p21." *Biochemical Pharmacology* 76 (2): 198–207. doi:10.1016/j.bcp.2008.05.004.

EUROPEAN MEDICINES AGENCY. 2013. "Lysodren Mitotane." Vol. 44.

Fang, Victor S. 1979. "Cytotoxic Activity of 1-(O-Chlorophenyl)-1-(P-Chlorophenyl)-2,2-Dichloroethane (Mitotane) and Its Analogs on Feminizing Adrenal Neoplastic Cells in Culture." *Cancer Research* 39: 139–45.

Fassnacht, Martin, and Bruno Allolio. 2009. "Clinical Management of Adrenocortical Carcinoma." *Best Practice & Research. Clinical Endocrinology & Metabolism* 23

151

(2). Netherlands: 273–89. doi:10.1016/j.beem.2008.10.008.

Fassnacht, Martin, Matthias Kroiss, and Bruno Allolio. 2013. "Update in Adrenocortical Carcinoma." *Journal of Clinical Endocrinology and Metabolism* 98 (12): 4551–64. doi:10.1210/jc.2013-3020.

Fassnacht, Martin, Massimo Terzolo, Bruno Allolio, Eric Baudin, Harm Haak, Alfredo Berruti, Staffan Welin, et al. 2012. "Combination Chemotherapy in Advanced Adrenocortical Carcinoma." *The New England Journal of Medicine* 366 (23). United States: 2189–97. doi:10.1056/NEJMoa1200966.

Feng, Xiaolan, Yi Zhang, Pan Wang, Quanhong Liu, and Xiaobing Wang. 2014. "Energy Metabolism Targeted Drugs Synergize with Photodynamic Therapy to Potentiate Breast Cancer Cell Death." *Photochemical & Photobiological Sciences : Official Journal of the European Photochemistry Association and the European Society for Photobiology* 13 (12): 1793–1803. doi:10.1039/c4pp00288a.

Fleseriu, Maria, and Frederic Castinetti. 2016. "Updates on the Role of Adrenal Steroidogenesis Inhibitors in Cushing's Syndrome: A Focus on Novel Therapies." *Pituitary*. Springer US. doi:10.1007/s11102-016-0742-1.

Fonseca, Annabelle, James Healy, John Kunstman, Reju Korah, and Tobias Carling. 2012. "Gene Expression and Regulation in Adrenocortical Tumorigenesis." *Biology* 2 (1): 26–39. doi:10.3390/biology2010026.

Fraipont, Florence de, Michelle El Atifi, Nadia Cherradi, Gwennaelle Le Moigne, Genevieve Defaye, Remi Houlgatte, Jerome Bertherat, et al. 2005. "Gene Expression Profiling of Human Adrenocortical Tumors Using Complementary Deoxyribonucleic Acid Microarrays Identifies Several Candidate Genes as Markers of Malignancy." *The Journal of Clinical Endocrinology and Metabolism* 90 (3). United States: 1819–29. doi:10.1210/jc.2004-1075.

Freya, Terrence G., and Carmen A. Mannellab. 2000. "The Internal Structure of Mitochondria." *Trends in Biochemical Sciences* 25 (7): 319–24. doi:10.1016/S0968-0004(00)01609-1.

Fukushima, David K, H Leon Bradlow, and Leon Hellman. 1971. "Effects of o,p'-DDD on Cortisol and 6-Beta-Hydroxycortisol Secretion and Metabolism in Man." *Journal of Clinical Endocrinology and Metabolism*.

Gaglio, Daniela, Christian M Metallo, Paulo A Gameiro, Karsten Hiller, Lara Sala Danna, Chiara Balestrieri, Lilia Alberghina, Gregory Stephanopoulos, and Ferdinando Chiaradonna. 2011. "Oncogenic K-Ras Decouples Glucose and Glutamine

152

Metabolism to Support Cancer Cell Growth." *Molecular Systems Biology* 7 (August). Nature Publishing Group: 523. doi:10.1038/msb.2011.56.

Gazdar, A F, H K Oie, C H Shackleton, T R Chen, T J Triche, C E Myers, G P Chrousos, M F Brennan, C A Stein, and R V La Rocca. 1990. "Establishment and Characterization of a Human Adrenocortical Carcinoma Cell Line That Expresses Multiple Pathways of Steroid Biosynthesis." *Cancer Research* 50 (17): 5488–96.

Gentilin, Erica, Federico Tagliati, Massimo Terzolo, Matteo Zoli, Marcello Lapparelli, Mariella Minoia, Maria Rosaria Ambrosio, Ettore C Degli Uberti, and Maria Chiara Zatelli. 2013. "Mitotane Reduces Human and Mouse ACTH-Secreting Pituitary Cell Viability and Function." *The Journal of Endocrinology* 218 (3). England: 275–85. doi:10.1530/JOE-13-0210.

Germano, Antonina. 2010. "o'p'-DDD MITOTANE." http://flipper.diff.org/app/items/info/2929.

Germano, Antonina, Ida Rapa, Marco Volante, Nicola Lo Buono, Sonia Carturan, Alfredo Berruti, Massimo Terzolo, and Mauro Papotti. 2014. "Cytotoxic Activity of Gemcitabine, Alone or in Combination with Mitotane, in Adrenocortical Carcinoma Cell Lines." *Molecular and Cellular Endocrinology* 382 (1): 1–7. doi:10.1016/j.mce.2013.08.023.

Ghataore, L, I Chakraborti, S J Aylwin, K-M Schulte, D Dworakowska, P Coskeran, and N F Taylor. 2012. "Effects of Mitotane Treatment on Human Steroid Metabolism: Implications for Patient Management." *Endocrine Connections* 1 (1): 37–47. doi:10.1530/EC-12-0028.

Grossman, Lawrence, and John Kamholz. 2015. "'Center for Molecular Medicine and Genetics', Wayne State University School of Medicine." http://genetics.wayne.edu/mitomed/research.php.

Hart, M M, R L Reagan, and R H Adamson. 1973. "The Effect of Isomers of DDD on the ACTH-Induced Steroid Output, Histology and Ultrastructure of the Dog Adrenal Cortex." *Toxicology and Applied Pharmacology* 24 (1): 101–13.

Hebe, David, George L. Blackburn, and John Miller, eds. 2011. *Nutritional Oncology.* 2nd ed. Academic Press.

Held, Paul G. 2001. "Nucleic Acid Purity Assessment Using A 260 / A 280 Ratios," no. 3: 1–5.

Hescot, Paci, Seck, Slama, Viengchareun, Trabado, Brailly-Tabard, et al. 2014. "The Lack of Antitumor Effects of o,p'DDA Excludes Its Role as an Active Metabolite

of Mitotane for Adrenocortical Carcinoma Treatment." *Hormones & Cancer* 5 (5). United States: 312–23. doi:10.1007/s12672-014-0189-7.

Hescot, Slama, Lombès, Paci, Remy, Leboulleux, Chadarevian, et al. 2013. "Mitotane Alters Mitochondrial Respiratory Chain Activity by Inducing Cytochrome c Oxidase Defect in Human Adrenocortical Cells." *Endocrine-Related Cancer* 20 (3): 371–81. doi:10.1530/ERC-12-0368.

Hilscherova, Klara, Paul D Jones, Tannia Gracia, John L Newsted, Xiaowei Zhang, J T Sanderson, Richard M K Yu, Rudolf S S Wu, and John P Giesy. 2004. "Assessment of the Effects of Chemicals on the Expression of Ten Steroidogenic Genes in the H295R Cell Line Using Real-Time PCR." *Toxicological Sciences : An Official Journal of the Society of Toxicology* 81 (1). United States: 78–89. doi:10.1093/toxsci/kfh191.

Hong, W K, American Association for Cancer Research, and W N Hait. 2010. *Holland Frei Cancer Medicine Eight*. Holland Frei Cancer Medicine. People's Medical Publishing House.

Horwitz, K B, M E Costlow, and W L McGuire. 1975. "MCF-7; a Human Breast Cancer Cell Line with Estrogen, Androgen, Progesterone, and Glucocorticoid Receptors." *Steroids* 26 (6). UNITED STATES: 785–95.

Howlett, T A, L H Rees, and G M Besser. 1985. "Cushing's Syndrome." *Clinics in Endocrinology and Metabolism* 14 (4). ENGLAND: 911–45.

Huang, G, Y Chen, H Lu, and X Cao. 2007. "Coupling Mitochondrial Respiratory Chain to Cell Death: An Essential Role of Mitochondrial Complex I in the Interferon-Beta and Retinoic Acid-Induced Cancer Cell Death." *Cell Death and Differentiation* 14 (2): 327–37. doi:10.1038/sj.cdd.4402004.

Huang, Hui, and Tito Fojo. 2008. "Adjuvant Mitotane for Adrenocortical Cancer--a Recurring Controversy." *The Journal of Clinical Endocrinology and Metabolism* 93 (10): 3730–32. doi:10.1210/jc.2008-0579.

Irizarry, Rafael, and Michael Love. 2014. *HarvardX: PH525x Data Analysis for Genomics*. EdX interactive online classe.

Jackson, Mark W, Mukesh K Agarwal, Jinbo Yang, Patrick Bruss, Takeshi Uchiumi, Munna L Agarwal, George R Stark, and Taylor William R. 2005. "p130/p107/p105Rb-Dependent Transcriptional Repression during DNA-Damage-Induced Cell-Cycle Exit at G2." *Journal of Cell Science* 118 (9): 1821 LP-1832.

Johnson, Madeleine. 2014. "Study Shows FFPE Pre-PCR Processing Problems Plague

Pathology Labs." https://www.genomeweb.com/sample-prep/study-shows-ffpe-pre-pcr-processing-problems-plague-pathology-labs-0.

Kasperlik-Zaluska, A.A. 2000. "Clinical Results of the Use of Mitotane for Adrenocortical Carcinoma." *Brazilian Journal of Medical and Biological Research = Revista Brasileira de Pesquisas Médicas E Biológicas / Sociedade Brasileira de Biofísica ... [et Al.]* 33 (10): 1191–96.

Kassi, Eva, Gregory Kaltsas, George Zografos, and George Chrousos. 2010. "Current Issues in the Diagnosis and Management of Adrenocortical Carcinomas." *Expert Review of Endocrinology & Metabolism* 5 (3). Expert Reviews: 451–66. doi:10.1586/eem.10.6.

Kroiss, Matthias, and Martin Fassnacht. 2016. "Inhibition of Cholesterol Esterification in the Adrenal Gland by ATR101/PD132301–2, a Promising Case of Drug Repurposing." *Endocrinology* 157 (5): 1719–21. doi:10.1210/en.2016-1210.

Krols, Michiel, Geert Bultynck, and Sophie Janssens. 2016. "ER-Mitochondria Contact Sites: A New Regulator of Cellular Calcium Flux Comes into Play." *Journal of Cell Biology* 214 (4): 367–70. doi:10.1083/jcb.201607124.

Kufe, Donald W.C, Robert C. Jr Bast, William N Hait, Waun Ki Hong, Raphael E. Pollock, Ralph R. Weichselbaum, James F. Holland, III Emil Frei, American Association for Cancer Research, and William N Hait. 2010. *Holland Frei Cancer Medicine Eight*. Edited by W K Hong and W N Hait. 8thed. Holland Frei Cancer Medicine. People's Medical Publishing House.

Lalli, E. 2015. "Mitotane Revisited: A New Target for an Old Drug." *Endocrinology* 156 (11): 3873–75. doi:10.1210/en.2015-1796.

LaPensee, Christopher R, Jacqueline E Mann, William E Rainey, Valentina Crudo, Stephen W 3rd Hunt, and Gary D Hammer. 2016. "ATR-101, a Selective and Potent Inhibitor of Acyl-CoA Acyltransferase 1, Induces Apoptosis in H295R Adrenocortical Cells and in the Adrenal Cortex of Dogs." *Endocrinology* 157 (5). United States: 1775–88. doi:10.1210/en.2015-2052.

Lehmann, Tomasz P, Tomasz Wrzesinski, and Pawel P Jagodzinski. 2013. "The Effect of Mitotane on Viability, Steroidogenesis and Gene Expression in NCI-H295R Adrenocortical Cells." *Molecular Medicine Reports* 7 (3). Greece: 893–900. doi:10.3892/mmr.2012.1244.

Libe, Rossella, and Guillaume Assie. 2014. "[Adrenocortical carcinoma: Update in 2014]." *Presse medicale (Paris, France : 1983)* 43 (4 Pt 1). France: 401–9.

doi:10.1016/j.lpm.2014.01.009.

Lin, Chia-Wen, Yen-Hwa Chang, and Hsiao-Fung Pu. 2012. "Mitotane Exhibits Dual Effects on Steroidogenic Enzymes Gene Transcription under Basal and cAMP-Stimulating Microenvironments in NCI-H295 Cells." *Toxicology* 298 (1–3): 14–23. doi:10.1016/j.tox.2012.04.007.

Livak, K J, and T D Schmittgen. 2001. "Analysis of Relative Gene Expression Data Using Real-Time Quantitative PCR and the 2(-Delta Delta C(T)) Method." *Methods (San Diego, Calif.)* 25 (4): 402–8. doi:10.1006/meth.2001.1262.

Lombardi, C P, M Raffaelli, G Pani, a Maffione, P Princi, E Traini, T Galeotti, E D Rossi, G Fadda, and R Bellantone. 2006. "Gene Expression Profiling of Adrenal Cortical Tumors by cDNA Macroarray Analysis. Results of a Preliminary Study." *Biomedicine & Pharmacotherapy = Biomédecine & Pharmacothérapie* 60 (4): 186–90. doi:10.1016/j.biopha.2006.03.006.

Maclaine, Nicola J., and Ted R. Hupp. 2009. "The Regulation of p53 by Phosphorylation: A Model for How Distinct Signals Integrate into the p53 Pathway." *Aging* 1 (5). United States: 490–502.

Maher, V M, P J Trainer, A Scoppola, J V Anderson, G R Thompson, and G M Besser. 1992. "Possible Mechanism and Treatment of o,p'DDD-Induced Hypercholesterolaemia." *The Quarterly Journal of Medicine* 84 (305): 671–79.

Martino, M C De, P M Koetsveld, R A Feeldes, S W J Lamberts, W W Herder, A Colao, P Pivonello, and L J & Hofland. 2015. "Combined Effects of Sirolimus and Mitotane in the Inhibition of Growth in Human Adrenocortical Carcinoma Cellsne." In *Endocrine Abstracts*, 37.EP94. doi:DOI:10.1530/endoabs.

Martz, F, and J A Straw. 1977. "The in Vitro Metabolism of 1-(O-Chlorophenyl)-1-(P-Chlorophenyl)-2,2-Dichloroethane (o,p'-DDD) by Dog Adrenal Mitochondria and Metabolite Covalent Binding to Mitochondrial Macromolecules: A Possible Mechanism for the Adrenocorticolytic Effect." *Drug Metabolism and Disposition: The Biological Fate of Chemicals* 5 (5): 482–86.

———. 1980. "Metabolism and Covalent Binding of 1-(O-Chlorophenyl)-1-(P-Chlorophenyl)-2,2-Dichloroethane (o,p,'-DDD). Correlation between Adrenocorticolytic Activity and Metabolic Activation by Adrenocortical Mitochondria." *Drug Metabolism and Disposition: The Biological Fate of Chemicals* 8 (3): 127–30.

Mearini, Luigi, Rachele Del Sordo, Elisabetta Costantini, Elisabetta Nunzi, and Massimo

Porena. 2013. "Adrenal Oncocytic Neoplasm: A Systematic Review." *Urologia Internationalis* 91 (2): 125–33. doi:10.1159/000345141.

Morishita, K, H Okumura, N Ito, and N Takahashi. 2001. "Primary Culture System of Adrenocortical Cells from Dogs to Evaluate Direct Effects of Chemicals on Steroidogenesis." *Toxicology* 165 (2–3). Ireland: 171–78.

Mpanaka, Ioanna, Vassiliki D Lyra, Gregory Kaltsas, and Sofia N Chatziioannou. 2011. "High (18)F-FDG Uptake by the Remaining Adrenal Gland Four Months after Surgery and Initiation of Mitotane Treatment in Two Patients with Adrenocortical Carcinoma." *Hellenic Journal of Nuclear Medicine* 14 (2): 168–72.

Nader, Nancy, Gérald Raverot, Agnès Emptoz-Bonneton, Henri Déchaud, Marc Bonnay, Eric Baudin, and Michel Pugeat. 2006. "Mitotane Has an Estrogenic Effect on Sex Hormone-Binding Globulin and Corticosteroid-Binding Globulin in Humans." *Journal of Clinical Endocrinology and Metabolism* 91 (6): 2165–70. doi:10.1210/jc.2005-2157.

"NCBI GENE RESOURCES." 2015.

Nelson, A A, and G Woodard. 1949. "Severe Adrenal Cortical Atrophy (Cytotoxic) and Hepatic Damage Produced in Dogs by Feeding 2,2-Bis(parachlorophenyl)-1,1-Dichloroethane (DDD or TDE)." *Archives of Pathology* 48 (5): 387–94.

Nijtmans, L. G. J., M. Artal Sanz, L. A. Grivell, and P. J. Coates. 2002. "The Mitochondrial PHB Complex: Roles in Mitochondrial Respiratory Complex Assembly, Ageing and Degenerative Disease." *Cellular and Molecular Life Sciences* 59: 143–55. doi:10.1007/s00018-002-8411-0.

Othumpangat, Sreekumar, John D. Noti, and Donald H. Beezhold. 2014. "Lung Epithelial Cells Resist Influenza A Infection by Inducing the Expression of Cytochrome c Oxidase VIc Which Is Modulated by miRNA 4276." *Virology* 468–470. Elsevier: 256–64. doi:10.1016/j.virol.2014.08.007.

Ovalle, William K., and Patrick C. Nahirney. 2013. "The Cell." In *Netter's Histology Flash Cards Updated Edition*, 1sted., 1.05. Elsevier.

Papa, Luena, and Doris Germain. 2011. "Estrogen Receptor Mediates a Distinct Mitochondrial Unfolded Protein Response." *Journal of Cell Science* 124 (Pt 9). England: 1396–1402. doi:10.1242/jcs.078220.

Perez-Novo, Claudina Angela, Cindy Claeys, Frank Speleman, Paul Van Cauwenberge, Claus Bachert, and Jo Vandesompele. 2005. "Impact of RNA Quality on Reference Gene Expression Stability." *BioTechniques* 39 (1). United States: 52,54,56.

157

Pfaffl, Michael W. 2004. "Relative Quantification," 63–82.

Pignatti, Emanuele, Sining Leng, Diana L. Carlone, and David T. Breault. 2017. "Regulation of Zonation and Homeostasis in the Adrenal Cortex." *Molecular and Cellular Endocrinology* 441. Elsevier Ireland Ltd: 146–55. doi:10.1016/j.mce.2016.09.003.

Pinton, P, C Giorgi, R Siviero, E Zecchini, and R Rizzuto. 2008. "Calcium and Apoptosis: ER-Mitochondria Ca2+ Transfer in the Control of Apoptosis." *Oncogene* 27 (50): 6407–18. doi:10.1038/onc.2008.308.

Poli, Giada, Daniele Guasti, Elena Rapizzi, Rossella Fucci, Letizia Canu, Alessandra Bandini, Nicoletta Cini, Daniele Bani, Massimo Mannelli, and Michaela Luconi. 2013. "Morphofunctional Effects of Mitotane on Mitochondria in Human Adrenocortical Cancer Cells." *Endocrine-Related Cancer* 20 (4): 537–50. doi:10.1530/ERC-13-0150.

Postlewait, Lauren M, Cecilia G Ethun, Thuy B Tran, Jason D Prescott, Timothy M Pawlik, Tracy S Wang, Jason Glenn, et al. 2016. "Outcomes of Adjuvant Mitotane after Resection of Adrenocortical Carcinoma: A 13-Institution Study by the US Adrenocortical Carcinoma Group." *Journal of the American College of Surgeons* 222 (4). United States: 480–90. doi:10.1016/j.jamcollsurg.2015.12.013.

Pópulo, Helena, José Manuel Lopes, and Paula Soares. 2012. "The mTOR Signalling Pathway in Human Cancer." *International Journal of Molecular Sciences* 13 (2). Molecular Diversity Preservation International (MDPI): 1886–1918. doi:10.3390/ijms13021886.

Pramanik, Kartick C., Srinivas Reddy Boreddy, and Sanjay K. Srivastava. 2011. "Role of Mitochondrial Electron Transport Chain Complexes in Capsaicin Mediated Oxidative Stress Leading to Apoptosis in Pancreatic Cancer Cells." *PLoS ONE* 6 (5).

Prince, Frederick P. 2002. "Lamellar and Tubular Associations of the Mitochondrial Cristae: Unique Forms of the Cristae Present in Steroid-Producing Cells." *Mitochondrion* 1 (4). Netherlands: 381–89.

Qiagen. 2010. "October 2010 RNAprotect ® Cell Reagent Handbook," no. October.

———. 2011a. "REPLI-G ® Mini / Midi Handbook Sample & Assay Technologies QIAGEN Sample and Assay Technologies," no. July 2005.

———. 2011b. "RT 2 PreAMP cDNA Synthesis Handbook Sample & Assay Technologies QIAGEN Sample and Assay Technologies," no. March.

QIAGEN. 2015. "mTOR Signaling RT2 Profiler PCR Array." https://www.qiagen.com/pl/products/genes and pathways/complete biology list/mtor signaling/rt2-profiler-pcr-arrays?catno=PAHS-098Z#geneglobe.

Rainey, William E., Karla Saner, and Bernard P. Schimmer. 2004. "Adrenocortical Cell Lines." *Molecular and Cellular Endocrinology* 228: 23–38. doi:10.1016/j.mce.2003.12.020.

Redick, J A, G F Kapke, L S 3rd Van Orden, and J Baron. 1977. "Immunohistochemical Localization of Adrenal Ferredoxin in Bovine Adrenal Cortex." *Life Sciences* 20 (7): 1139–47.

Rosa, V. De, F. Iommelli, M. Monti, R. Fonti, G. Votta, M. P. Stoppelli, and S. Del Vecchio. 2015. "Reversal of Warburg Effect and Reactivation of Oxidative Phosphorylation by Differential Inhibition of EGFR Signaling Pathways in Non-Small Cell Lung Cancer." *Clinical Cancer Research*. doi:10.1158/1078-0432.CCR-15-0375.

Rulli, Samuel. 2014. "Introduction To Real-Time Quantitative PCR (qPCR)." In .

Sbiera, Silviu, Ellen Leich, Gerhard Liebisch, Iuliu Sbiera, Andreas Schirbel, Laura Wiemer, Silke Matysik, et al. 2015. "Mitotane Inhibits Sterol-O-Acyl Transferase 1 Triggering Lipid-Mediated Endoplasmic Reticulum Stress and Apoptosis in Adrenocortical Carcinoma Cells." *Endocrinology* 156 (11): 3895–3908. doi:10.1210/en.2015-1367.

Schapira, Anthony H. V., and S Dimauro. 1994. *Mitochondrial Disorders in Neurology*. Edited by Anthony H V Schapira and S Dimauro. Oxford OX2 8DP: Butterworth-Heinemann International Medical Reviews.Burlington : Elsevier Science.

Schteingart, D. E. 2000. "Conventional and Novel Strategies in the Treatment of Adrenocortical Cancer." *Brazilian Journal of Medical and Biological Research* 33 (10): 1197–1200. doi:10.1590/S0100-879X2000001000009.

Schteingart, D E, J E Sinsheimer, R E Counsell, G D Abrams, N McClellan, T Djanegara, J Hines, N Ruangwises, R Benitez, and L L Wotring. 1993. "Comparison of the Adrenalytic Activity of Mitotane and a Methylated Homolog on Normal Adrenal Cortex and Adrenal Cortical Carcinoma." *Cancer Chemotherapy and Pharmacology* 31 (6): 459–66.

Schteingart, D E, H S Tsao, C I Taylor, A McKenzie, R Victoria, and B A Therrien. 1980. "Sustained Remission of Cushing's Disease with Mitotane and Pituitary Irradiation." *Annals of Internal Medicine* 92 (5): 613–19. doi:10.7326/0003-4819-92-5-613.

Simon, H. U., A. Haj-Yehia, and F. Levi-Schaffer. 2000. "Role of Reactive Oxygen Species (ROS) in Apoptosis Induction." *Apoptosis* 5 (5): 415–18. doi:10.1023/A:1009616228304.

Singh, Keshav K., and Leslie C. Costello. 2009. "Mitochondria and Cancer." *Mitochondria and Cancer*. Nature Publishing Group, 1–289. doi:10.1007/978-0-387-84835-8.

Sotgia, Federica, Ubaldo E Martinez-Outschoorn, Stephanos Pavlides, Anthony Howell, Richard G Pestell, and Michael P Lisanti. 2011. "Understanding the Warburg Effect and the Prognostic Value of Stromal Caveolin-1 as a Marker of a Lethal Tumor Microenvironment." *Breast Cancer Research : BCR* 13 (4). BioMed Central: 213. doi:10.1186/bcr2892.

Stigliano, A, L Cerquetti, M Borro, G Gentile, B Bucci, S Misiti, P Piergrossi, E Brunetti, M Simmaco, and V Toscano. 2008. "Modulation of Proteomic Profile in H295R Adrenocortical Cell Line Induced by Mitotane." *Endocrine-Related Cancer* 15 (1): 1–10. doi:10.1677/ERC-07-0003.

Szabo, P M, V Tamasi, V Molnar, M Andrasfalvy, Z Tombol, R Farkas, K Kovesdi, et al. 2010. "Meta-Analysis of Adrenocortical Tumour Genomics Data: Novel Pathogenic Pathways Revealed." *Oncogene* 29 (21). England: 3163–72. doi:10.1038/onc.2010.80.

Tait, Stephen W G, and Douglas R Green. 2012. "Mitochondria and Cell Signalling." *Journal of Cell Science* 125 (Pt 4): 807–15. doi:10.1242/jcs.099234.

Takeshita, Akira, Junko Igarashi-Migitaka, Noriyuki Koibuchi, and Yasuhiro Takeuchi. 2013. "Mitotane Induces CYP3A4 Expression via Activation of the Steroid and Xenobiotic Receptor." *The Journal of Endocrinology* 216 (3). England: 297–305. doi:10.1530/JOE-12-0297.

Temperley, Richard J, Mateusz Wydro, Robert N Lightowlers, and Zofia M Chrzanowska-Lightowlers. 2010. "Human Mitochondrial mRNAs—like Members of All Families, Similar but Different." *Biochimica et Biophysica Acta* 1797 (6–7). Elsevier Pub. Co: 1081–85. doi:10.1016/j.bbabio.2010.02.036.

Terzolo, Massimo, Alberto Angeli, Martin Fassnacht, Fulvia Daffara, Libuse Tauchmanova, Pier Antonio Conton, Ruth Rossetto, et al. 2007. "Adjuvant Mitotane Treatment for Adrenocortical Carcinoma." *The New England Journal of Medicine* 356 (23): 2372–80. doi:10.1056/NEJMoa063360.

Terzolo, Massimo, and Alfredo Berruti. n.d. "Efficacy of Adjuvant Mitotane Treatment
160

in Prolonging Recurrence-Free Survival in Patients with Adrenocortical Carcinoma at Low-Intermediate Risk of Recurrence Submitted to Radical Resection." https://www.epiclin.it/adiuvo.

Touitou, Y, A Bogdan, and J P Luton. 1978. "Changes in Corticosteroid Synthesis of the Human Adrenal Cortex in Vitro, Induced by Treatment with o,p'-DDD for Cushing's Syndrome: Evidence for the Sites of Action of the Drug." *Journal of Steroid Biochemistry* 9 (12): 1217–24.

Tripto-Shkolnik, Liana, Zeev Blumenfeld, Moshe Bronshtein, Asher Salmon, and Anat Jaffe. 2013. "Pregnancy in a Patient with Adrenal Carcinoma Treated with Mitotane: A Case Report and Review of Literature." *Journal of Clinical Endocrinology and Metabolism* 98 (2): 443–47. doi:10.1210/jc.2012-2839.

Vafai, Scott B, and Vamsi K Mootha. 2012. "Mitochondrial Disorders as Windows into an Ancient Organelle." *Nature* 491 (7424). England: 374–83. doi:10.1038/nature11707.

Veytsman, Irina, Lynnette Nieman, and Tito Fojo. 2009. "Management of Endocrine Manifestations and the Use of Mitotane as a Chemotherapeutic Agent for Adrenocortical Carcinoma." *Journal of Clinical Oncology : Official Journal of the American Society of Clinical Oncology* 27 (27): 4619–29. doi:10.1200/JCO.2008.17.2775.

Wallace, Douglas C. 2012. "Mitochondria and Cancer." *Nature Reviews. Cancer* 12 (10): 685–98. doi:10.1038/nrc3365.

Waszut, U, P Szyszka, and D Dworakowska. 2017. "Understanding Mitotane Mode of Action." *Journal of Physiology and Pharmacology : An Official Journal of the Polish Physiological Society* 68 (1). Poland: 13–26.

Watts, R W E, R A Harkness, E Spellacy, and N F Taylor. 1987. "Lesch-Nyhan Syndrome: Growth Delay, Testicular Atrophy and a Partial Failure of the 11β-Hydroxylation of Steroids." *Journal of Inherited Metabolic Disease* 10 (3). Kluwer Academic Publishers: 210–23. doi:10.1007/BF01800063.

Wei, Huijun, Lili Guo, Lin Li, Qinghua Zhou, and Zhihao Wu. 2015. "Mechanism of Warburg effect and its effect on tumor metastasis." *Chinese journal of lung cancer* 18 (3). China: 179–83. doi:10.3779/j.issn.1009-3419.2015.03.09.

Wey, Raymond E. Counsell, David E. Schteingart, Joseph E. Sinsheimer, Alfin D N Vaz, and Linda L. Wotring. 1997. "Adrenal Proteins Should Be a Reactive Intermediate of Mitotane." *Cancer Chemotherapy and Pharmacology* 39: 537–40.

doi:10.1007/s002800050610.

Whelan, Sean P., and Brian S. Zuckerbraun. 2013. "Mitochondrial Signaling: Forwards, Backwards, and in between." *Oxidative Medicine and Cellular Longevity* 2013 (351613). United States: 1–11. doi:10.1155/2013/351613.

Wu, Yanjing, Warren G. Foster, and Edward V. Younglai. 2006. "Rapid Effects of Pesticides on Human Granulosa-Lutein Cells." *Reproduction* 131 (2): 299–310. doi:10.1530/rep.1.00922.

Young, B R, M J Bryson, M L Sweat, and J C. Street. 1973. "Complexing of DDT and O' P 'DDD with Adrenal Cytochrome P-450 Hydroxylating Systems." *Joumal of Sreroid Biochemisry,* 4 (Pergamon Press): 585–91.

Zatelli, Maria Chiara, Erica Gentilin, Fulvia Daffara, Federico Tagliati, Giuseppe Reimondo, Gianni Carandina, Maria Rosaria Ambrosio, Massimo Terzolo, and Ettore C. Degli Uberti. 2010. "Therapeutic Concentrations of Mitotane (o,p'-DDD) Inhibit Thyrotroph Cell Viability and TSH Expression and Secretion in a Mouse Cell Line Model." *Endocrinology* 151 (6): 2453–61. doi:10.1210/en.2009-1404.

Zeviani, Massimo, Michal Minczuk, Mike Murphy, John Walker, and Edmund Kunji. 2015. "Expression and Repair of the Mitochondrial Genome | Mitochondrial Biology Unit." http://www.mrc-mbu.cam.ac.uk/research/mitochondrial-genetics/expression-and-repair-mitochondrial-genome.

Zhang, Jitao David, Markus Ruschhaupt, and Rudolf Biczok. 2015. "ddCt Method for qRT–PCR Data Analysis."

Zhao, Bao-Xia, Jing Wang, Bo Song, Hong Wei, Wei-Peng Lv, Li-Min Tian, Mei Li, and Shen Lv. 2015. "Establishment and Biological Characteristics of Acquired Gefitinib Resistance in Cell Line NCI-H1975/gefinitib-Resistant with Epidermal Growth Factor Receptor T790M Mutation." *Molecular Medicine Reports* 11 (4). Greece: 2767–74. doi:10.3892/mmr.2014.3058.

Zsippai, A, DR Szabó, Z Tömböl, K Eder, E Pállinger, RC Gaillard, A Patócs, et al. 2012. "Effects of Mitotane on Gene Expression in the Adrenocortical Cell Line NCI-H295R : A Microarray Study." *Pharmacogenomics* 13 (12): 1351–61.

Zsippai, Adrienn, DR Szabó, Z Tömböl, Katalin Eder, E Pállinger, RC Rolf C Gaillard, A Patócs, et al. 2012. "Effects of Mitotane on Gene Expression in the Adrenocortical Cell Line NCI-H295R : A Microarray Study." *Pharmacogenomics* 13 (12). England: 1351–61. doi:10.2217/pgs.12.116.